Distribution Agreement

In presenting this thesis or dissertation as a partial fulfillment of the requirements for an advanced degree from Emory University, I hereby grant to Emory University and its agents the non-exclusive license to archive, make accessible, and display my thesis or dissertation in whole or in part in all forms of media, now or hereafter known, including display on the world wide web. I understand that I may select some access restrictions as part of the online submission of this thesis or dissertation. I retain all ownership rights to the copyright of the thesis or dissertation. I also retain the right to use in future works (such as articles or books) all or part of this thesis or dissertation.

Signature:

_____ _____

Courtney St Clair Ardita Date

Lactobacillus rhamnosus GG-induced probiotic effects require Nox1-generated ROS and SpaC-mediated adhesion

By

Courtney St Clair Ardita
Doctor of Philosophy

Graduate Division of Biological and Biomedical Science
Microbiology and Molecular Genetics

_____

Andrew Neish, M.D.
Advisor

_____

Daniel Kalman, Ph.D.
Committee Member

_____

Ken Moberg, Ph.D
Committee Member

_____

Martin Moore, Ph.D.
Committee Member

_____

David Weiss, Ph.D.
Committee Member

Accepted:

_____

Lisa A. Tedesco, Ph.D.
Dean of the James T. Laney School of Graduate Studies

_____

Date

Lactobacillus rhamnosus GG-induced probiotic effects require Nox1-generated ROS and SpaC-mediated adhesion

By

Courtney St Clair Ardita
B.S., The College of William and Mary, 2007

Advisor: Andrew S. Neish, M.D.

An abstract of
A dissertation submitted to the Faculty of the
James T. Laney School of Graduate Studies of Emory University
in partial fulfillment of the requirements for the degree of
Doctor of Philosophy in
Graduate Division of Biological and Biomedical Science
Microbiology and Molecular Genetics
2014

Abstract

Lactobacillus rhamnosus GG-induced probiotic effects require Nox1-generated ROS and SpaC-mediated adhesion

By

Courtney St Clair Ardita

Lactobacilli preparations are marketed for their health benefits and have shown promising efficacy as treatments for intestinal disease. Studies exploring the effect of lactobacilli in the alimentary canals of two common laboratory models, *Drosophila* and mice, have demonstrated that exposure to lactobacilli positively impacts development, homeostasis, and immune functioning in these systems. However, despite their clinical potential and the existence of laboratory models to investigate them, the nature of the relationship between commensal lactobacilli and host health is poorly characterized. The studies described in this dissertation elucidate some molecular mechanisms behind how probiotic lactobacilli induce salutary effects in the gastrointestinal tracts of flies and mice. Here, we found that *Lactobacillus plantarum* naturally colonizes laboratory-raised strains of *Drosophila* and that this bacterium induces cellular reactive oxygen species (ROS) generation in the *Drosophila* midgut. This cellular ROS generation also activates cell proliferation in the fly midgut. Lactobacilli-induced ROS generation was also shown to occur in cultured mammalian cells, and in the murine intestine. Indeed, *Lactobacillus rhamnosus* GG (LGG) induces particularly robust ROS generation in mammalian systems. We also established that ROS-generation is dependent on cellular expression of NADPH oxidase (Nox). Lactobacilli-induced ROS generation is significantly diminished in enterocyte specific dNox null *Drosophila* and in gut epithelial-specific Nox1 null mice. Furthermore, we demonstrated that the LGG pilin adhesion protein, SpaC, is required for LGG-induced ROS generation. An isogenic *Lactobacillus rhamnosus* GG strain that lacks SpaC (LGGΩ*spaC*) does not adhere to intestinal mucus or murine intestines as well as the wild type strain. SpaC was shown to contribute to the capacity of LGG to induce cellular ROS generation, potentiate ERK MAPK signaling in enterocytes, stimulate cellular proliferation, and protect against radiation-induced injury. Collectively, these data show that commensal lactobacilli found in the alimentary canal lead to beneficial effects in their hosts by inducing cellular ROS generation through a Nox-dependent mechanism. In addition, LGG requires intimate contact with intestinal epithelial cells in order to elicit this ROS induction and its probiotic effects are dependent on bacterial expression of the SpaC pilin protein.

Lactobacillus rhamnosus GG-induced probiotic effects require Nox1-generated ROS and SpaC-mediated adhesion

By

Courtney St Clair Ardita
B.S., The College of William and Mary, 2007

Advisor: Andrew S. Neish, M.D.

A dissertation submitted to the Faculty of the
James T. Laney School of Graduate Studies of Emory University
in partial fulfillment of the requirements for the degree of
Doctor of Philosophy in
Graduate Division of Biological and Biomedical Science
Microbiology and Molecular Genetics
2014

Table of Contents

List of Figures

Chapter 1: Introduction

Commensal Bacteria

Eukaryotic organisms evolved in the presence of prokaryotes and over the course of biotic history this developing relationship has not only allowed multicellular organisms to develop mechanisms to protect their selves from harmful single celled pathogens but it has also allowed the evolution of trans-kingdom symbiotic relationships. Only 1/10th of the cells in the human body are eukaryotes; the other 9/10^{ths} are comprised of the prokaryotic commensal bacteria that are play integral roles in the body's every functions (1). The human **microbiota** is a term that refers to the commensal bacteria, archaea, fungi, and viruses that colonize the skin, gut, and mucosal surfaces of the human body. The collective genome of these organisms is referred to as the human **microbiome**. It is becoming increasingly apparent just how critical the human microbiota is to human health; doctors and researchers are continually demonstrating how the organisms residing in our oral cavity, urogenital tract, upper respiratory system, and gastrointestinal tract as well as those living on our skin have important roles in our well-being. The bacteria residing in and on the human body benefit from a stable, nutrient rich environment and in turn provide the host with a wealth of beneficial effects including; competitive exclusion of pathogens, extraction of otherwise indigestible calories, activation of epithelial transcription programs, stimulation of adaptive immune system, and stimulation of cytoprotective pathways (2, 3).

The commensal bacteria occupying a given anatomical location depend on the local microenvironment's characteristics (e.g. pH, temperatures, redox

potential, as well as oxygen, water and nutrient levels) and therefore the flora changes with the area of the body being studied. The four most common phyla found living in or on any area in the human body are: Actinobacteria, Bacteroidetes, Firmicutes, and Proteobacteria (4-6). The percentage of the total microbial community each phyla represents, however, varies significantly with location. Actinobacteria make up the largest portion of bacteria on the skin where as Firmicutes and Bacterioidetes are the most abundant phyla in the oral and gasterointestinal microbiotas (4). In reproductive age women, the vaginal microbiota belongs to one of five groups. Lactic acid bacteria, members of the Firmicutes phyla, dominate four of these groups. In fact, 73% of vaginal communities are dominated by one or more *Lactobacillus* species (7). Interestingly, the vaginal flora changes with age and hormonal level: from one month of age until the onset of puberty, the vaginal flora is comprised of skin like flora, while after puberty contains more lactic acid bacteria, and finally returns to its prepubescent state following menopause (8). In the oral cavity, Firmicutes represented 36.7 % of the taxa sampled while Bacteriodetes and Proteobacteria represent about 17.3% and 17.1 % of the taxa sampled respectively (6). Together, Firmicutes and Bacteriodetes account for over 90% of the taxa sampled in the gastrointestinal tract (5).

Intestinal Microbiota

The human gastrointestinal tract is one of the best-studied bacterial ecosystems on the planet. The microbes found in the gastrointestinal tract form one of the most complex bacterial ecosystems ever discovered, a notion perhaps

not surprising, when one considers that the intestinal microbiome is estimated to have over 100 fold more genes than the human genome (9, 10). When metagenomic sequencing was performed on DNA isolated from fecal samples of 124 European individuals, Qin et al found that 3.3 million non-redundant genes and determined that over 99% of them were of bacterial origin (11).

Microbes within the intestines can exist in a free living planktonic state in the luminal stream of the gastrointestinal tract or they can exist in a more sessile state where they remain in intimate contact with the mucous layer that forms a barrier between intestinal enterocytes and the luminal contents. These populations consist of both **autochthonous** or indigenous species that originated in the area being sampled as well as **allochthonous** species or ones that have originated elsewhere and were likely ingested along with food or have traveled from more proximal or in some cases even distal areas of the gastrointestinal tract (1)

Due to the fact that the mammalian intestinal microbiota changes as one travels along the alimentary canal, varies temporally within a host, differs between hosts, and is largely comprised of obligate anaerobic bacteria that are unculturable, studies that precisely define the bacterial-members of the microbiota have not been possible. However, with the use of more recently developed nucleic acid based techniques such as next generation sequencing and the genomic informatics to analyze the data, our knowledge of specific members of the microbiota continues to grow rapidly. The human intestinal microbiota has the highest recorded density of any bacterial ecosystem (Figure 1) yet its diversity with respect to phyla levels is among the lowest; while there are over 50 bacteria

phyla in existence, human intestinal microbes belong to just 13 of these and the greatly dominated by just two phyla specifically Firmicutes and Bacteroidetes (10, 12).

In 2011, a metagenomic study comparing the microbiota from 33 European, American, and Japanese individuals identified three robust clusterings across individuals. These clusters, termed enterotypes, where characterized by an enrichment in one of three bacteria genera, specifically *Bacteroides, Prevotella*, or *Ruminococcus*, and named enterotype 1, 2, and 3, respectively. Interestingly, enterotype was not related to gender, body mass index, age, or nationality. Moreover, when the same analysis was performed on previously published metagenomic data sets from 239 individuals the same three groupings were detected (13). The same year, however, research published by a different group suggested that gut microbiotas should be grouped into two rather than three enterotypes that were related to long term diets; those high in protein and animal fat were associated with *Bacteroides* while diets high in carbohydrates were associated with *Prevetella* (14). Further studies have continued to blur the concept of enterotypes and suggest that microbiotas fall along a gradient or continuum of *Bacteriodes*-enriched versus *Prevetella*-enriched populations rather than into three distinct groups (15). In conclusion, the application of nucleic acid based techniques is continually adding to our knowledge this complex ecosystem. And, this further characterization is allowing researchers to link subsets of the microbiota to specific functions that were originally only possible to attribute to the entire microbiota as a whole, as well as allowing them to link specific microbial compositions to clinical traits.

Anatomy of the Intestine

Murine and human intestines are divided into two main portions, the small intestine and the large intestine, which can be further divided. The small intestine include, proximal to distal, the duodenum, the jejunum and the ileum. Microscopically, the lining or **mucosa** is characterized by finger shaped projections that reach into the lumen perpendicular to the length of the intestine. These projections, known as villi, serve as the primary site of digestive and greatly increase the surface area of this organ that is responsible for much of the body's digestion and food absorption. The villi are longest in the duodenum and become progressively shorter as one travels along the small intestine until the structures disappear in the large intestine (16). The large intestine is comprised of the cecum, colon, and rectum, which functions in absorbing the remaining water in indigestible food material and compacting it into fecal pellets before it is excreted. The colon, especially the cecum, is home to the highest density population of intestinal commensal bacteria and will absorb various products resulting from the metabolic and fermentation processes occurring in its prokaryotic residents. Short chain fatty acids (SCFAs) and essential amino acids produced by the commensal population serve as key energy sources for the gut epithelial cells and, in the case of SCFAs, also have anti-carcinogenic and anti-inflammatory effects (17). The ceca of mice are proportionally much larger than human ceca because more of their diet consists of plant derived materials requiring extensive fermentation. While to large intestine does not have evaginated villi, both the small intestine and colon contain test tube shaped

invaginations known as **crypts of Lieberkuhn**. These crypts are protective areas that house the intestinal stem cells, which divide and differentiate to maintain the highly dynamic intestinal epithelial layer.

Types of Intestinal Epithelial Cells

The intestinal epithelial layer is comprised of three main cell types: absorptive enterocytes, goblet cells, and enteroendocrine cells. Enterocytes are the most abundant type and perform most intestinal digestive and absorptive functions. Goblet cells are specialized secretory cells that produce mucus and associated substances, which together protect the epithelial layer from the luminal contents and provide lubrication for the passage of digestive material along the intestines. Enteroendocrine cells are specialized endocrine cells that produce specific regulatory hormones. Paneth cells, which secrete a variety of antimicrobial substances, can be found in the crypts of the small intestines as well as the crypts of the proximal colon (16, 18, 19).

The intestinal epithelial layer is under a state of constant renewal and is completely replaced every 3 to 5 days (18). This process allows this critical barrier to remain intact despite the vast amount of cells that are lost or damaged due to the continuous flow of luminal contents along that gastrointestinal tract. Intestinal stem cells located near the base of the intestinal crypts replenish the epithelial cell population; the stem cells first divide to create highly proliferative progenitor cells which further divide and differentiate as the move up the crypt and eventually develop into one of three main cell types. Cells exiting the crypt stop proliferating but continue to migrate to replenish the rest of the epithelial

layer. In the small intestine, where over 300 million new epithelial cells are produced daily, the epithelial cells will migrate upwards towards the tips of villi (18). Interestingly, Paneth cells are only replaced every 3-6 weeks and are replenished by cells that migrate abluminally (down) from the stem cell niche (18).

Pattern Recognition Receptors on Intestinal Epithelial Cells

The single cell epithelial layer, measuring only 20 um in thickness, and the surrounding mucus that this specialized layer of cells secretes serve as the sole boundary between the trillions of bacteria in the intestinal lumen and the interior of the body (19). Thus, in addition to its simple barrier function, this layer must have mechanisms to sense the bacteria it comes in contact with and determine whether these bacteria are commensal or pathogenic, and have a way to rely these finding to the rest of the body.

To this end, epithelial cells have evolved pattern recognition receptors, or PRRs, that can detect conserved structural motifs present in wide ranges of microbes. These conserved motifs are known as MAMPs or microbial associated molecular patterns. PRRs, which include toll-like receptors (TLRs), the related nucleotide-binding oligomerization domain (NOD) proteins, and the formyl peptide receptors (FPRs), are expressed on the apical side of the enterocytes. The activation of these receptors leads to the activation signaling cascades involving mitogen activate protein kinases (MAPKs) and nuclear-factor κB (NF κB). The combination of the receptors activated as well as the magnitude of the signal and the physical location of the activated receptor allows the cells to differentiate

between stimulation from commensal versus pathogenic organisms. While Toll-like receptors are critical for the detection of pathogens and the initiation of the immune responses to these pathogens, the commensal bacteria present in the gastrointestinal tract also express the MAMPs that are detected by TLRs. Of the ten TLRs, four are dedicated to sensing bacteria. TLR2 and TLR4 detect lipoteichoic acid (LTA) and lipopolysaccharide (LPS) on found on gram-positive and gram-negative bacteria, respectively. TLR5 responses to flagellin and TLR9 reacts with unmethylated CpG DNA that is present in prokaryotes (19).

Commensal bacteria stimulation of intestinal epithelial expressed TLRs has been shown to be important to intestinal homeostasis (20). MyD88 -/- mice, which have dysfunctional TLR signaling, are more susceptible to DSS-induced colitis; however, when the commensal microbiota is removed from wild type mice via broad spectrum antibiotic treatment, wild type mice display this same susceptibility to DSS-colitis (20). This observation highlights the conclusion that commensal bacteria contribute to a basal level of TLR induced protective factors like heat shock proteins and cytokines. While commensal bacteria constantly signal TLRs to facilitate homeostasis and “prime the pump” for further more serious insults, mammals have evolved mechanisms to limit the amount of TLR-commensal signaling that occurs as well. For example, TLR5 can induce a proinflammatory response after exposure to flagellin but constant inflammation in intestinal epithelial cells exposed to commensal microbiota is prevented because these cells keep their TLR5s physically sequestered from the microbiota present in the intestinal lumen. IEC only express TLR5 on their basolateral membrane which prevents the commensal bacteria on the apical side from

stimulating a proinflammatory response but allows the IECs to detect any bacteria that has managed to invade or translocate its flagellin to the more protected basolateral side of the epithelial layer (21). While macrophages express TLR4 on their cellular surface, TLR4 expressed by intestinal epithelial cells is found in the Golgi apparatus and therefore cannot react with LPS until it has been internalized by the cell (22).

Formyl peptide receptors (FPR) are PRRs that respond to the formylated bacterial and mitochondrial products. After the 1975 discovery that formylated peptides served as neutrophilic chemoattractants (23), Williams et al demonstrated FPRs were present on human polymorphonuclear leukocytes in 1977 (24). Humans and non-human primates have 3 types of FPRs, FPR1, FPR2, and FPR3, while there are at least 7 in the murine genome. These receptors are promiscuous G-coupled receptors that contain seven transmembrane regions and all three types bind to the N-formyl peptides that are produced prokaryotic protein synthesis is initiated by N-formylmethionine (25). While FPRs are expressed throughout the body, we are most interested in FPR1 due to its presence on colonic epithelial cells. FPR1 localizes to the lateral membrane of crypt epithelial cells in the human colon and its activation by fMLF plays an important role in wound closure due to the receptors ability to stimulate PI3K activity (26).

Mucus Layer

The gastrointestinal tract is covered by mucus that is secreted from epithelial surfaces. This mucus is comprised of two layers; a firm layer directly on

top of the apical side of the epithelial cells and a loose layer found between the firm layer and the lumen (27, 28). While the firm layer is patchy in the small intestines, it is continuous in the colon (27). The mucus layer is thickest in the colon where the loose layer is approximately twice as thick as the firm layer (for example measurements in murine colon were around 100 μm and 50 μm respectively). The composition of both layers is almost identical and while a variety of proteins, antimicrobial peptides, and antibodies can be found in the mucin, it is predominantly comprised of the mucin (28).

Muc2 is produce by goblet cells in the small and large intestines. After production, Muc2 is extensively postranslationally modified and individual Muc2 proteins are covalently bound together into net-like structures. These structures are stored in goblet cells mucin granules until they are released extracellularly. Once released, the net-link structure further expands and becomes the firm mucus layer. The loose layer is created by proteolytic cleavage of the firm layer (29, 30).

While the two layers of mucus are comprised of the same components and are adjacent to each other, FISH studies using pan-bacterial probes have demonstrated that while the loose layer contains a plethora of microbes where as the firm layer is completely devoid of bacteria (28). This physical separation is one of the ways the colon can tolerate being so near the millions of microbes it contains; a mucus layer devoid of bacteria is not observed in many patients with inflammatory bowel disease or Muc2 -/- mice that develop spontaneous colitis (31).

Germ Free Intestines

Studies employing the use of germ free, or axenic, animals that have been raised in a completely sterile environment have demonstrated that exposure to microbes in critical for normal intestinal development as well as gut homeostasis (32). The microbiota influences the architecture of the intestinal epithelial layer; distal small intestine villi of germ free mice are longer, thinner, and have less developed vasculature than those of conventionally raised mice, the crypts of germ free mice are shallower and have less proliferating stem cells than conventional crypts and the mucus layer in a germ free intestine is thinner than normal (33). Normal lymphoid structures are underdeveloped in germ free animals as well (33). The proper development of the mesenchymal microvascular network found in the small intestinal villi (34) and the enteric nervous system in the jejunum and ileum (35) requires exposure key members of the microbiota. Collectively, these experiments are strongly suggestive of beneficial, physiological roles of the microbiota in mammalian gut homeostasis.

Mucosa-Associated Bacteria

Recent improvements in our ability to characterize bacteria by sequencing and analyzing its 16s rDNA is proving that, like other microbial communities, the commensal bacteria within the gastrointestinal tract is more organized that was initially realized. The mucosa-associated bacteria represent a different group of organisms than the bacteria that can be found in the lumen or free flowing digesta (5, 36, 37). Therefore, studies analyzing bacteria found in fecal samples will result in different findings than those analyzing bacteria found in biopsy

samples. As mentioned above, there are great inter-individual differences with respect to the intestinal microbiota and the only variable that has consistently been found to be greater than this inter-individual difference is the intra-individual differences between the microbial population residing in the stool and that found residing within the mucosal layer attached to the intestinal epithelium (5).

When referring human or murine intestinal microbes, the vast majority of the population belongs to one of two phyla, either the Firmicutes or Bacteriodetes, whether samples are taken fecal samples or mucosa associated and most of the time Firmicutes outnumber the Bacteriodetes (36-38). The ratio of these two species, however, changes depending on which kind of sample is being analyzed. Using laser capture microdissection to isolate the microbial population associated with the folds found in the ascending mouse colon, Nava et al determined that this populations was 78% Firmicutes and 16% Bacteriodetes while the microbial population isolated from the luminal contents of the same mice was 56% Firmicutes and 40% Bacteriodetes (36). Interestingly, a study looking at the difference between mucosal-associated bacteria found in human biopsies from individuals with and without IBD found significantly more Firmicutes than Bacteriodetes in healthy individuals only (39).

With more and more studies highlighting differences between luminal and mucosal-associated bacteria populations, it is becoming increasingly likely that many of the beneficial functions originally attributed to the entire microbiota are actually derived specifically from mucosal-associated populations. This population remains in the gastrointestinal tract longer than the luminal

population and is more intimately associated with the host epithelium allowing it to exert disproportional effect on host (30).

Inflammatory Bowel Disease and Dysbiosis

Inflammatory bowel disease (IBD) is a chronic condition that is characterized by relapsing inflammation of the gut. IBD is a general term that can refer to either ulcerative colitis (UC) or Crohn's disease (CD) both of which have unidentified etiologies and have not been linked to an infectious agent. Patients with IBD often have persistent ulcerations in their small or large bowel mucosa. People suffering from UC have diffuse inflammation in the mucosal layer of their colons. CD can occur in any part of the gastrointestinal tract and presents as stricturing, inflammatory, or penetrating Crohn's (40). The prevalence of IBD has been reported to be as high 827 in 100,000 individuals in Europe and 568 in 100,000 in North America. While Western nations have much higher incidence and prevalence rates than developing countries, both these rates are increasing worldwide (41).

The causative agents behind IBD are unknown but genetic predispositions and environmental factors have been attributed to developing these diseases. It is also becoming increasingly apparent that the symptoms associated with IBD are caused by excessive or dysregulated immune responses to normal commensal microbes in the gut IBD. In addition, numerous studies have linked **dysbiosis** or abnormal microbiota compositions to IBD; it remains to be determined whether this alteration in the intestinal flora is the causative factor behind IBD or whether it develops as a result of the inflammation associated with IBD (42). One study

using murine models, demonstrated that intestinal inflammation, whether induced by infection, chemical treatment, or genetic predisposition led to an overgrowth of *Enterobacteriaceae* and suggests that dysbiosis is a result altered intestinal inflammation (43).

However, regardless of whether these changes are causative or not, it is clear that the microbiota is involved in the process since mice genetically predisposed to IBD do not development disease under germ free conditions. IBD is associated with a decreased abundance of diversity in the intestinal microbiota. The total amount of genes present in the microbiome in individuals suffering from IBD has been determined to be on average 25% less than healthy individuals (11). As mentioned previously, unlike healthy individuals, those with IBD do not have significantly more Firmicutes than Bacteriodetes in their mucosal-associated bacteria population (39). Analysis of the *Bacteriodes fragilis* group population size in fecal samples revealed that this population, particular species *B. vulgatus*, was significantly decreased in samples taken from individuals with IBD. Interestingly, the same study indicated that while differences in *Bacteriodes fragilis* group population size were seen between healthy controls and those with IBD, significant differences where not observed between individuals with active IBD and those in remission (44). The continued effort to identify differences between the microbial composition of healthy individuals and those with IBD will not only provide valuable incite into the causative mechanism behind IBD but could specific ways to actively reverse IBD-linked dysbiosis, and in turn ameliorate IBD symptoms.

Reactive Oxygen Species

In order to generate energy, aerobic organisms have evolved to use molecular oxygen as the final electron acceptor in their electron transport chain. While capable of producing energy effectively, the mitochondrial respiration process also generates a number of byproducts including reactive oxygen species (ROS). These ROS, including O_2-, H_2O_2, and OH-, can cause damage to the aerobic cells that produce them by nonspecifically reacting with nucleic acids, proteins, and membrane lipids leading to genetic mutations, loss or change in enzymatic activity, and change in cell membrane permeability, respectively. In addition to the ROS created my mitochondrial respiration, cells are exposed to ROS generated from external sources, including, UV light, ionizing radiation, and oxidative chemicals. Perhaps most interesting, however, is the fact that cells have also developed enzymes to generate ROS deliberately.

The most well-studied example is Phox, or the Nox of phagocytes, that is responsible for generating the super oxide during the microbicidal respiratory burst seen in phagocytes. Phox is made up of a catylatic subunit, gp91phox and regulatory subunits p22phox, p47phox, p40phox, p67phox and small GTPase RAC. Nox2 uses NADPH as an electron donor to reduce molecular oxygen to superoxide (45).

In addition to gp91phox (referred to as Nox2 hereafter), six other NADPH oxidases have been identified in humans. Beginning with the discovery of Nox1, originally named Mox1, in 1999, researchers have also identified Nox3, Nox4, Nox5, and two dual oxidases, Duox1 and Duox2 that are expressed in a variety of cell types throughout the body. Nox1, Nox3, and Nox4 are organized like Nox2.

Nox5 has an additional amino terminal calcium binding domain and the Duoxes have an additional transmembrane alpha helix that extend from the calcium binding domain found in Nox5 and attaches to an extracellular peroxidase domain (45).

The study, which initially identified Nox1, found that Nox1 mRNA was expressed highly expressed in the colon and to a much lesser extent in the prostrate and uterus (46). The same study also demonstrated that human nox1 was 86% identical to rat nox1. Further work established that Nox1 is highly expressed in the lower two-thirds of murine colon crypts and that, while Nox1 is highly expressed throughout the entire length of the human colon and rectum, it is also expressed in the jejunum, ileum, and ileocecal region albeit at much lower levels. Nox1 is present in human colon cancer samples and has the highest expression in the most differentiated tumors (47). This finding has prompted several groups to explore the proliferative effects of Nox1 expression.

Physiological production of ROS

The production of ROS via Nox enzymes is an evolutionarily ancient phenomenon and occurs in virtually all forms of multicellular life. Examples of deliberately created and beneficial ROS can have been identified in plants, sea urchins, social amoebas, nematodes, and fruit flies. Although it might initially seem paradoxical, the high reactivity of ROS allows them to be utilized as tightly controlled universal signals. The distance ROS can travel is short and these species must be generated near their intended target molecules to relay specific signals. Organisms have evolved mechanisms to enhance this specificity; the

cytosolic environment of cells contains several antioxidant enzymes and ROS generating enzymes are generally confined to a specific subcellular location. These enzymes are associated with the cytoskeleton, membrane rafts, and specific organelles where their location can be highly regulated (48). In some cases, ROS targets are further limited because the Nox enzymes are physically linked to their intended target molecules (e.g. peroxidase domain of Duox enymes).

ROS influence signal transduction pathways by oxidizing reactive cysteine residues that are often found in the active cites of common regulatory proteins. Importantly, this oxidation not only occurs rapidly but is also reversible and therefore well suited for signaling purposes (49, 50). Most cysteine residues have a pKa of about 8.5 and remain protonated at physiological levels but reactive cysteine residues are special in that their low pKa (4.7-5.4) allow them to exist as cysteine thiolate anions (Cys-S-) within the cell (50). Cysteine thiolate anions can be reversibly oxidized into cysteine sulfenic acid (Cys-SOH). Sulfenic acid can then be stabilized into disulfide bonds or be further oxidized into sulfinic acid (Cys-SO_2H) and sulfonic acid (Cys-SO_3H). This further oxidation is irreversible (Figure 2). Protein tyrosine phosphatase (PTP), the lipid phosphatase (PTEN), MAP kinase phosphatases (MAPKP), low molecular weight protein tyrosine phosphatases (LMW-PTP), and enzymes involved in sumoylation and neddylation reactions all contain redox-sensitive thiolates that can be regulated by ROS (49, 51-53).

Commensal bacteria induces ROS production

By employing the use of fluorescent dyes and cell culture monolayers, we demonstrated that commensal bacterial induce the production of ROS *in vitro* (54-56). Compared to other enteric bacteria, *Lactobacillus rhamnosus* GG elicits a particularly strong ROS induction in human intestinal cell lines (54). Similar results have been obtained *in vivo*. Oral doses of commensal bacteria lead to ROS upregulation in the murine jejunum while rectal doses will lead to ROS production in the colon (54). This effect is not limited to adults; small intestinal samples from preweaned mice gavaged with LGG also show ROS upregulation when compared to controls (55). This induction of ROS may not be entirely dependent on epithelial contact with live bacteria. For example, butyrate is a bacterial fermentation product. Cells treated with butyrate also produce ROS, however, the levels of ROS produced are less than cells treated with whole bacteria (57). As mentioned, formyl peptides are prokaryotic derived peptides that have been translationally modified with the bacterial specific amino acid N-formyl-methionine. Interestingly, the well-studied synthetic peptide N-formylmethionyl-leucyl-phenylalanine (fMLF) can also induce epithelial cell ROS production (58, 59).

While all the details of the molecular pathway leading to ROS production by intestinal Nox1 remains to be fully established, studies from our laboratory have shown that bacterial induced ROS production is dependent on FPR1 and Nox1. LGG induced ROS production is greatly diminished in FPR null mice and tissue specific Nox1 knockout mice that lack the enzyme in their intestinal epithelial cells (60, 61).

Beneficial Effects of Microbial Induced ROS

Epithelial Growth and Differentiation

As previously discussed, the microbes present in the gastrointestinal tract can influence intestinal growth and differentiation; the crypt to villus tip migration rate of epithelial cells is reduced in germ free mice (62), the intestinal epithelial renewal rate is reduced in germ free flies, and ingested pathogens will disrupt this renewal rate in flies (63). Physiological levels of ROS also play a role in cellular proliferation and differentiation in diverse organisms. For example, ROS is involved in plant root hair development (64) and promotes hematopoietic differentiation in *Drosophila* (65). Our lab has demonstrated that bacterial-induced ROS can activate the pro-proliferative MAPK ERK in intestinal epithelial cells via the oxidative inactivation of DUSP3 (58, 59) and shown that this ERK phosphorylation requires both FPR1 and Nox1. Additionally, Nox1 is plays a role in determining the fate of intestinal progenitor cells. Nox1 knockout mice have less enterocytes and more goblet cells in their intestinal epithelial layer than their wild type counterparts. Wnt and Notch1 signaling, two pathways that control the fate of intestinal progenitor cells in the murine colon, are repressed in Nox1-null animals (66). Therefore, bacterially stimulated Nox1 ROS generation has an effect on both epithelial cell differentiation and proliferation in both *in vitro* and *in vivo* models.

Inflammatory Signaling

Intestinal microbiota can modulate eukaryotic inflammatory signaling pathways including the MAPK and NF-κB pathways and, not surprisingly, this

ability is being exploited for its use in the probiotic treatment of IBD. Numerous studies have demonstrated that lactic acid bacteria are among the intestinal commensals capable of dampening inflammatory processes (67-69). One way the eukaryotic cell regulates its signaling pathways is through the process of ubiquitination; proteins that are poly-ubiquitinated are targeted to proteasomes for degradation. Commensal and pathogenic intestinal bacteria can influence the ubiquitin-proteosome pathway (70-73). The ability to influence this process allows microbes to influence the NF-κB pathway because ubiquitination plays a role in regulating it. NF-κB is activated after its inhibitor molecule, IκB, has been poly-ubiquitinated.

More specifically, commensal bacteria have been shown to interfere with *in vitro* and *in vivo* epithelial NF-κB activation by preventing SCFβ^{TrCP} (Skp1, Cdc53/Cullin, F box receptor), the IκB ubiquitin ligase, from ubiquitinated its target. SCFβ^{TrCP} is not active unless its regulatory subunit, cullin-1 (Cul-1), has been neddylated. The Ubc12 Nedd8 ligase is redox sensitive and oxidative signaling will transiently block neddylation. Studies by members of our laboratory have demonstrated that *Lactobacillus rhamnosus* GG can block NF-κB production in both primary human fetal intestinal cells and immature murine intestines by inducing cullin-1 deneddylation through production of cellular ROS (55). Considering the significant amount of data showing that the microbiota is capable of dampening the inflammatory process in the intestines and our laboratory's work that has demonstrated that LGG can accomplish this feat by inducing cellular ROS production, it likely that this ROS induced immunomodulation is general mechanism used many commensal bacteria.

Furthermore, bacterial induced prevention of $SCF\beta^{TrCP}$ neddylation quite possibly influences other aspects of mucosal homeostasis because by this enzymatic complex is involved in regulating the Wnt, Hedgehog, and Snail pathways (74).

Epithelial Cell Motility

Epithelial cell motility in the intestines is important for the normal renewal process and also plays a critical role in wound healing. When the intestinal epithelial layer is damaged cells from surrounding areas must quickly migrate to cover the wounded area in order to keep the barrier between lumen contents and the rest of the body intact. The microbiota likely influences these processes because germ-free animals have deficiencies in epithelial cell proliferation and wound healing. Epithelial cells are able to migrate through a process that involves the regulated restructuring of their actin cytoskeleton cytoskeleton. Focal adhesions (FAs), found on the edges of the extracellular matrix, rapidly assemble at the leading edge of the cell while simultaneously disassemble at the trailing edge along the cell to move in a particular direction. The assembly/disassembly process is regulated by focal adhesion kinases (FAKs). FAKs are kept in an inactive dephosphorylated state by the LMW-PTPase and SHP-2 tyrosine phosphatases. As mentioned earlier, these phosphatases are redox-sensitive and are inactivated in the presence of ROS. Cell motility is initiated in epithelial cells after growth factors and integrins induce the activation of Nox1 resulting in a local increase in ROS levels that leads to FAK phosphorylation (75). Our laboratory has demonstrated that commensal bacterial contact with intestinal epithelial cells induces rapid ROS generation in these cells

particularly at the leading edges of migrating monolayers and at the edges of wounds *in vivo*. This ROS goes on to reversibly oxidize redox-sensitive low pKa cysteines in LMW-PTP and SHP-2, which results in more FAs at the edges of migrating cells via the upregulation of FAK phosphorylation. Importantly, these events increase the healing time in both *in vitro* and *in vivo* injury models (76). Because we have demonstrated that commensal induced ROS upregulation is dependent on FPR and Nox1, our data suggests that commensal bacteria can mediate the maintenance of gut barrier and integrity.

In summary, these findings demonstrate that microbial-elicited ROS has been shown to mediate epithelial growth and differentiation, inflammatory signaling, and epithelial cell motility. Together, they demonstrate how the intestinal microbiota can influence intestinal epithelial cell homeostasis and suggest that known effects of the microbiota are at least partially mediated by ROS-dependent mechanism (Figure 3).

Lactobacilli

The genus *Lactobacilli* are facultative anerobic rod shaped Gram-positive bacteria that belong the phylum *Firmicutes*, class *Bacilli*, order *Lactobacillales,* and family *Lactobacillus* (77). Lactobacilli can be found in a wide range of niches including dairy production, the production of fermented meats and vegetables, mammalian microbiotas, sewage, and decaying plant material. Members of the genus produce lactic acid through the fermentation of carbohydrates. The wide range of niches that this genus occupies has produced considerable genetic variation among its member species and as well as produced significant intra-

species heterogenicity. There is also great intra-species various with respect to metabolomic capabilities. The ability to use a particular carbohydrate source and synthesize amino acids de novo can be better predicted by a strain's particular niche than its by its phylogenetic relationship within the genus. For example, the strains found in dairy production and the gastrointestinal tract are more likely to use lactose as a carbohydrate source and less likely to synthesize amino acids de novo than plant-derived strains belonging to the same species (77).

While the genus makes up a subdominant portion of human intestinal microbiota and many species are considered allochthonous rather than human commensals, the genus has been extensively studied as promising intestinal probiotic candidates for several reasons. First, due to their historical use in food production, lactobacilli are considered GRAS or "generally regarded as safe." Second, their ubiquitous presence throughout different anatomical sites on the human body highlights the low likelihood of their administration leading to disease. And, finally, lactobacilli possess mechanisms to interact with the intestinal mucosa, which is increasingly being recognized as the site at which commensal bacteria exert many of their beneficial effects.

Several species of lactobacilli produce surface proteins that have mucin adhesive properties. In 2002, Roos et al identified a protein on the surface of *L. reuteri* 1063 that was designated Mub due to its ability to bind mucus *in vitro*. The mannose specific adhesion (Msa) protein was identified through the genomic comparison of several *L. plantarum* strains with varying abilities to agglutinate the yeast *S. cerevisiae*; the *msa* gene was present only present in strains with

agglutination capacities. Interestingly, the Msa protein was also demonstrated to contain two Mub domains (78). *L. rhamnosus* GG (LGG) has greater persistence ability and mucus-adhesion activity than related *L. rhamnosus* LC705. As with the Msa protein, genomic comparison of these two strains led to the identification of a sortase-dependent pilus that was only present in LGG (79). This pilus, encoded by *spaCBA*, was later demonstrated to bind intestinal mucin (80) and contribute to the capacity of LGG to bind cultured intestinal epithelial cells (81). The *L. johnsonii* surface protein GroEL also binds mucin and epithelial cells (82). Interestingly, the presence of mucus binding genes in probiotic lactobacilli may be important for more than facilitating the close proximity between the bacterium and its host and increasing bacterial persistence. A study by Gross et al demonstrated that in addition to a slight competitive disadvantage with respect to persistence *L plantarum* mutants lacking msa also lost their ability to regulate host gene expression (83). In conclusion, the mucus binding genes present in some lactobacilli used as probiotics allows these strains to remain in intimate contact with the intestinal mucosa and may explain why these can exert recognizable effects on their host despite being a subdominant component of the intestinal microbiota.

Pili

Pili are long proteinaceous hair-like appendages that are present on the surface of many bacteria and their functions include DNA transfer, biofilm formation, immune evasion, adhesions to host cells, and bacterial cell movement (84). Their presence was first detected on Gram-negative bacteria by electron microscopy in the late

1940s while Gram-positive pili were first observed using immunoelectron microscopy in 1968. Unlike Gram-negative pili, which are generally formed by non-covalent homopolymerization of major pilus subunit, Gram-positive pili are formed by covalent polymerization of pili subunits in a process that involves a dedicated sortase enzyme (Figure 4). Pili genes in Gram-positive bacteria occur in clusters; the genes that encode the subunits are found near a pilin-specific sortase gene (85, 86). This clustering has facilitated their identification in commensal organism for which the genomic sequence is available. And in turn, Gram-positive pili are being increasingly recognized as important components of commensal biology.

Chapter 1 Figures

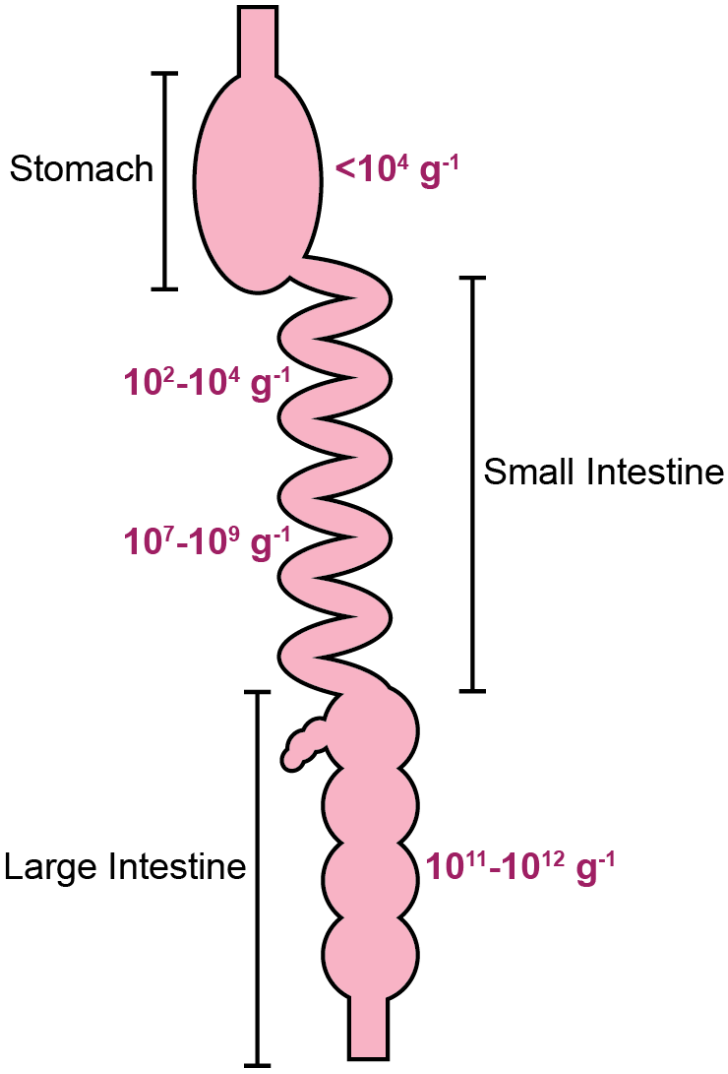

Figure 1. Current estimates of the bacterial population size within the gastrointestinal tract. Adapted from (87).

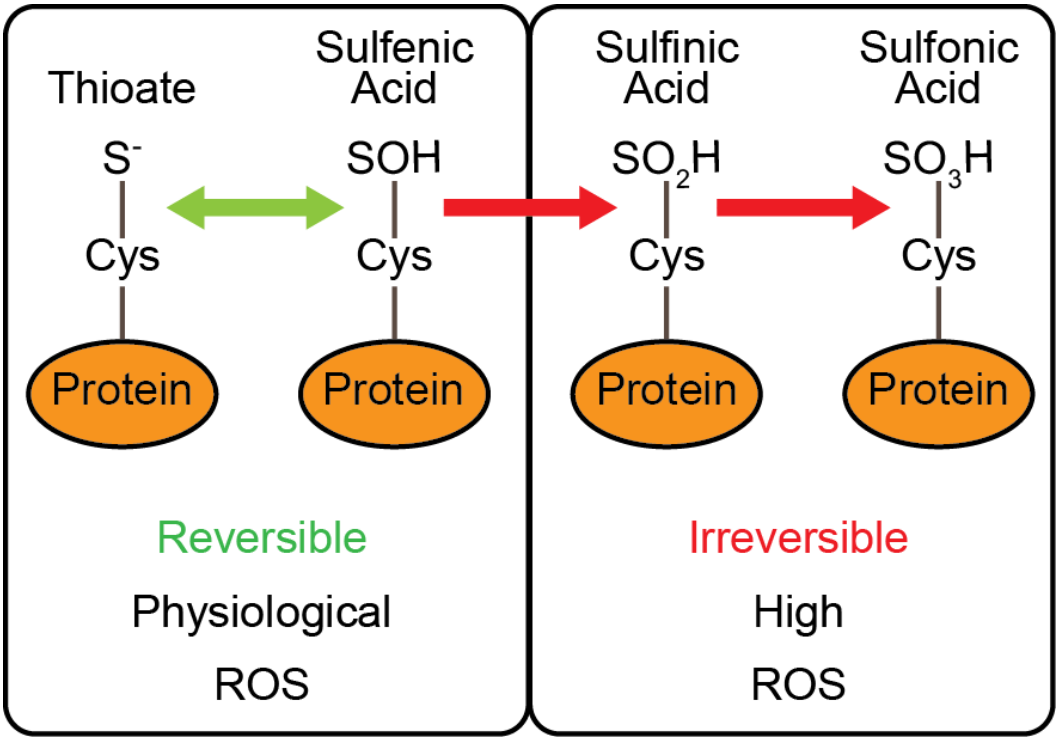

Figure 2. Modification of reactive cysteines by ROS. Physiological levels of ROS reversibly oxidize thiolate anions in reactive cysteines to produce sulfenic acid, which can be stabilized through the production of disulfide bonds. High levels of ROS can oxidize sulfenic acid into sulfinic and then sulfonic acid. This process is irreversible and has pathological effects.

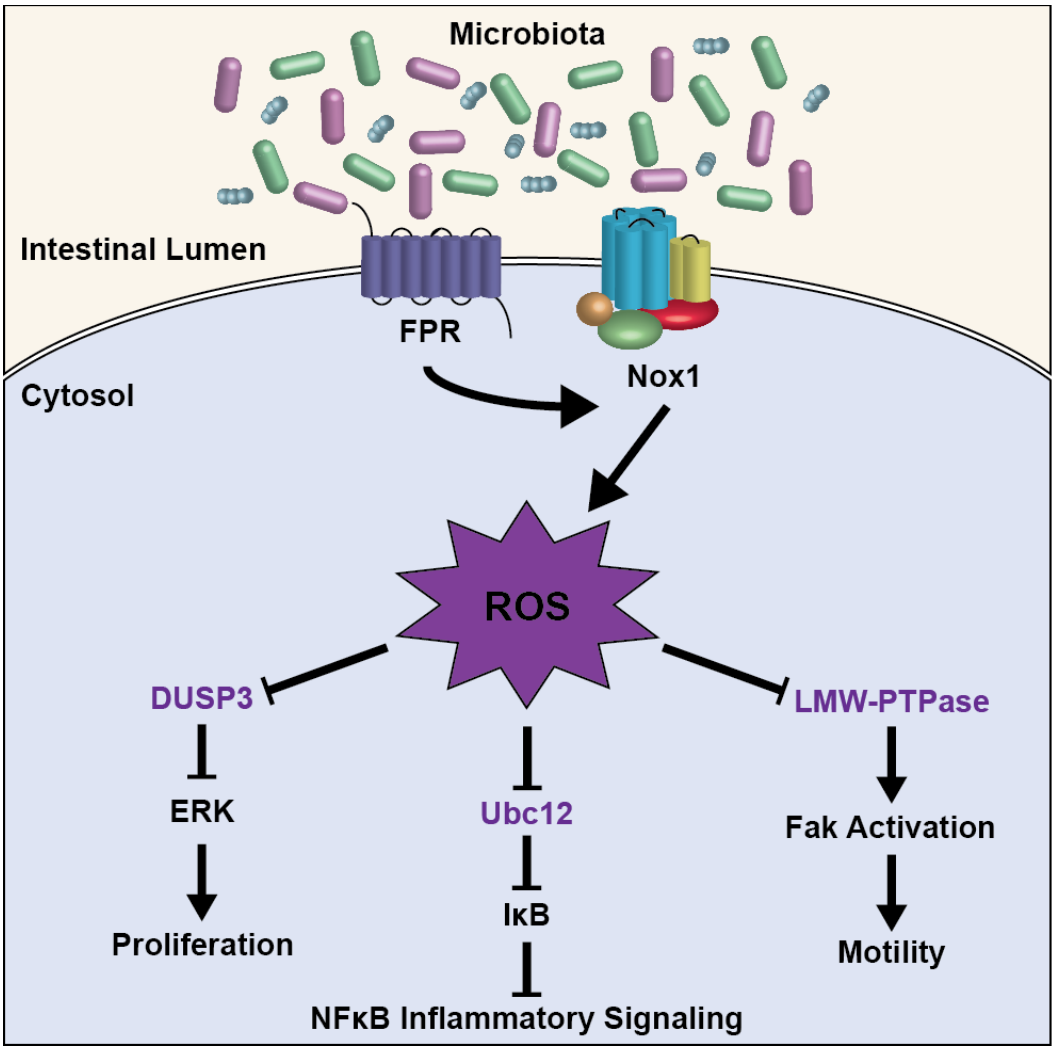

Figure 3. Microbial induced ROS influences basic cellular processes. Commensal bacteria and/or their products stimulate FPR1, which leads to the production of Nox1-generated ROS. This ROS oxidizes reactive cysteines in DUSP2, Ubc12, and LMW-PTPase, key players in the ERK MAPK, the NF-κB, and the FAK pathways, respectively, and influences basic cellular processes involved in intestinal homeostasis. Adapted from (88).

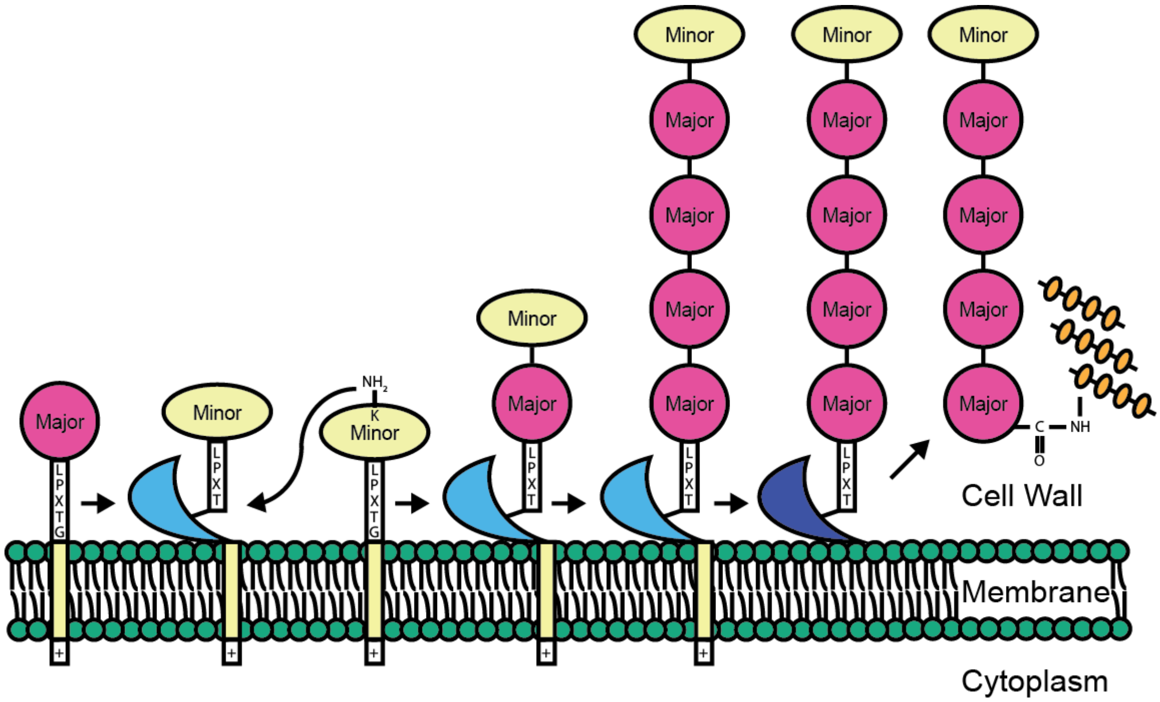

Figure 4. The assembly of Gram-positive pili. The pilin subunits are transported out of the cell via the Sec pathway but remain attached to the membrane through their C-terminal hydrophobic tails. A membrane associated pilin specific sortase (shown in light blue) recognizes LPxTG-like domains on the subunits and covalently joins the subunits together to form a functional pilus. The shaft of a functional pilus is generally comprised of major pilin subunits (shown in pink) and has one minor pilin subunit (shown in yellow) located at its tip. Once all the subunits have been polymerized, a house keeping sortase (shown in dark blue) will covalently attach the pilus to the cell wall. Depending on the bacteria, additional minor subunits may also be distributed allow the pilus shaft (not shown). Adapted from (86, 89).

Chapter 1 References

1. **Savage DC.** 1977. Microbial ecology of the gastrointestinal tract. Annu. Rev. Microbiol. **31:**107-133.
2. **Hooper LV, Gordon JI.** 2001. Commensal host-bacterial relationships in the gut. Science **292:**1115-1118.
3. **Neish AS.** 2009. Microbes in gastrointestinal health and disease. Gastroenterology **136:**65-80.
4. **Grice EA, Segre JA.** 2011. The skin microbiome. Nature reviews. Microbiology **9:**244-253.
5. **Eckburg PB, Bik EM, Bernstein CN, Purdom E, Dethlefsen L, Sargent M, Gill SR, Nelson KE, Relman DA.** 2005. Diversity of the human intestinal microbial flora. Science **308:**1635-1638.
6. **Dewhirst FE, Chen T, Izard J, Paster BJ, Tanner AC, Yu WH, Lakshmanan A, Wade WG.** 2010. The human oral microbiome. J. Bacteriol. **192:**5002-5017.
7. **Ravel J, Gajer P, Abdo Z, Schneider GM, Koenig SS, McCulle SL, Karlebach S, Gorle R, Russell J, Tacket CO, Brotman RM, Davis CC, Ault K, Peralta L, Forney LJ.** 2011. Vaginal microbiome of reproductive-age women. Proc. Natl. Acad. Sci. U. S. A. **108 Suppl 1:**4680-4687.
8. **Baron S.** 1996. Medical microbiology, 4th ed. University of Texas Medical Branch at Galveston, Galveston, Tex.
9. **Gill SR, Pop M, Deboy RT, Eckburg PB, Turnbaugh PJ, Samuel BS, Gordon JI, Relman DA, Fraser-Liggett CM, Nelson KE.** 2006.

Metagenomic analysis of the human distal gut microbiome. Science **312:**1355-1359.

10. **Backhed F, Ley RE, Sonnenburg JL, Peterson DA, Gordon JI.** 2005. Host-bacterial mutualism in the human intestine. Science **307:**1915-1920.

11. **Qin J, Li R, Raes J, Arumugam M, Burgdorf KS, Manichanh C, Nielsen T, Pons N, Levenez F, Yamada T, Mende DR, Li J, Xu J, Li S, Li D, Cao J, Wang B, Liang H, Zheng H, Xie Y, Tap J, Lepage P, Bertalan M, Batto JM, Hansen T, Le Paslier D, Linneberg A, Nielsen HB, Pelletier E, Renault P, Sicheritz-Ponten T, Turner K, Zhu H, Yu C, Li S, Jian M, Zhou Y, Li Y, Zhang X, Li S, Qin N, Yang H, Wang J, Brunak S, Dore J, Guarner F, Kristiansen K, Pedersen O, Parkhill J, Weissenbach J, Meta HITC, Bork P, Ehrlich SD, Wang J.** 2010. A human gut microbial gene catalogue established by metagenomic sequencing. Nature **464:**59-65.

12. **Dethlefsen L, McFall-Ngai M, Relman DA.** 2007. An ecological and evolutionary perspective on human-microbe mutualism and disease. Nature **449:**811-818.

13. **Arumugam M, Raes J, Pelletier E, Le Paslier D, Yamada T, Mende DR, Fernandes GR, Tap J, Bruls T, Batto JM, Bertalan M, Borruel N, Casellas F, Fernandez L, Gautier L, Hansen T, Hattori M, Hayashi T, Kleerebezem M, Kurokawa K, Leclerc M, Levenez F, Manichanh C, Nielsen HB, Nielsen T, Pons N,**

Poulain J, Qin J, Sicheritz-Ponten T, Tims S, Torrents D, Ugarte E, Zoetendal EG, Wang J, Guarner F, Pedersen O, de Vos WM, Brunak S, Dore J, Meta HITC, Antolin M, Artiguenave F, Blottiere HM, Almeida M, Brechot C, Cara C, Chervaux C, Cultrone A, Delorme C, Denariaz G, Dervyn R, Foerstner KU, Friss C, van de Guchte M, Guedon E, Haimet F, Huber W, van Hylckama-Vlieg J, Jamet A, Juste C, Kaci G, Knol J, Lakhdari O, Layec S, Le Roux K, Maguin E, Merieux A, Melo Minardi R, M'Rini C, Muller J, Oozeer R, Parkhill J, Renault P, Rescigno M, Sanchez N, Sunagawa S, Torrejon A, Turner K, Vandemeulebrouck G, Varela E, Winogradsky Y, Zeller G, Weissenbach J, Ehrlich SD, Bork P. 2011. Enterotypes of the human gut microbiome. Nature **473:**174-180.

14. **Wu GD, Chen J, Hoffmann C, Bittinger K, Chen YY, Keilbaugh SA, Bewtra M, Knights D, Walters WA, Knight R, Sinha R, Gilroy E, Gupta K, Baldassano R, Nessel L, Li H, Bushman FD, Lewis JD.** 2011. Linking long-term dietary patterns with gut microbial enterotypes. Science **334:**105-108.

15. **Jeffery IB, Claesson MJ, O'Toole PW, Shanahan F.** 2012. Categorization of the gut microbiota: enterotypes or gradients? Nature reviews. Microbiology **10:**591-592.

16. **Bjerknes M, Cheng H.** 2006. Intestinal epithelial stem cells and progenitors. Methods Enzymol. **419:**337-383.

17. **Rajilic-Stojanovic M.** 2013. Function of the microbiota. Best Pract. Res. Clin. Gastroenterol. **27:**5-16.

18. **Barker N.** 2014. Adult intestinal stem cells: critical drivers of epithelial homeostasis and regeneration. Nat. Rev. Mol. Cell Biol. **15:**19-33.

19. **Ismail AS, Hooper LV.** 2005. Epithelial cells and their neighbors. IV. Bacterial contributions to intestinal epithelial barrier integrity. Am. J. Physiol. Gastrointest. Liver Physiol. **289:**G779-784.

20. **Rakoff-Nahoum S, Paglino J, Eslami-Varzaneh F, Edberg S, Medzhitov R.** 2004. Recognition of commensal microflora by toll-like receptors is required for intestinal homeostasis. Cell **118:**229-241.

21. **Gewirtz AT, Navas TA, Lyons S, Godowski PJ, Madara JL.** 2001. Cutting edge: bacterial flagellin activates basolaterally expressed TLR5 to induce epithelial proinflammatory gene expression. J. Immunol. **167:**1882-1885.

22. **Hornef MW, Frisan T, Vandewalle A, Normark S, Richter-Dahlfors A.** 2002. Toll-like receptor 4 resides in the Golgi apparatus and colocalizes with internalized lipopolysaccharide in intestinal epithelial cells. J. Exp. Med. **195:**559-570.

23. **Schiffmann E, Corcoran BA, Wahl SM.** 1975. N-formylmethionyl peptides as chemoattractants for leucocytes. Proc. Natl. Acad. Sci. U. S. A. **72:**1059-1062.

24. **Williams LT, Snyderman R, Pike MC, Lefkowitz RJ.** 1977. Specific receptor sites for chemotactic peptides on human polymorphonuclear leukocytes. Proc. Natl. Acad. Sci. U. S. A. **74:**1204-1208.

25. **Migeotte I, Communi D, Parmentier M.** 2006. Formyl peptide receptors: a promiscuous subfamily of G protein-coupled receptors controlling immune responses. Cytokine Growth Factor Rev. **17:**501-519.

26. **Babbin BA, Jesaitis AJ, Ivanov AI, Kelly D, Laukoetter M, Nava P, Parkos CA, Nusrat A.** 2007. Formyl peptide receptor-1 activation enhances intestinal epithelial cell restitution through phosphatidylinositol 3-kinase-dependent activation of Rac1 and Cdc42. J. Immunol. **179:**8112-8121.

27. **Atuma C, Strugala V, Allen A, Holm L.** 2001. The adherent gastrointestinal mucus gel layer: thickness and physical state in vivo. Am. J. Physiol. Gastrointest. Liver Physiol. **280:**G922-929.

28. **Johansson ME, Phillipson M, Petersson J, Velcich A, Holm L, Hansson GC.** 2008. The inner of the two Muc2 mucin-dependent mucus layers in colon is devoid of bacteria. Proc. Natl. Acad. Sci. U. S. A. **105:**15064-15069.

29. **Johansson ME, Larsson JM, Hansson GC.** 2011. The two mucus layers of colon are organized by the MUC2 mucin, whereas the outer layer is a legislator of host-microbial interactions. Proc. Natl. Acad. Sci. U. S. A. **108 Suppl 1:**4659-4665.

30. **Ouwerkerk JP, de Vos WM, Belzer C.** 2013. Glycobiome: bacteria and mucus at the epithelial interface. Best Pract. Res. Clin. Gastroenterol. **27:**25-38.

31. **Van der Sluis M, De Koning BA, De Bruijn AC, Velcich A, Meijerink JP, Van Goudoever JB, Buller HA, Dekker J, Van**

Seuningen I, Renes IB, Einerhand AW. 2006. Muc2-deficient mice spontaneously develop colitis, indicating that MUC2 is critical for colonic protection. Gastroenterology **131:**117-129.

32. **Smith K, McCoy KD, Macpherson AJ.** 2007. Use of axenic animals in studying the adaptation of mammals to their commensal intestinal microbiota. Semin. Immunol. **19:**59-69.
33. **Sommer F, Backhed F.** 2013. The gut microbiota--masters of host development and physiology. Nature reviews. Microbiology **11:**227-238.
34. **Stappenbeck TS, Hooper LV, Gordon JI.** 2002. Developmental regulation of intestinal angiogenesis by indigenous microbes via Paneth cells. Proc. Natl. Acad. Sci. U. S. A. **99:**15451-15455.
35. **Collins J, Borojevic R, Verdu EF, Huizinga JD, Ratcliffe EM.** 2014. Intestinal microbiota influence the early postnatal development of the enteric nervous system. Neurogastroenterol. Motil. **26:**98-107.
36. **Nava GM, Friedrichsen HJ, Stappenbeck TS.** 2011. Spatial organization of intestinal microbiota in the mouse ascending colon. The ISME journal **5:**627-638.
37. **Hong PY, Croix JA, Greenberg E, Gaskins HR, Mackie RI.** 2011. Pyrosequencing-based analysis of the mucosal microbiota in healthy individuals reveals ubiquitous bacterial groups and micro-heterogeneity. PLoS One **6:**e25042.
38. **Shen XJ, Rawls JF, Randall T, Burcal L, Mpande CN, Jenkins N, Jovov B, Abdo Z, Sandler RS, Keku TO.** 2010. Molecular

characterization of mucosal adherent bacteria and associations with colorectal adenomas. Gut microbes **1:**138-147.

39. **Walker AW, Sanderson JD, Churcher C, Parkes GC, Hudspith BN, Rayment N, Brostoff J, Parkhill J, Dougan G, Petrovska L.** 2011. High-throughput clone library analysis of the mucosa-associated microbiota reveals dysbiosis and differences between inflamed and non-inflamed regions of the intestine in inflammatory bowel disease. BMC Microbiol. **11:**7.

40. **Manichanh C, Borruel N, Casellas F, Guarner F.** 2012. The gut microbiota in IBD. Nature reviews. Gastroenterology & hepatology **9:**599-608.

41. **Molodecky NA, Soon IS, Rabi DM, Ghali WA, Ferris M, Chernoff G, Benchimol EI, Panaccione R, Ghosh S, Barkema HW, Kaplan GG.** 2012. Increasing incidence and prevalence of the inflammatory bowel diseases with time, based on systematic review. Gastroenterology **142:**46-54 e42; quiz e30.

42. **Sartor RB.** 2008. Microbial influences in inflammatory bowel diseases. Gastroenterology **134:**577-594.

43. **Lupp C, Robertson ML, Wickham ME, Sekirov I, Champion OL, Gaynor EC, Finlay BB.** 2007. Host-mediated inflammation disrupts the intestinal microbiota and promotes the overgrowth of Enterobacteriaceae. Cell host & microbe **2:**119-129.

44. **Takaishi H, Matsuki T, Nakazawa A, Takada T, Kado S, Asahara T, Kamada N, Sakuraba A, Yajima T, Higuchi H, Inoue N, Ogata**

H, Iwao Y, Nomoto K, Tanaka R, Hibi T. 2008. Imbalance in intestinal microflora constitution could be involved in the pathogenesis of inflammatory bowel disease. Int. J. Med. Microbiol. **298:**463-472.

45. **Lambeth JD.** 2004. NOX enzymes and the biology of reactive oxygen. Nat. Rev. Immunol. **4:**181-189.

46. **Suh YA, Arnold RS, Lassegue B, Shi J, Xu X, Sorescu D, Chung AB, Griendling KK, Lambeth JD.** 1999. Cell transformation by the superoxide-generating oxidase Mox1. Nature **401:**79-82.

47. **Geiszt M, Lekstrom K, Brenner S, Hewitt SM, Dana R, Malech HL, Leto TL.** 2003. NAD(P)H oxidase 1, a product of differentiated colon epithelial cells, can partially replace glycoprotein 91phox in the regulated production of superoxide by phagocytes. J. Immunol. **171:**299-306.

48. **Terada LS.** 2006. Specificity in reactive oxidant signaling: think globally, act locally. J. Cell Biol. **174:**615-623.

49. **Barford D.** 2004. The role of cysteine residues as redox-sensitive regulatory switches. Curr. Opin. Struct. Biol. **14:**679-686.

50. **Rhee SG, Kang SW, Jeong W, Chang TS, Yang KS, Woo HA.** 2005. Intracellular messenger function of hydrogen peroxide and its regulation by peroxiredoxins. Curr. Opin. Cell Biol. **17:**183-189.

51. **Chiarugi P, Buricchi F.** 2007. Protein tyrosine phosphorylation and reversible oxidation: two cross-talking posttranslation modifications. Antioxidants & redox signaling **9:**1-24.

52. **Le NT, Corsetti JP, Dehoff-Sparks JL, Sparks CE, Fujiwara K, Abe J.** 2012. Reactive Oxygen Species, SUMOylation, and Endothelial Inflammation. International journal of inflammation **2012:**678190.

53. **Luo Z, Pan Y, Jeong LS, Liu J, Jia L.** 2012. Inactivation of the Cullin (CUL)-RING E3 ligase by the NEDD8-activating enzyme inhibitor MLN4924 triggers protective autophagy in cancer cells. Autophagy **8:**1677-1679.

54. **Kumar A, Wu H, Collier-Hyams LS, Hansen JM, Li T, Yamoah K, Pan ZQ, Jones DP, Neish AS.** 2007. Commensal bacteria modulate cullin-dependent signaling via generation of reactive oxygen species. EMBO J. **26:**4457-4466.

55. **Lin PW, Myers LE, Ray L, Song SC, Nasr TR, Berardinelli AJ, Kundu K, Murthy N, Hansen JM, Neish AS.** 2009. Lactobacillus rhamnosus blocks inflammatory signaling in vivo via reactive oxygen species generation. Free Radic. Biol. Med. **47:**1205-1211.

56. **Wentworth CC, Alam A, Jones RM, Nusrat A, Neish AS.** Enteric commensal bacteria induce extracellular signal-regulated kinase pathway signaling via formyl peptide receptor-dependent redox modulation of dual specific phosphatase 3. J Biol Chem **286:**38448-38455.

57. **Kumar A, Wu H, Collier-Hyams LS, Kwon YM, Hanson JM, Neish AS.** 2009. The bacterial fermentation product butyrate influences epithelial signaling via reactive oxygen species-mediated changes in cullin-1 neddylation. J. Immunol. **182:**538-546.

58. **Wentworth CC, Alam A, Jones RM, Nusrat A, Neish AS.** 2011. Enteric commensal bacteria induce extracellular signal-regulated kinase pathway signaling via formyl peptide receptor-dependent redox modulation of dual specific phosphatase 3. J. Biol. Chem. **286:**38448-38455.

59. **Wentworth CC, Jones RM, Kwon YM, Nusrat A, Neish AS.** 2010. Commensal-epithelial signaling mediated via formyl peptide receptors. Am. J. Pathol. **177:**2782-2790.

60. **Alam A, Leoni G, Wentworth CC, Kwal JM, Wu H, Ardita CS, Swanson PA, Lambeth JD, Jones RM, Nusrat A, Neish AS.** 2013. Redox signaling regulates commensal-mediated mucosal homeostasis and restitution and requires formyl peptide receptor 1. Mucosal Immunol.

61. **Jones RM, Luo L, Ardita CS, Richardson AN, Kwon YM, Mercante JW, Alam A, Gates CL, Wu H, Swanson PA, Lambeth JD, Denning PW, Neish AS.** 2013. Symbiotic lactobacilli stimulate gut epithelial proliferation via Nox-mediated generation of reactive oxygen species. EMBO J.

62. **Savage DC, Siegel JE, Snellen JE, Whitt DD.** 1981. Transit time of epithelial cells in the small intestines of germfree mice and ex-germfree mice associated with indigenous microorganisms. Appl. Environ. Microbiol. **42:**996-1001.

63. **Buchon N, Broderick NA, Chakrabarti S, Lemaitre B.** 2009. Invasive and indigenous microbiota impact intestinal stem cell activity through multiple pathways in Drosophila. Genes Dev. **23:**2333-2344.

64. **Tsukagoshi H, Busch W, Benfey PN.** 2010. Transcriptional regulation of ROS controls transition from proliferation to differentiation in the root. Cell **143:**606-616.

65. **Owusu-Ansah E, Banerjee U.** 2009. Reactive oxygen species prime Drosophila haematopoietic progenitors for differentiation. Nature **461:**537-541.

66. **Coant N, Ben Mkaddem S, Pedruzzi E, Guichard C, Treton X, Ducroc R, Freund JN, Cazals-Hatem D, Bouhnik Y, Woerther PL, Skurnik D, Grodet A, Fay M, Biard D, Lesuffleur T, Deffert C, Moreau R, Groyer A, Krause KH, Daniel F, Ogier-Denis E.** 2010. NADPH oxidase 1 modulates WNT and NOTCH1 signaling to control the fate of proliferative progenitor cells in the colon. Mol. Cell. Biol. **30:**2636-2650.

67. **Pena JA, Versalovic J.** 2003. Lactobacillus rhamnosus GG decreases TNF-alpha production in lipopolysaccharide-activated murine macrophages by a contact-independent mechanism. Cell. Microbiol. **5:**277-285.

68. **Menard S, Candalh C, Bambou JC, Terpend K, Cerf-Bensussan N, Heyman M.** 2004. Lactic acid bacteria secrete metabolites retaining anti-inflammatory properties after intestinal transport. Gut **53:**821-828.

69. **Kelly D, Campbell JI, King TP, Grant G, Jansson EA, Coutts AG, Pettersson S, Conway S.** 2004. Commensal anaerobic gut bacteria attenuate inflammation by regulating nuclear-cytoplasmic shuttling of PPAR-gamma and RelA. Nat. Immunol. **5:**104-112.

70. **Neish AS, Gewirtz AT, Zeng H, Young AN, Hobert ME, Karmali V, Rao AS, Madara JL.** 2000. Prokaryotic regulation of epithelial responses by inhibition of IkappaB-alpha ubiquitination. Science **289:**1560-1563.

71. **Petrof EO, Claud EC, Sun J, Abramova T, Guo Y, Waypa TS, He SM, Nakagawa Y, Chang EB.** 2009. Bacteria-free solution derived from Lactobacillus plantarum inhibits multiple NF-kappaB pathways and inhibits proteasome function. Inflamm. Bowel Dis. **15:**1537-1547.

72. **Petrof EO, Kojima K, Ropeleski MJ, Musch MW, Tao Y, De Simone C, Chang EB.** 2004. Probiotics inhibit nuclear factor-kappaB and induce heat shock proteins in colonic epithelial cells through proteasome inhibition. Gastroenterology **127:**1474-1487.

73. **Iyer C, Kosters A, Sethi G, Kunnumakkara AB, Aggarwal BB, Versalovic J.** 2008. Probiotic Lactobacillus reuteri promotes TNF-induced apoptosis in human myeloid leukemia-derived cells by modulation of NF-kappaB and MAPK signalling. Cell. Microbiol. **10:**1442-1452.

74. **Zhou BP, Hung MC.** 2005. Wnt, hedgehog and snail: sister pathways that control by GSK-3beta and beta-Trcp in the regulation of metastasis. Cell cycle **4:**772-776.

75. **Chiarugi P, Pani G, Giannoni E, Taddei L, Colavitti R, Raugei G, Symons M, Borrello S, Galeotti T, Ramponi G.** 2003. Reactive oxygen species as essential mediators of cell adhesion: the oxidative

inhibition of a FAK tyrosine phosphatase is required for cell adhesion. J. Cell Biol. **161:**933-944.

76. **Swanson PA, 2nd, Kumar A, Samarin S, Vijay-Kumar M, Kundu K, Murthy N, Hansen J, Nusrat A, Neish AS.** 2011. Enteric commensal bacteria potentiate epithelial restitution via reactive oxygen species-mediated inactivation of focal adhesion kinase phosphatases. Proc. Natl. Acad. Sci. U. S. A. **108:**8803-8808.

77. **O'Callaghan J, O'Toole PW.** 2013. Lactobacillus: host-microbe relationships. Curr. Top. Microbiol. Immunol. **358:**119-154.

78. **Pretzer G, Snel J, Molenaar D, Wiersma A, Bron PA, Lambert J, de Vos WM, van der Meer R, Smits MA, Kleerebezem M.** 2005. Biodiversity-based identification and functional characterization of the mannose-specific adhesin of Lactobacillus plantarum. J. Bacteriol. **187:**6128-6136.

79. **Kankainen M, Paulin L, Tynkkynen S, von Ossowski I, Reunanen J, Partanen P, Satokari R, Vesterlund S, Hendrickx AP, Lebeer S, De Keersmaecker SC, Vanderleyden J, Hamalainen T, Laukkanen S, Salovuori N, Ritari J, Alatalo E, Korpela R, Mattila-Sandholm T, Lassig A, Hatakka K, Kinnunen KT, Karjalainen H, Saxelin M, Laakso K, Surakka A, Palva A, Salusjarvi T, Auvinen P, de Vos WM.** 2009. Comparative genomic analysis of Lactobacillus rhamnosus GG reveals pili containing a human-mucus binding protein. Proc. Natl. Acad. Sci. U. S. A. **106:**17193-17198.

80. **von Ossowski I, Reunanen J, Satokari R, Vesterlund S, Kankainen M, Huhtinen H, Tynkkynen S, Salminen S, de Vos WM, Palva A.** 2010. Mucosal adhesion properties of the probiotic Lactobacillus rhamnosus GG SpaCBA and SpaFED pilin subunits. Appl. Environ. Microbiol. **76:**2049-2057.

81. **Lebeer S, Claes I, Tytgat HL, Verhoeven TL, Marien E, von Ossowski I, Reunanen J, Palva A, Vos WM, Keersmaecker SC, Vanderleyden J.** 2012. Functional analysis of Lactobacillus rhamnosus GG pili in relation to adhesion and immunomodulatory interactions with intestinal epithelial cells. Appl. Environ. Microbiol. **78:**185-193.

82. **Bergonzelli GE, Granato D, Pridmore RD, Marvin-Guy LF, Donnicola D, Corthesy-Theulaz IE.** 2006. GroEL of Lactobacillus johnsonii La1 (NCC 533) is cell surface associated: potential role in interactions with the host and the gastric pathogen Helicobacter pylori. Infect. Immun. **74:**425-434.

83. **Gross G, van der Meulen J, Snel J, van der Meer R, Kleerebezem M, Niewold TA, Hulst MM, Smits MA.** 2008. Mannose-specific interaction of Lactobacillus plantarum with porcine jejunal epithelium. FEMS Immunol. Med. Microbiol. **54:**215-223.

84. **Proft T, Baker EN.** 2009. Pili in Gram-negative and Gram-positive bacteria - structure, assembly and their role in disease. Cell. Mol. Life Sci. **66:**613-635.

85. **Danne C, Dramsi S.** 2012. Pili of gram-positive bacteria: roles in host colonization. Res. Microbiol. **163:**645-658.

86. **Scott JR, Zahner D.** 2006. Pili with strong attachments: Gram-positive bacteria do it differently. Mol. Microbiol. **62:**320-330.

87. **Kleerebezem M, Vaughan EE.** 2009. Probiotic and gut lactobacilli and bifidobacteria: molecular approaches to study diversity and activity. Annual review of microbiology **63:**269-290.

88. **Jones RM, Mercante JW, Neish AS.** 2012. Reactive oxygen production induced by the gut microbiota: pharmacotherapeutic implications. Curr. Med. Chem. **19:**1519-1529.

89. **Marraffini LA, Dedent AC, Schneewind O.** 2006. Sortases and the art of anchoring proteins to the envelopes of gram-positive bacteria. Microbiol. Mol. Biol. Rev. **70:**192-221.

Chapter 2 Symbiotic lactobacilli stimulate gut epithelial proliferation via Nox-mediated generation of reactive oxygen species

Rheinallt M. Jones,[a] Liping Luo,[a] Courtney S. Ardita,[a] Arena N. Richardson,[b] Young Man Kwon,[a] Jeffrey W. Mercante,[a] Ashfaqual Alam,[a] Cymone L. Gates,[a] Huixai Wu,[a] Phillip A. Swanson,[a] J. David Lambeth,[a] Patricia W. Denning,[b] Andrew S. Neish [a]

Epithelial Pathobiology Unit, Department of Pathology and Laboratory Medicine, Emory University School of Medicine, Atlanta, Georgia, USA[a]

Department of Pediatrics, Emory University School of Medicine, Atlanta, Georgia, USA[b]

Chapter 2 Abstract

The resident prokaryotic microbiota of the metazoan gut elicits profound effects on the growth and development of the intestine. However, the molecular mechanisms of symbiotic prokaryotic–eukaryotic cross-talk in the gut are largely unknown. It is increasingly recognized that physiologically generated reactive oxygen species (ROS) function as signaling secondary messengers that influence cellular proliferation and differentiation in a variety of biological systems. Here, we report that commensal bacteria, particularly members of the genus *Lactobacillus*, can stimulate NADPH oxidase 1 (Nox1)-dependent ROS generation and consequent cellular proliferation in intestinal stem cells upon initial ingestion into the murine or Drosophila intestine. Our data identify and highlight a highly conserved mechanism that symbiotic microorganisms utilize in eukaryotic growth and development. Additionally, the work suggests that specific redoxmediated functions may be assigned to specific bacterial taxa and may contribute to the identification of microbes with probiotic potential.

Chapter 2 Introduction

It is becoming increasingly evident that an optimal metazoan gut microbiota serves beneficial functions for the host that includes energy extraction, stimulation of immune development, and competitive exclusion of pathogenic microorganisms (1). In addition, experiments in germ-free animals have demonstrated a physiological role for the microbiota in regulation of epithelial homeostasis, as well as host immunity and metabolism (2, 3). Consistently, abnormalities (‘dysbiosis’) in the intestinal microbiota may be sufficient to

provoke intestinal inflammation as seen in inflammatory bowel disease (IBD), and quantitative and/or qualitative abnormalities of the microbiota have been associated with other allergic, metabolic, systemic immune, and infectious disorders (4). Indeed, therapeutic administration of exogenous viable bacteria, termed probiotics, has also been reported to dampen inflammation, improve barrier function, and promote intestinal reparative responses in response to inflammatory and developmental disorders of the intestinal tract (5).

Eukaryotes have evolved dedicated perception and signaling systems for monitoring potential pathogens, and necessarily, their own symbiotic microbiota. These pathways allow for recognition of microbes via pattern recognition receptors (PRRs) and activation of signal transduction cascades such as the MAPK and NF-**k**B pathways. While generally considered pro-inflammatory, basal low level PRR signalling has been implicated in normal homeostatic maintenance in the gut (6). Additionally, our research group has reported that the microbiota in the intestinal lumen modulates host redox biochemistry to limit proinflammatory signaling and activate reparative responses (7-11). Thus, there is increasing evidence that the gut microbiota is perceived by the host, and influences a wide range of physiological processes. However, little is known of how the microbiota mechanistically influences gut biology. Moreover, delineation of the molecular mechanisms that underlies host and microbe interactions would be instrumental in understanding this important symbiotic relationship, its role in heath and disease, and therapeutic the exploitation of beneficial bacteria.

The gut epithelium of both mammals and invertebrates is a highly adapted tissue that has evolved for both digestive and absorptive functions as well as

providing a vital mechanical and immunological barrier against gut luminal contents. The epithelia of both are a two-dimensional, single cell sheet of enterocytes interspersed with pluripotent stem cell niches that serve as sources of cellular renewal (12-14). In mammals, the stem cell compartment is at the base of the three-dimensional epithelial invaginations forming the crypt niche. The daughter progeny of mammalian stem cells further proliferate and migrate luminally defining the adjacent transient amplifying compartment prior to terminal differentiation into absorptive, mucus secreting, and neuroendocrine epithelial cells. It is estimated that the dynamic renewal of murine epithelia occurs within 4–5 days (14). In Drosophila, the epithelial cells of the larval fly gut are initially supplied by dispersed single intestinal stem cells (ISCs) that proliferate into a multicellular niche over the course of larval life. The stem cells and progeny represent adult midgut precursors (AMPs) that serve as the primordial of the adult intestinal epithelium that forms during pupal metamorphosis. The adult Drosophila midgut comprises an enterocyte monolayer interspersed with hormone-producing enteroendocrine cells. The adult midgut enterocytes are continuously replenished by ISCs that adjoin the intestinal basement membrane (12, 13). Together, these systems form an attractive and genetically tractable target system for the study of gut stem cell dynamics and the role of environmental influences in this process (15).

Reactive oxygen species (ROS) are short-lived molecules derived from incomplete reduction of oxygen metabolites that at high levels have a microbicidal function in professional phagocytes. However, a lower ‘physiological’ level of ROS is increasingly recognized in the mediation of

intracellular signaling events in a wide variety of cell types (16). Importantly, ROS are induced in response to bacteria in virtually all forms of multicellular life ranging from plants and social amoebae to humans, thus representing a primordial form of microbial perception and control (17, 18)(Ha et al, 2005b; Kotchoni et al, 2006). Significantly, ROS are also increasingly recognized as mediators of cellular proliferation and differentiation in disparate biological systems such as plant root hair development (19), and *Drosophila* haematopoiesis (20). Recently, we reported that some species of human gut bacteria can induce rapid, physiological generation of ROS that has potent regulatory effects on host immune function, intracellular signaling, and cytoskeletal dynamics (7-10). Cellular ROS are often produced *via* the catalytic action of NADPH oxidases. The archetypal member of this family, Nox2, was first identified in neutrophils, and was shown to play an important role in phagocyte microbicidal ROS generation in response to bacteria (oxidant burst). Subsequently, paralogues of Nox2 were identified in non-phagocytic tissues, including Nox1 and Duox2, which are strongly expressed in colonic intestinal epithelia of both flies and mice (21-23).

Herein, we show that the commensal *Lactobacillus* spp. are potent inducers of endogenous ROS generation, and of ROS-dependent cellular proliferation within intestines of two metazoan models, namely the fruitfly *Drosophila melanogaster* and the mouse. In addition, we show that *Lactobacillus*-induced ROS generation and cell proliferation is dependent on a functional Nox1 enzyme in intestinal epithelial cells. ROS production was absent in germ-free animals and was associated with suppressed epithelial growth.

Together, these data indicate that bacteria-induced activation of an ROS generating enzyme in enterocytes influences cellular proliferation.

Chapter 2 Materials and Methods

Isolation Of Bacterial Strains From The *Drosophila* Intestine. *w1118* third-instar larvae propagated on conventional *Drosophila* media were dissected and the gut homogenized in a 1.5-ml microcentrifuge tube in sterile PBS using a sterile plastic pestle. Serial dilutions of the homogenate were plated on three separate solid media: brain heart infusion (BD, Sparks, MD), tryptic soy (BD, Sparks, MD), and de-Man-Rogosa-Sharpe (BD, Sparks, MD) under both aerobic and anaerobic conditions. Anaerobiosis was achieved using a sealed chamber together with the Gas-Pak EZ system (BD, Sparks, MD). After incubation at 30°C for 24–48 h, individual, morphologically distinct colonies were inoculated into the corresponding liquid media and grown at 30°C for 24 h with or without aeration.

Purification of bacterial genomic DNA, 16S PCR and Dna sequencing, and quantitative PCR. Genomic DNA was purified from each bacterial isolate using the QIAamp DNA Stool Mini Kit (Qiagen, Valencia, CA). Short segments of 16S rDNA were amplified from each isolate by PCR using a combination of forward (16S63F, 5′-CAGGCCTAACACATGCAAGTC-3′; 16S338FV3, 5′-ACTCCTACGGGAGGCAGCAG-3′) and reverse (6S1387R, 5′-GGGCGGWGTGTACAAGGC-3′; 16S518RV3, 5′-ATTACCGCGGCTGCTGG-3′) primers. Amplified 16S rDNA products were purified using the Qiaquick PCR

Purification Kit (Qiagen), and sequence analysis was performed at SeqWright DNA Technology Service (Houston, TX). The following bacterial strains were identified in the *Drosophila* gut: *Bacillus cereus; Achromobacter xylosoxidans; Lactobacillus plantarum; Achromobacter piechaudii; Stenotrophomonas maltophilia; Staphylococcus capitis; Acetobacter pomorum* (Supplementary Table S1). To determine the extent to which RNAi (IR) constructs obtained from the Vienna Drosophila RNAi Center (VDRC) silenced *nox* and *duox* expression, respectively, we dissected five adult *Drosophila* intestines and immerse them directly in TRIzol before RNA extraction. For each *Drosophila* line examined, RNA from three independent replicates (each containing five intestines) was extracted. Transcript levels were measured for each replicate in duplicate by qRT-PCR. *nox* transcript levels were amplified using primers Nox-RT-F 5′-ggctatctcctgcaagatcg-3′, and Nox-RT-R 5′-ccaactcaatcaggcggtat-3′, and *duox* transcripts amplified using primers Duox-RT-F, 5′-tggccaacgagatagtgatg-3′, and Duox-RT-R 5′-aaactgccatcaatccaagc-3′. *nox* and *duox* transcript levels were normalized against *rp49* transcript levels measured using Rp49-F, 5′-tacaggcccaagatcgtgaa-3′ and Rp49-R, 5′-tctccttgcgcttcttgga-3′.

Fly culture and strains. Flies were maintained on standard media. The *gstD-gfp* reporter line was a gift from Dirk Bohmann (Sykiotis and Bohmann, 2008). *MyoIA-GAL4* was a gift from Shigeo Takashima (24), and Vienna Drosophila RNAi Center (VDRC) stocks 4913 (d*nox*IR) and stock 2593 (d*duox*IR) were used for depleting levels of NADPH oxidases in the midgut.

Detection of ROS generation and cell proliferation in the germ-

free or colonized first and third instar *Drosophila* larvae. *Drosophila* embryos were collected and transferred to a cell strainer. Under a sterile hood, embryos were washed three times with sterile PBS, soaked in 50% bleach for 5 min, before washing again with sterile PBS. The mesh of the cell strainer was cut with a sterile blade, and transferred into a sterile Perti dish containing sterilize *Drosophila* food, and incubated for 24 h at 25°C. Then, first-instar larvae were transferred into another Petri dish containing 2 ml liquefied sterile *Drosophila* food containing a total of 1×10^6 cfu pure bacterial culture, and a final concentration of 100 μM of hydro-Cy3 ROS-sensitive reagent. After 30 min, the intestinal tract of first-instar larvae were dissected, fixed in 4% paraformaldehyde, and fluorescence detected by confocal microscopy. The procedure was similar for the detection of ROS generation in the intestine of third-instar larvae, save that embryos were incubated at 25°C for 4 days before transfer into liquefied *Drosophila* food. To determine that the first-instar larvae ingested similar numbers of bacterial monoculture, larval intestines were dissected into 1 ml sterile PBS, and cfu calculated by the plate count method. We detected 5.5×10^4 cfu *L. plantarum* per first-instar larval intestine (s.d.=2×10^4, n=5), 1.04×10^4 cfu *B. cereus* per intestine (s.d.=7.8×10^3, n=5), 1.16×10^4 cfu *S. capitis* per intestine (s.d.=3.4×10^3, n=5), 6.8×10^4 cfu *E. coli* per intestine (s.d.=1.51×10^4, n=5) 9.96×10^3 cfu *A. piechaudii* per intestine (s.d.=2.8×10^3, n=5), 3.3×10^4 cfu *A. xylosoxidans* per intestine (s.d.=1.1×10^4, n=5), and 6.2×10^4 cfu *S. maltophilia* per intestine (s.d.=1.6×10^4, n=5), respectively. For the detection of cellular proliferation in the intestine of third-instar larvae, EdU

(final concentration of 0.4 mM) was added to liquefied sterile food (germ free) or to liquefied food containing 1×10^6 cfu pure bacterial culture. Larvae were incubated in the milieu for 4 h, the intestines dissected and EdU incorporation determined according to the manufacturer's protocol (Roche Diagnostics GmbH, Germany).

Detection of ROS generation in cultured cells and murine models. ROS generation was measured using the Hydro-Cy3 ROS sensitive dye (25). Briefly, cultured Caco-2 cells were grown to confluence on a 96-well plate. Then, 100 μM Hydro-Cy3 was added to the culture media (DMEM with 0.4% serum) incubated at 37°C and 5% CO2. After 1 h, media containing the Hydro-Cy3 dye was removed by washing with KRH (Krebs–Ringer–Hepes) buffer, before contacting cells with a total of 5×10^8 cfu bacteria suspended in KRH buffer. Fluorescence was measured using a fluorescence microplate reader (SpectraMax M2; Molecular Devices, Sunnyvale, CA, USA) after various time intervals with excitation at 544 nm and emission at 574 nm for Hydro-Cy3. For qualitative detection of ROS, cultured Caco-2 cells were grown to confluency in 8-well chamber slides, treated as described above, before detection of fluorescence by Confocal microscopy at 40 × objective. In some experiments, cells were incubated in the presence of 5 mM TEMPOL before bacterial contact. For the detection of ROS generation in the 6-week-old murine distal small intestine of 6-week-old mice, mice were fasted for 16 h before IP administration of 100 μl of 40 mM Hydro Cy-3 for 15 min. Then, 200 μl of 1×10^{10} cfu/ml of bacteria, or buffer control was fed to mice by oral gavage. After 1 h ingestion of

bacteria, mice were sacrificed and tissues of the distal intestine sliced to small pieces, before visualization by confocal microscopy. All ROS fluorescence experiments repeated at least three times. The procedures for 2-day-old mice were identical to those for 6-week-old mice, save for no fasting period, 25 µl of 40 mM Hydro Cy-3 administered by IP for 15 min, and 100 µl of 1×10^9 cfu of bacteria fed by oral gavage and ingested for 30 min before sacrifice. For the detection of cell proliferation in murine tissues, 6-week-old mice were fed 200 µl of 5×10^9 cfu of bacteria for 2 h, and 2-day-old mice, were fed 100 µl of 1×10^9 cfu/ml of bacteria for 1 h before sacrifice.

Detection of EdU-positive cells and phospho-histone H3-positive cells in the murine model. Proliferating cells in the intestine were identified by detecting EdU-positive or phospho-histone H3-positive cells. For EdU analysis, mice were fed the 1×10^9 cfu of the indicated bacteria by oral gavage for 3 h. Then, mice were administered EdU by IP at a rate of 100 µg EdU per gram of mouse weight. Following a further 2 h, mice were euthanized and the intestinal epithelium was assessed for EdU-positive cells under confocal microscopy. For p-Histone H3 analysis, mice were fed 1×10^9 cfu of the indicated bacteria by oral gavage for 5 h. Frozen sections of the intestinal tissue were immunostained using the anti-phospho-histone H3 antibody (Cell Signaling, Danvers, MA), followed by (3,3′-diaminobenzidine) DAB detection. Numbers of p-Histone H3-positive cells were assessed by light microscopy. At least three mice were included in each experimental point, and 40 field views at × 20 magnification of each intestinal preparation were numerated for both EdU and p-

histone H3-positive cells.

Chapter 2 Results

Colonization of the *Drosophila* midgut by *Lactobacillus plantarum* induces cellular ROS generation. We previously demonstrated that contact with the human commensal (and commonly used probiotic) *Lactobacillus rhamnosus* GG with cultured epithelial cells induces the endogeneous generation of cellular ROS (10). Here, we assessed the ability of diverse strains of bacteria to elicit this response in viable *Drosophila* gut epithelia. To undertake these analyses, and as an improvement on previous techniques that used ROS detection dyes that were prone to auto-oxidation or photobleaching, we employed a new class of hydrocyanine dyes (hereafter referred to as hydro-Cy3) that exhibit far greater specificity and stability, enabling detection of ROS generation in tissue compartments *in vivo* (25). Whereas the mammalian gut microbiota includes several hundred distinct species of bacteria, the *Drosophila* gut microbiota is markedly less complex (26). We isolated and cultured six distinct bacteria (three Gram negative and three Gram positive) from the luminal content of adult *Drosophila* (Supplementary Table S1). Pure cultures of the isolated bacteria were mixed with sterile media, and germ-free *Drosophila* embryos introduced into the vial. Thus, emerged first-instar larvae gnotobiotically ingested sterile media supplemented with pure cultures of the respective bacteria. Culture-based quantification revealed that each first-instar larvae typically ingested a total of about 10^3–10^4 CFUs (see Materials and

Methods). Fluorescent imaging revealed that gnotobiotic ingestion of *L. plantarum* potently induced the rapid generation of ROS in midgut enterocytes within 30 min, as detected by the oxidation of the hydro-Cy3 dye, and activation of the ROS-responsive *gstD1-gfp* reporter element (Sykiotis and Bohmann, 2008) (Figure 1). Ingestion of pure cultures of other members of the microbiota, particularly Gram-negative bacteria, elicited nearly undetectable levels of cellular ROS generation (Figure 1), and no ROS generation was detected when emerged germ-free larvae consumed sterilized food (Figure 1), although minor fragments of auto-fluorescent particles were visible. In addition to first-instar larvae, *L. plantarum* ingestion by germ-free third-instar larvae also induced the generation of cellular ROS, and ROS-responsive genetic elements within 30 min of feeding (Figures 2A and B). Importantly, ingestion of *B. cereus* isolated from the *Drosophila* gut, or the *Drosophila* pathogen *Erwinia carotovora,* did not induce ROS generation at up to 4 h post ingestion (Figures 2C and D). These results were recapitulated in adult *Drosophila* where ingestion of *L. plantarum* but not *E. carotovora* (detected in the figure by GFP activity) induced ROS generation after 4 h (Figure 2E).

As stated in the introduction, bacterial-induced ROS generation occurs in phagocytes *via* the enzymatic activity of the Nox2 NADPH oxidase. Indeed, it is well established that NADPH oxidases function in the anti-microbial response in mammalian phagocytes, and in epithelial cells of the *Drosophila* gut (27, 28). However, the function of ROS generated in response to colonization with commensal bacteria is not understood. We thus examined the extent to which the

dNox or dDuox (the sole NADPH oxidases in *Drosophila*) function in *L. plantarum*-induced ROS generation within enterocytes. We expressed RNAi constructs against dNox and dDuox under the enterocyte-specific *myoIA*-GAL4 driver fly (29). We confirm that the stock used significantly reduced the expression of d*nox* and d*duox* respectively compared to w1118 or *gal4*IR control flies (Supplementary Figure S1). Our analyses show that depletion in the levels of dNox but not dDuox markedly dampened induced ROS generation following the *L. plantarum* ingestion (Figure 2F and G). We conclude that initial ingestion of *L. plantarum* induces the rapid generation of ROS by a dNox-dependent mechanism.

***Lactobacillus* induces ROS-Dependent cellular proliferation in the *Drosophila* intestine.** The *Drosophila* larvae midgut enterocytes are large polyploid cells that form the interface with the gut luminal contents. The stem cells are interspersed between enterocytes, and the stem cells expand over the larval life to form proliferative stem cell niches. These niches harbor adult midgut progenitors (AMPs), from which the adult intestinal epithelium is derived during pupal metamorphosis (15), whereas the adult midgut enterocytes are continuously replenished by pluripotent ISCs (12, 13). We assessed the number of proliferative niche cells in the midguts of conventionally raised and germ-free *Drosophila* larvae. Germ-free third-instar larvae had significantly fewer numbers of EdU-positive cells in the midgut stem cell niches, compared to conventionally raised larvae (Figure 3A and B), as well as fewer GFP-positive cells in germ-free *esg*-GAL4 UAS-*gfp*, a genetic marker of midgut niche stem cells and their

progeny (12), compared to isogenic conventionally raised flies (Supplementary Figure S2). Strikingly, colonization of germ-free third instar *Drosophila* larvae with *L. plantarum* for 2 h significantly increased the number of proliferating niche cells in the midgut (Figure 3A and B). As stated in Introduction, ROS have been shown to function in cell proliferation within diverse tissues (19, 20). We corroborate these reports by showing that supplementing the *N*-acetylcysteine (NAC) (a glutathione precursor and direct antioxidant) into the fly media for 12 h before bacterial ingestion significantly decreased *L. plantarum*-induced cell proliferation (Figure 3A and B). We also detected similar responses in adult *Drosophila*. Germ-free adult *Drosophila* had significantly fewer EdU-positive ISCs and progeny than conventionally raised flies (Figure 3C and D). Similar to the response in larvae, *L. plantarum* ingestion for 12 h resulted in a significant increase in the number of EdU-positive ISCs and their progeny in the adult midgut while *E. carotovora* ingestion did not (Figure 3C and D).

As shown in Figure 2, the NADPH oxidase, dNox is required for *L. plantarum*-induced ROS generation in enterocytes. Here, we show that depletion of dNox, but not dDuox levels also significantly reduced the numbers of proliferating cells in conventionally raised larval midgut (Supplementary Figure S3), and in the 5-day-old adult midgut (Figure 3E and F). Consequentially, examination of the DNA counter stain in Figure 3E indicated changes in midgut histological architecture, and we detected significantly shorter lifespan in *Drosophila* expressing enterocyte-specific d*nox*IR compared to control flies (Supplementary Figure S4). Examination of the adult midgut at 10, 20, and 30

days following the eclosure reveals only few detectable EdU-positive cells and marked observable changes in midgut histological architecture (Supplementary Figure S5). Similarly, using a GFP marker for enterocyte cells (30), markedly altered enterocyte histological architecture was detected in d*nox*IR compared to control flies (Supplementary Figure S6). Intriguingly, we also examined the influence of diminishing dNox levels in midgut ISCs using the ISC-specific *escargot*-GAL4 driver fly. We detected less influence on the numbers of EdU-positive cells in the midgut, although subtle changes in cell arrangement were seen (Supplementary Figure S7), suggesting that dNox-mediated pro-proliferative ROS production occurs predominantly in enterocytes. Together, these observations demonstrate that *Lactobacillus*-induced ROS generation promotes cell proliferation in the *Drosophila* intestine, by a mechanism dependent on dNox activity in enterocytes.

Contact of lactobacilli with cultured mammalian cells induces ROS generation. To determine whether the specific influence of ROS-inducing lactobacilli is conserved in mammalian systems, we assessed the ability of diverse strains of mammalian commensal bacteria to elicit this response in cultured Caco-2 cells. Cells were grown to confluency and pre-loaded with hydro-Cy3 for 30 min, before contact with 1×10^8 cfu of the candidate bacteria. Consistent with previous experiments, lactobacilli rapidly induced the generation of cellular ROS within minutes of contact (Figure 4A and B). Other *Lactobacillus* species tested, including *L. acidophilus* or *L. casei*, as well as the Gram-positive intestinal bacteria *Bifidobacteria bifidum and Lactococcus lactis* also induced the

generation of cellular ROS, albeit to a lower extent than *L. rhamnosus* (Figure 4A and B). Importantly, *L. rhamnosus*-induced ROS generation was abolished in the presence of the superoxide dismutase (SOD) mimetic TEMPOL (Figure 4B). In contrast, *Bacteroides thetaiotaomicron*, a well-known enteric Gram-negative anaerobic microbe, as well as Gram-negative *Escherichia coli* or the mammalian pathogen *Salmonella typhimurium* could not induce cellular ROS generation. In addition, contact of cultured cells with the luminal contents isolated from conventionally raised mice also induced the generation of cellular ROS, whereas similar fecal preparations from germ-free mice could not (Figure 4C). These data confirm the conserved ability of members of the lactobacilli to induce the epithelial ROS generation across distant metazoan phyla.

Ingestion of *Lactobacillus* induces Nox1-dependent generation of cellular ROS in murine enterocytes. To examine the extent to which bacterially stimulated and Nox1-mediated ROS generation following the ingestion of lactobacilli can be detected *in vivo* in the murine model, we assessed the effects of feeding *L. rhamnosus* GG in 6-week-old and 2-day-old wild-type mice, and in intestinal epithelial cell-specific Nox1-deficient (B6.Nox1ΔIEC) animals. We recently described the generation of B6.Nox1ΔIEC mice and the intestinal epithelial expression pattern of Nox1 (31). In addition, previous publications have reported strong expression of *nox1* in colonic tissue (32, 33). We confirm these findings, and also detect Nox1 activity in the distal small intestine (Supplementary Figure S8). To assess ROS generation, wild-type and B6.Nox1ΔIEC littermates were administered hydro-Cy3 by IP injection 30 min

before oral gavage feeding with preparations of 1×10^9 cfu *L. rhamnosus* or *E. coli*. Preliminary experiments indicated the bacterial gavage contents reached the colon within 1 h. Examination of colonic tissues at 1 h post feeding revealed that *L. rhamnosus*, but not *E. coli* ingestion resulted in the generation of ROS within colonic and small intestine epithelial cells in 6-week-old mice (Figure 5A and B), and in 2-day-old mice (Supplementary Figure S9) by a Nox1-dependent mechanism. Furthermore, feeding germ-free 6-week-old mice *L. rhamnosus* potently induced ROS generation in the enterocytes of the small intestine (Supplementary Figure S10). Finally, pretreatment of murine subjects with the anti-oxidant NAC administered by IP at 1 h before oral gavage of *L. rhamnosus* GG completely abolished detectable ROS in the small intestine (Supplementary Figure S11). These data show that ingestion of *L. rhamnosus* GG results in the potent induction of Nox1-dependent ROS generation in enterocytes of the distal small intestine and the colon.

Ingestion of *Lactobacillus* induces Nox1-dependent cell proliferation in the murine gut epithelium. As stated previously, endogeneous and presumably enzymatic generation of ROS in cells have been implicated in the control of cellular proliferation in other biological systems (19, 20). We thus examined the extent to which *L. rhamnosus*-induced, and Nox1-dependent ROS generation influenced cellular proliferation in the murine intestine. Our experiments show that 6-week-old mice fed *L. rhamnosus* GG had significantly elevated levels of proliferating cells in the colon compared to controls at 5 h following the bacterial ingestion, as measured by the number of

phospho-Histone H3- and EdU-positive cells (Figure 6A and B; Supplementary Figure S12), consistent with previous reports (34). Importantly, we confirm that *L. rhamnosus* GG-induced cell proliferation in the colon is Nox1 dependent at 6 weeks and 2 days old (Figure 6A and B; Supplementary Figure S12). In addition, these data were recapitulated in the small intestines of or 6-week-old mice fed *L. rhamnosus* GG, again in a Nox1-dependent manner (Figure 6C and D), and upon initial colonization of 2-day-old mice (Supplementary Figure S13). Together, these data support the conclusion that *L. rhamnosus* is a potent inducer of Nox1-dependent ROS generation in enterocytes, and of ROS-dependent cellular proliferation in gut tissues (Supplementary Figure S14).

Chapter 2 Discussion

A growing body of evidence indicates that the gut microbiota beneficially affects intestinal homeostasis and, by extension, systemic organismal health. However, relatively little is known of how the host perceives non-pathogenic bacteria, or how the microbiota mechanistically influences gut biology. Here, we describe a highly conserved response (the generation of endogenous cellular ROS *via* the action of NADPH oxidases) of host intestinal cells upon perception of bacteria that likely forms a fundamental component of the host–microbiota interaction.

Besides being by-products of metabolism, or active antimicrobial molecules, data are emerging that certain ROS species, especially non-radical forms such as H_2O_2, function as essential signaling molecules (16). This notion became relevant with our recent discovery demonstrating that commensal gut

bacteria induced rapid, generation of physiological levels of ROS from an unknown source within mammalian epithelial cells that had regulator effects (7, 9, 10). Cellular redox signaling requires 'sensor' proteins, which are generally regulatory enzymes whose activity can be modulated by ROS (35, 36). These redox-sensitive proteins are modified by reversible H_2O_2-mediated oxidation of their active site cysteines, thus allowing for graded perception of intracellular H_2O_2 concentrations and control of critical steps in signal transduction pathways. As we and others have shown, such redox-sensitive thiolates are present in a limited but increasingly recognized subset of enzymes, including tyrosine phosphatases, MAP kinase phosphatases (MAPK-P or DUSPs) and regulatory enzymes of ubiquitin and ubiquitin-like proteins such as SUMO and Nedd8 (35). However, to date, little was known about the extent to which ROS modulates proteins that function to control cellular proliferation in the mammalian or insect intestine. Here, we propose a new paradigm where ROS generation stimulated by an exogenous source—the gut microbiota—elicits the enzymatic generation of epithelial ROS, and subsequent modulatory effects on epithelial proliferation (Supplementary Figure S14). Identifying ROS-sensitive proteins that control cell proliferation and/or differentiation in the stem cell microenvironment will yield further insights into the molecular mechanisms that mediate symbiotic bacterial-induced promotion of epithelial homeostasis.

We show that candidate bacterial strains induce variable levels of ROS generation in contacted cells. *Lactobacilli* were found to be especially potent inducers of ROS generation in cultured cells and *in vivo*. On the basis of 16S

ribosomal RNA sequencing, the candidate lactobacilli tested, *L. rhamnosus*, *L. acidophilus* and *L. casei* on mammalian cells, and *L. plantarum* in flies have been grouped into disparate phylogenic clades (37). Despite the divergence, each lactobacilli tested have seemingly evolved the ability to induce cellular ROS generation within its adapted host. Members of the *Lactobacillus* genus are well-known members of the human microbiota, and are prominently represented as candidate probiotic agents. These biological effects were highlighted in a recent report where *Lactobacillus* sp. stimulated intestinal epithelial growth (34). Lactobacilli have been utilized in fermented food products for centuries. Their ability to catabolize milk, utilized by yogurt and cheese makers, may have also been exploited during evolution by the gut of neonatal mammals, which may explain the development of lactobacilli-mediated beneficial effects on mammals. Likewise, the role of lactobacilli in fruit spoilage may be relevant to the ability of *Drosophila* to use these organisms as a signal for growth. This notion is consistent with the recent reported that *L. plantarum* stably colonizes the *Drosophila* gut, is transmitted vertically, and promotes *Drosophila* systemic growth by modulating hormonal signals through TOR-dependent nutrient sensing (38). This study concluded that the *Drosophila* microbiota sustains optimal larval development and that mono-ingestion of *L. plantarum* is sufficient to recapitulate the effects of the normal microbiota. Our investigations describe another role for *L. plantarum* in local epithelial development, that is, the stimulation of Nox-dependent epithelial ROS generation and the ROS-dependent promotion of gut proliferation under homeostatic conditions. In addition to ROS

generation, we also detect activation of the Nrf2 pathway-responsive and ROS-sensitive anti-oxidant response element (ARE) (Figure 2E, lower panels). The Nrf2 pathway induces the upregulation of a battery of anti-oxidative genes that counterbalance ROS levels in the cytoplasm (39). Thus, ROS generation following the long-term colonization with lactobacilli is likely to be spatially and temporally variable, where ROS levels (and cell proliferation) are dynamically modulated. These events are the focus of current investigations within our research group.

We also identify the enzymatic basis of bacterial-induced ROS generation. Recently, Nox family members have been identified in many non-phagocytic cell types, with Nox1 and Duox2 strongly expressed in intestinal epithelia (22). Importantly, Nox1 has been shown to be important for migration of cultured colonic epithelial cells (40), suggesting direct effects on intestinal epithelial related processes, including proliferation and/or migration. In this study, we confirm this function by showing that Nox1 is required for bacterial-induced intestinal cell proliferation in mice and *Drosophila*. In addition, depletion of Nox in *Drosophila* enterocytes reduced lifespan, although decreased viability was only detected following 30 days (Supplementary Figure S4). Depletion of dNox also resulted in markedly altered enterocyte histological architecture, with the degree of altered architecture correlating with age (Supplementary Figures S5 and S6). These observations strongly implicate dNox as functioning in a critical role during midgut development and/or homeostasis, consistent with previous reports (41). Further examination of signalling events in the ISC microenvironments where dNox levels are depleted will yield critical insights into

the exact mechanisms by which dNox generated ROS controls and modulates pro-proliferative and differentiation events in the gut.

Orthologues of the Nox family mediate ROS generation throughout multicellular life, including *Drosophila* (27)(Ha et al, 2005a). Interestingly, in the fly, ROS generation occurs in the epithelia, and is necessary for control of the luminal flora. In this case, the dDuox enzyme was shown to be responsible for antimicrobial ROS generation in response to pathogenic infection (17, 42)(Ha et al, 2005b; Chakrabarti et al, 2012). Furthermore, it was reported that the *Drosophila* intestine responds to *E. carotovora* infection and tissue damage by inducing ISC proliferation, through a mechanism regulated by the Imd and JAK-STAT pathways following 16 h infection (43). Importantly, in our studies, *E. carotovora* did not induce detectable ROS generation using the hydro-Cy3 dye at the much shorter time points we examined, and moreover, we show that cell proliferation is also induced by a dNox-dependent response to symbiotic bacteria in conditions and time scale that do not involve tissue injury. It is important to contrast our results to recent studies that report the generation of HOCl in the gut following 2 h ingestion of *E. carotovora* by a Duox-dependent mechanism (44). HOCl generation is formed from hydrogen peroxide and chlorine by the enzyme myeloperoxide (MPO). In addition, the R19S dye used by Lee et al (44) is sensitive only to HOCl (45), whereas the hydro-Cy3 dye used in our studies is sensitive to a broad range of ROS (25). Thus, these data support the conclusion that Nox-catalysed ROS generation in response to lactobacilli modulates homeostatic cell signalling in the gut, whereas Duox and MPO-catalysed

generation of HOCl is a response to pathogens.

In the mammalian gut, epithelial ROS generated in response to bacteria serves a signaling role and likely there are numerous ROS-sensitive enzymes that could be influenced by changes in cellular redox status. As has been discussed, reversible oxidative inactivation of a wide range of regulatory enzymes is an increasingly recognized mechanism of signal transduction (36). Delineating ROS-dependent outcomes on multiple cell signaling pathways *in vivo* will be the challenging future work. Alternatively (but not contradictorily), a role of bacterial-elicited ROS stimulating an epithelial antimicrobial response (as occurs in phagocytes and the *Drosophila* gut), especially in limited locations such as the intestinal crypt, is still to be resolved. Taken together, we suggest that ROS generation for signaling and microbicidal functions in the gut epithelia may represent the primordial ancestral response to bacteria, and that Nox1-dependent ROS generation in epithelial cells plays an important role in critical ROS-mediated intestinal homeostatic processes.

Chapter 2 Tables

Experimental ID	Propagation media	Strain Identity by 16s	Gram stain
FC1, BHI-M	BHI, Aerobic	*Bacillus cereus* SJ1	Positive
FC2, BHI-N	BHI, Aerobic	*Achromobacter xylosoxidans* C54	Negative
FC4, TSA-K	TSA, Aerobic	*Lactobacillus plantarum* subsp. Plantarum strain ATCC 14917	Positive
FC5, TSA-I	TSA, Aerobic	*Achromobacter piechaudii*	Negative
FC6, TSA-H	TSA, Aerobic	*Stenotrophomonas maltophilia*	Negative
FC7, TSA-L	TSA, Aerobic	*Staphylococcus capitis*	Positive
FC14, MRS-Q	MRS Anaerobic	*Lactobacillus plantarum* subsp. Plantarum strain ATCC 14917	Positive

Table S1. List of bacteria isolated from the midgut contents of 5-day-old adult *w1118* Drosophila.

Chapter 2 Figures

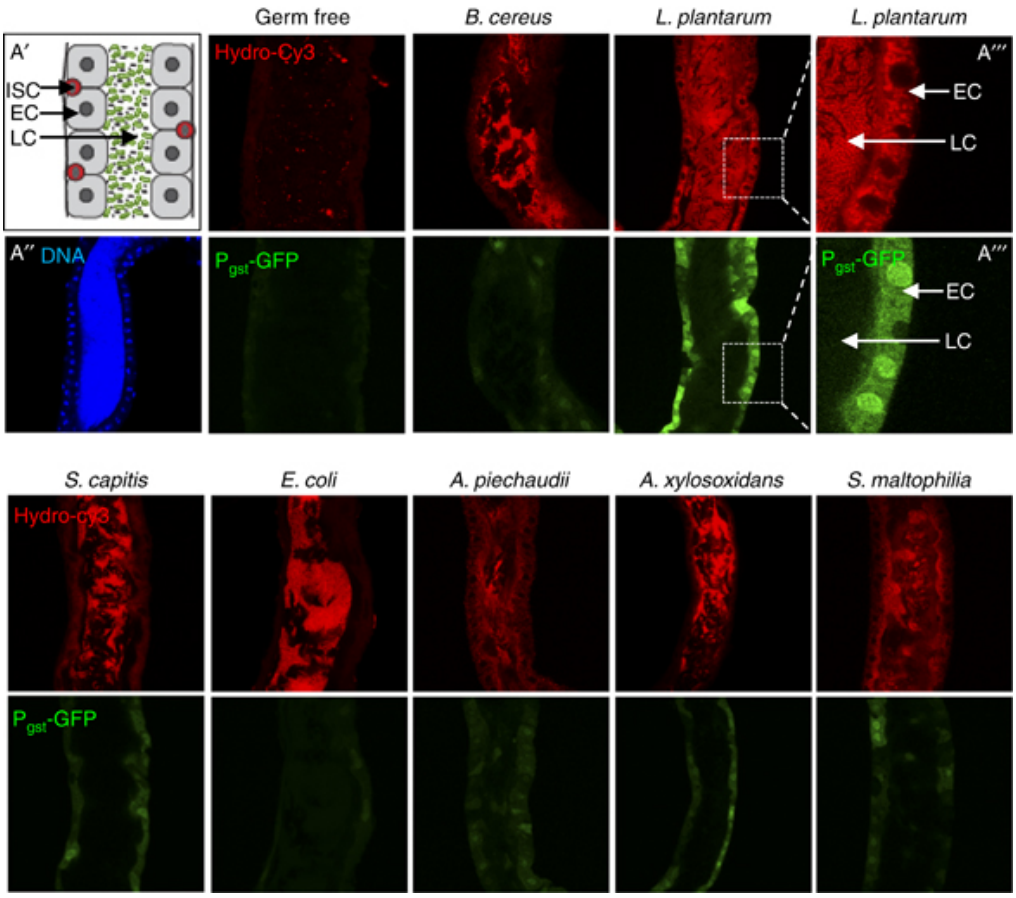

Figure 1. Ingestion of *Lactobacillus plantarum* by first-instar *Drosophila* larvae induces cellular ROS generation. Detection of ROS generation following the ingestion of indicated bacteria by germ-free newly emerged *gstD1-gfp* first-instar larvae for 30 min with the indicated Gram-positive or Gram-negative bacteria isolated from *Drosophila* midguts (Supplementary Table S1). Germ-free *gstD1-gfp* embryos were placed in a vial containing sterilized *Drosophila* growth media inoculated with 1×10^8 cfu of the indicated bacteria. ROS were detected by oxidation of the hydrocyanin ROS-sensitive dye (upper panels), that is present in

the larval food. Larvae used also harbour an ROS inducible *gstD1-gfp* reporter gene (green lower panels). (**A′**) Cartoon of first-instar midgut. Enterocyte (EC), intestinal stem cell (ISC), luminal contents (LCs). (**A″**) Tissue orientation control by staining of first-instar midgut stained for DNA. (**A‴**) Exploded view of the interface between the ECs and the LC in larvae fed *L. plantarum*. Numbers of bacteria ingested by larva were quantified and results are presented in Materials and methods.

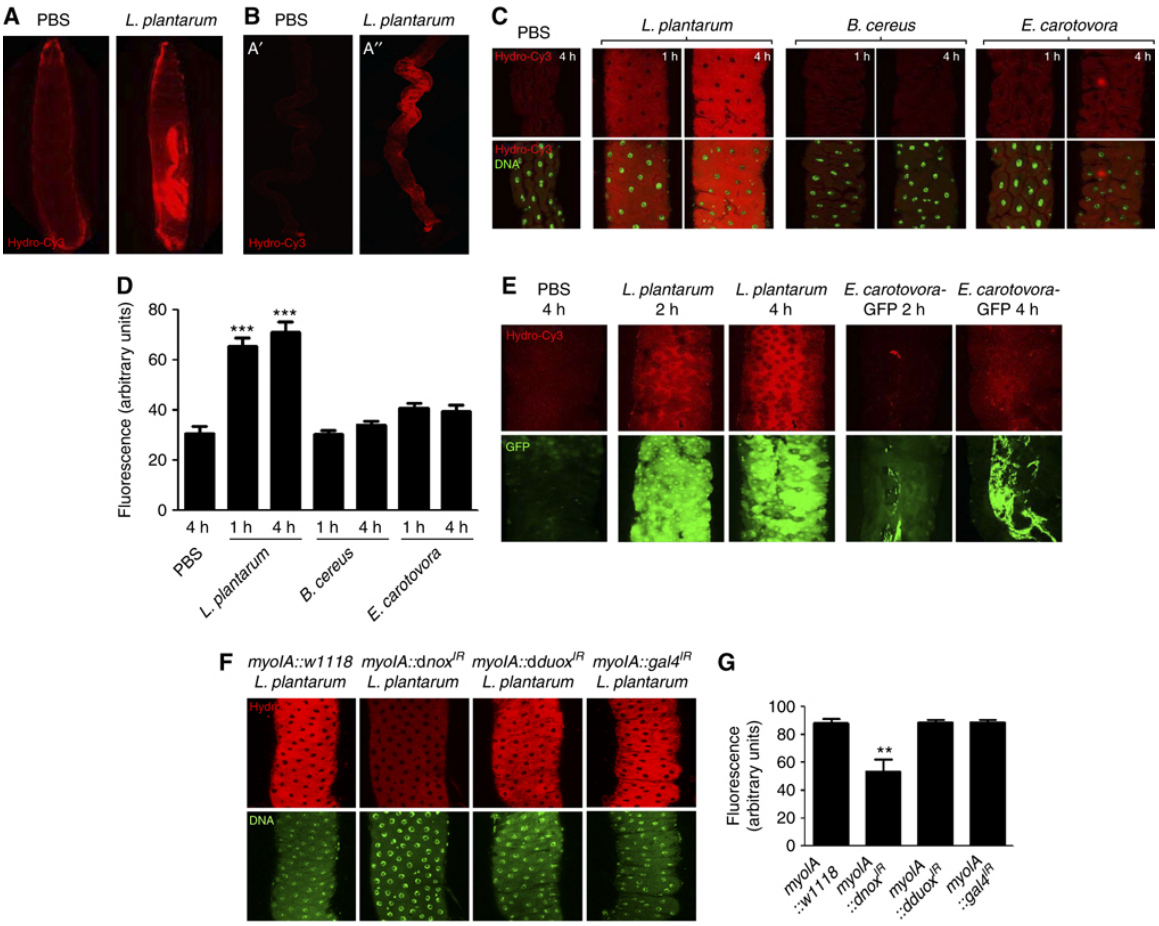

Figure 2. Ingestion of *Lactobacillus plantarum* by *Drosophila* induces cellular ROS generation in the midgut. (**A**) ROS generation following the ingestion of *L. plantarum* by germ-free third-instar larvae over 1 h. ROS were detected by oxidation of the hydrocyanin ROS-sensitive dye also included in the media. (**B**) Microscopic analysis at × 4 magnification of larval midgut dissected from (**A**). (**C**) ROS generation in the third-instar midgut following the ingestion of *L. plantarum*, *Bacillus cereus* or *Erwinia carotovora* for up to 4 h. (**D**) Densitometric analysis of larval midguts described in (**C**). Results are an average for 5 dissected midguts from each assay. (**E**) ROS generation in the gstD1-*gfp*

adult *Drosophila* midgut following the ingestion of *L. plantarum*, or *Erwinia carotovora*-GFP for up to 4 h. Note Hydro-Cy3 fluorescence and expression of GFP in enterocytes following the *L. plantarum* ingestion. Also note GFP fluorescence detected in the midgut following the ingestion of *E. carotovora*-GFP. (**F**) ROS generation following the ingestion of *L. plantarum* in adult *Drosophila* midguts of the indicated genotypes for 1 h. (**G**) Densitometric analysis of larval midguts described in (**F**). Results are an average for five dissected midguts from each assay. All histograms report densitometric analysis (arbitrary units) of hydro-Cy3 oxidation, using the ImageJ software. Ten identically sized areas within an image were measured. n=50. $^{**}P<0.01$, $^{***}P<0.0001$.

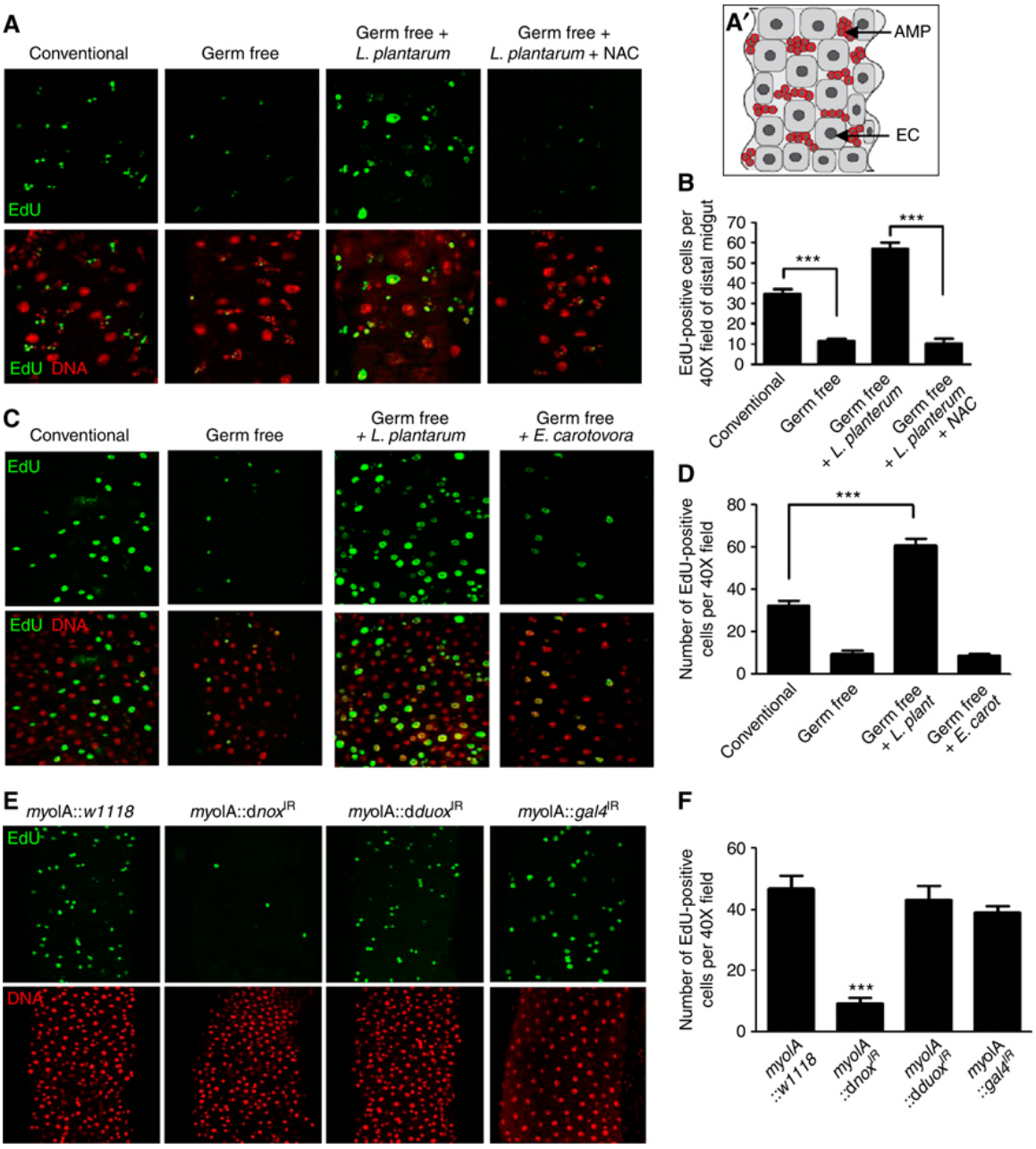

Figure 3. Ingestion of *Lactobacillus plantarum* induces ROS-dependent cellular proliferation in the *Drosophila* intestine. (**A**) EdU-positive cells in the midgut of *w1118* germ-free third-instar larvae, or germ-free larvae fed with 1×10^8 cfu *L. plantarum* for 4 h. Where indicated, the media also contained 1 mM *N*-

acetylcysteine (NAC). (**A′**) Cartoon of *en face* third-instar midgut. Enterocyte (EC) in grey, adult midgut progenitors (AMPs) in red. Note some large enterocytes are EdU positive due to endonuclear DNA replication in maturing larval. (**B**) Number of EdU-positive cells under conditions described in (**A**) n=20, ***P<0.001. (**C**) Detection of EdU-positive cells in the midgut of adult conventionally raised, germ-free, or germ-free adult *Drosophila* following the ingestion of *L. plantarum* or *Erwinia carotovora* for 12 h. (**D**) Number of EdU-positive cells under conditions described in (**C**) n=20, ***P<0.001. (**E**) Detection of EdU-positive cells in the midgut of adult where the levels of Nox or Duox are diminished under the enterocyte-specific *myoIA-GAL4* driver. Full genotypes *myoIA*-GAL4;UAS-d*nox*-RNAi and *myoIA*-GAL4;UAS-d*duox*-RNAi, and *myoIA*-GAL4;UAS-*gal4*-RNAi. (**F**) Number of EdU-positive cells in (**A**). n=10, ***P<0.001.

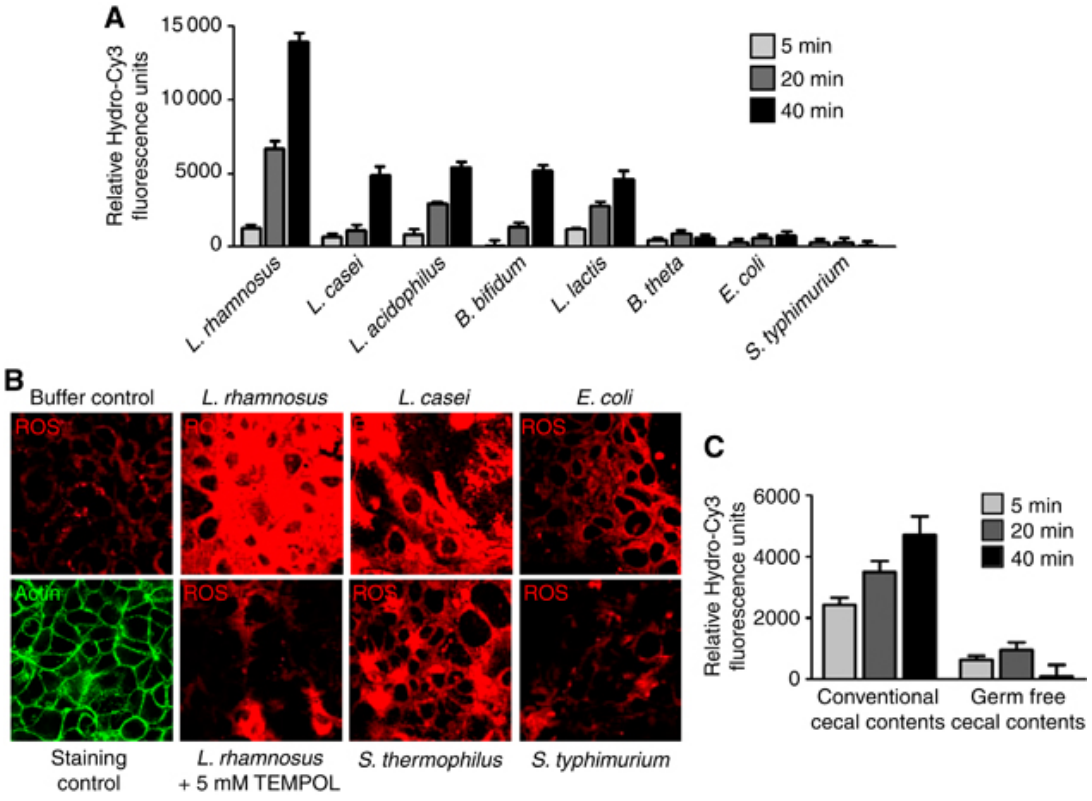

Figure 4. Contact of cultured cells with lactobacilli induces the generation of cellular ROS. (A) Bacterial-induced ROS in cells contacted by the indicated bacteria for up to 40 min. Caco-2 cells seeded in a 96-well format were preloaded with 100 µM hydro-Cy3, then contacted with 3×10^8/100 µl viable bacteria for the indicated times. Cells were then washed three times with PBS before fluoromometric analysis at 575 nm. (B) Bacterial-induced ROS in cells treated as described in (A) detected by confocal microscopy at 585 nm. In some experiments, 5 mM TEMPOL (a membrane-permeable oxygen radical scavenger) was also included. (C) ROS generation in response to contact of Caco-2 cells as described in (A) by the cecal contents of a conventionally raised BL6, or of germ-free BL6 mice. ROS was detected by fluoromometric analysis at 575 nm.

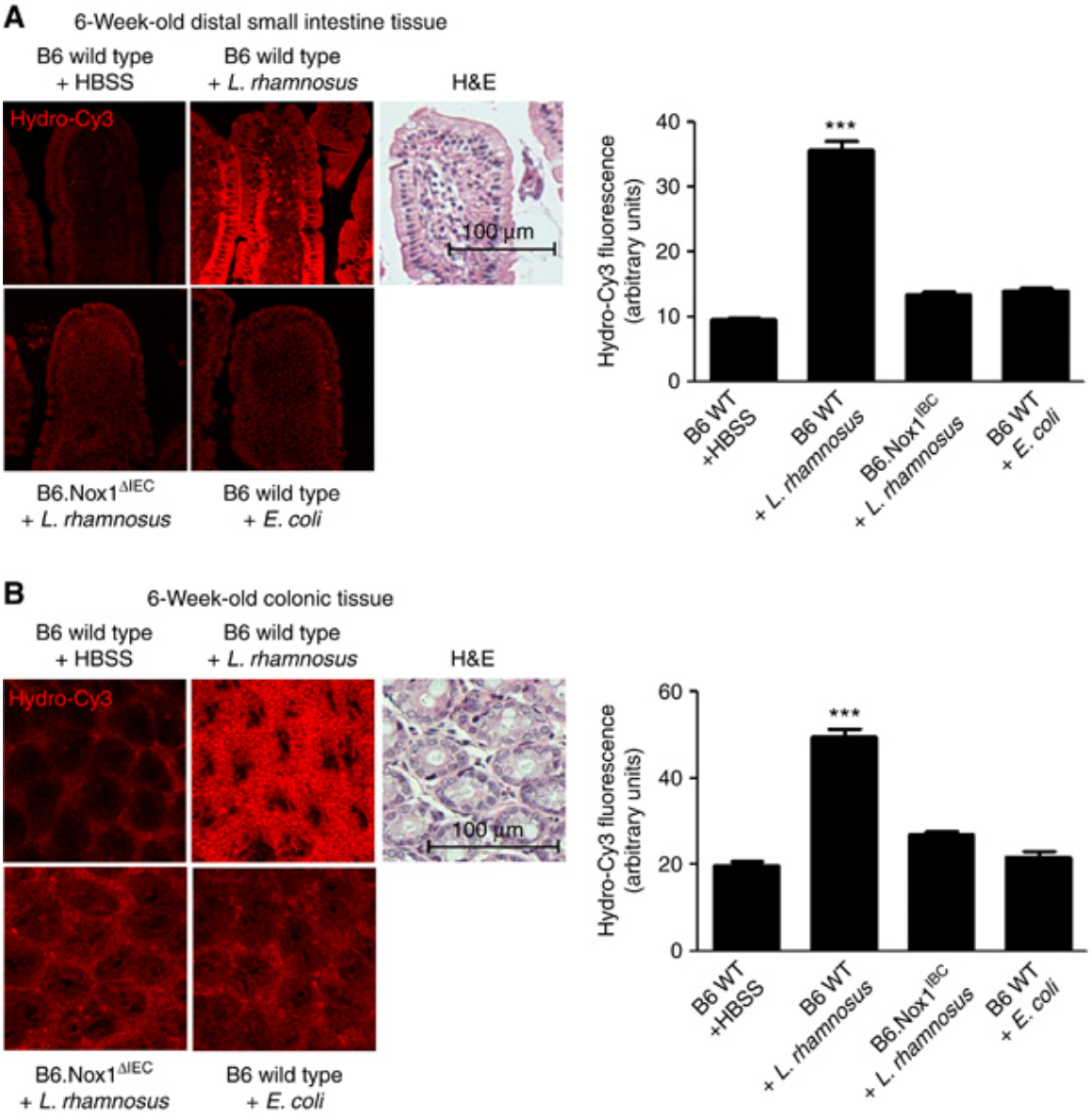

Figure 5. Ingestion of *Lactobacillus* induces Nox1-dependent generation of cellular reactive oxygen species (ROS) in murine enterocytes. (A) Detection of ROS generation in the distal small intestine of B6.wild type or B6.Nox1ΔIEC 6-week-old mice at 1 h following the oral gavage feeding of *L. rhamnosus* GG or *E. coli*. Mice were administered 5 µl of 200 µM hydro-Cy3 at 15 min before bacterial feeding. (B) Detection of ROS generation in the colon of 6-week-old mice treated

as described in (A). In each figure, Haematoxylin and Eosin (H&E) stain is included for tissue orientation and scale. Scale bar=100 μm. Histograms report densitometric analysis (arbitrary units) of hydro-Cy3 oxidation, using the ImageJ software. The densitometry of 10 identically sized areas within an image was measured. Results are an average for three mice for each treatment. n=30. $^{***}P$<0.001. Error bars indicate S.E.M.

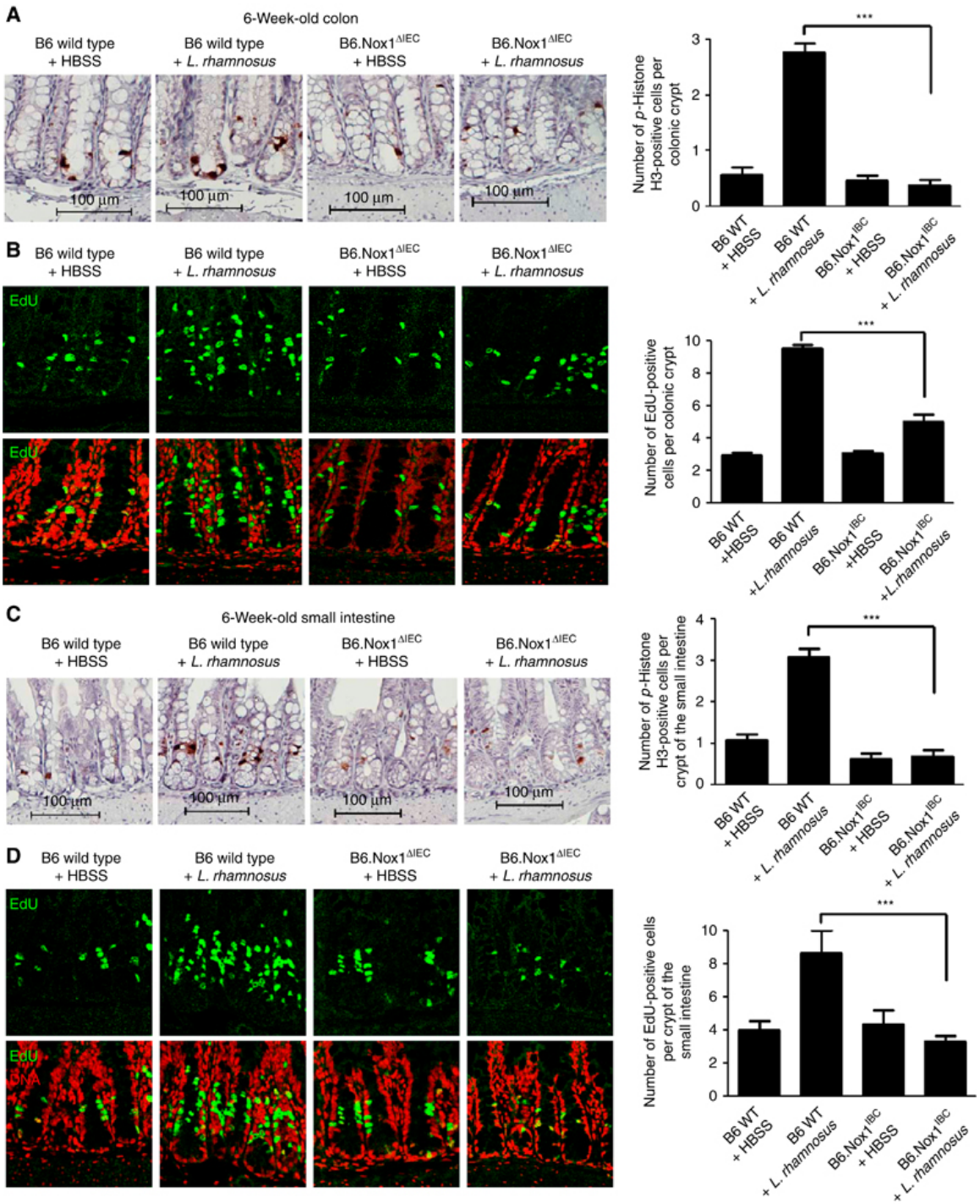

Figure 6. Ingestion of *Lactobacillus* induces Nox1-dependent cell proliferation in the murine gut epithelium. (A) Detection and numeration of p-Histone H3 in cells within the colon of 6-week-old w.t. or B6.Nox1ΔIEC mice at 4 h following

the oral gavage feeding of HBSS or *L. rhamnosus* GG. (B) Detection and numeration of EdU-positive cells within the colon of 6-week-old w.t. or B6.Nox1ΔIEC mice at 4 h following the oral gavage feeding of HBSS or *L. rhamnosus* GG. (C) Detection and numeration of p-Histone H3 in cells within the small intestine of 6-week-old w.t. or B6.Nox1ΔIEC mice at 4 h following the oral gavage feeding of HBSS or *L. rhamnosus* GG. (D) Detection and numeration of EdU-positive cells within the small intestine of 6-week-old w.t. or B6.Nox1ΔIEC mice at 4 h following the oral gavage feeding of 1×10^8 cfu of HBSS or *L. rhamnosus* GG. For each numeration, 40 × 20 fields were counted in three mice for each treatment. ***$P<0.001$.

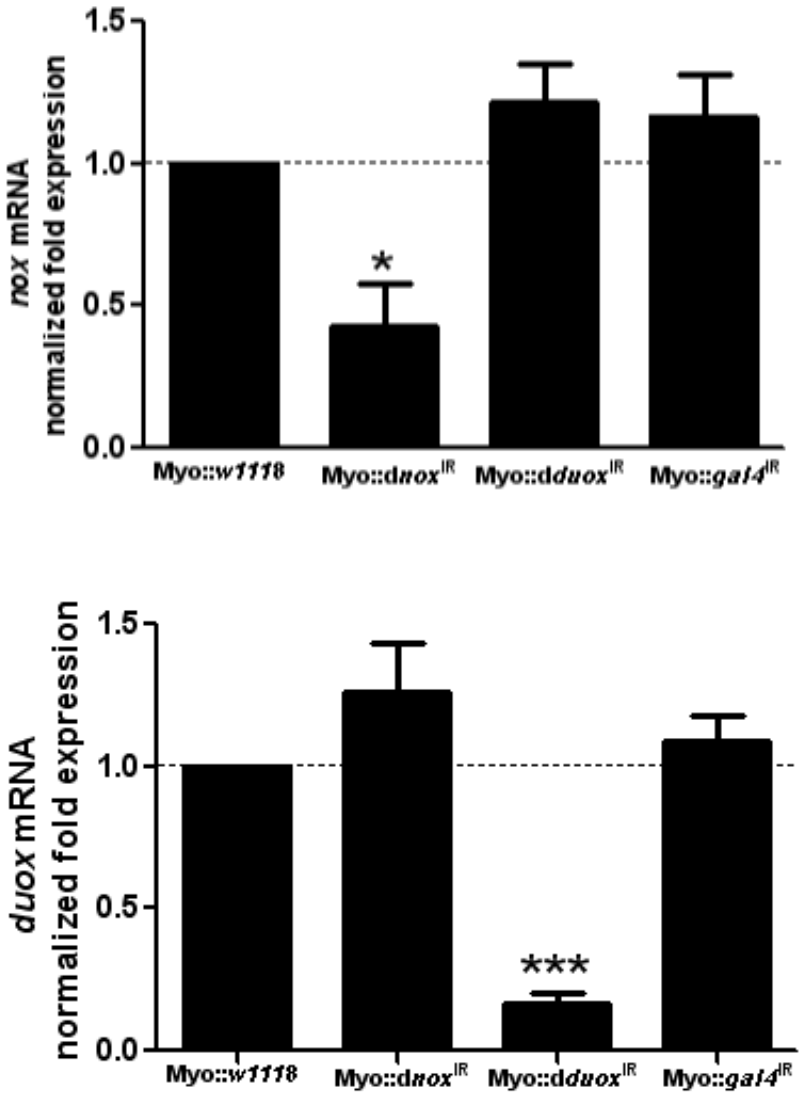

Figure S1. Knockdown of dnox and dduox mRNA in the of dissected 10-day-old adult *Drosophila* midgut. Relative levels of dnox and dduox in the midgut were quantified by qRTPCR. Levels were normalized to transcript levels measured in myoIA-GAL4 w1118. For each genotype, three replicates of five intestines were dissected and pooled for RNA preparation. n=15, *= $P < 0.01$, ***= $P < 0.0001$.

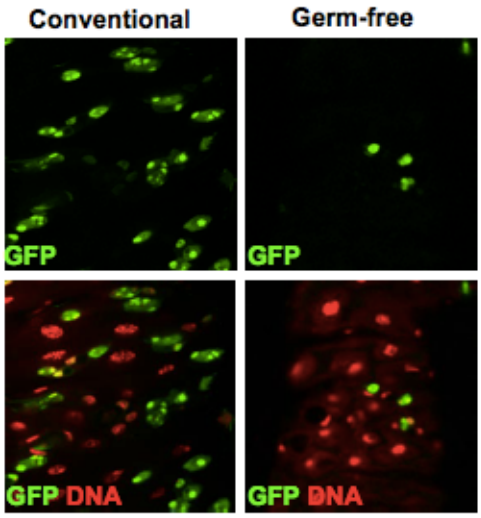

Figure S2. Detection of GFP-positive cells in the midgut of *Drosophila* larvae harboring the ISC-specific driver esg-GAL4 UAS-gfp raised in conventional or germ-free conditions. Note fewer GFP-positive (ISCs) in germ-free larvae.

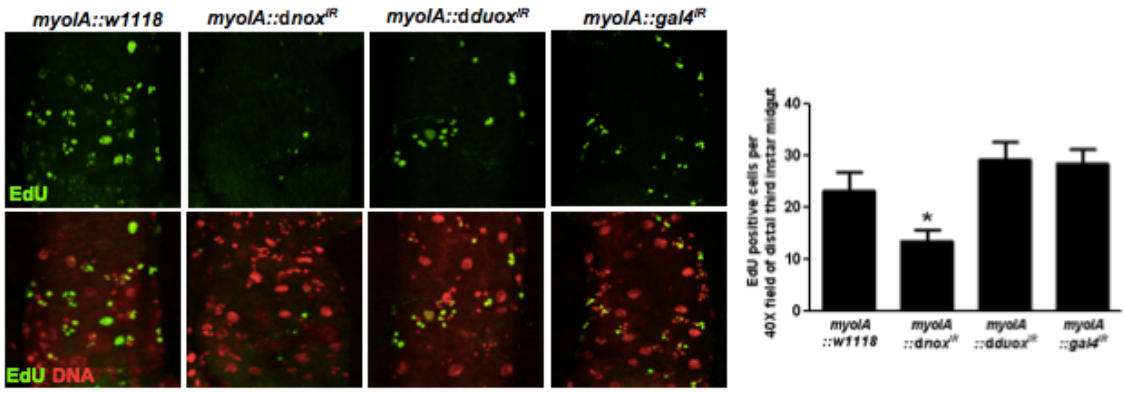

Figure S3. (A) Detection of EdU positive cells in the midgut of third instar larvae where the levels of Nox or Duox are diminished under the enterocyte specific myoIA-GAL4 driver. Full genotypes myoIA-GAL4;UAS-nox-RNAi and myoIA-GAL4;UAS-duox-RNAi. Note markedly lower numbers of EdU positive cells following diminished levels of Nox. (B) Numeration of EdU positive cells in (A). n=10, *= $P < 0.01$.

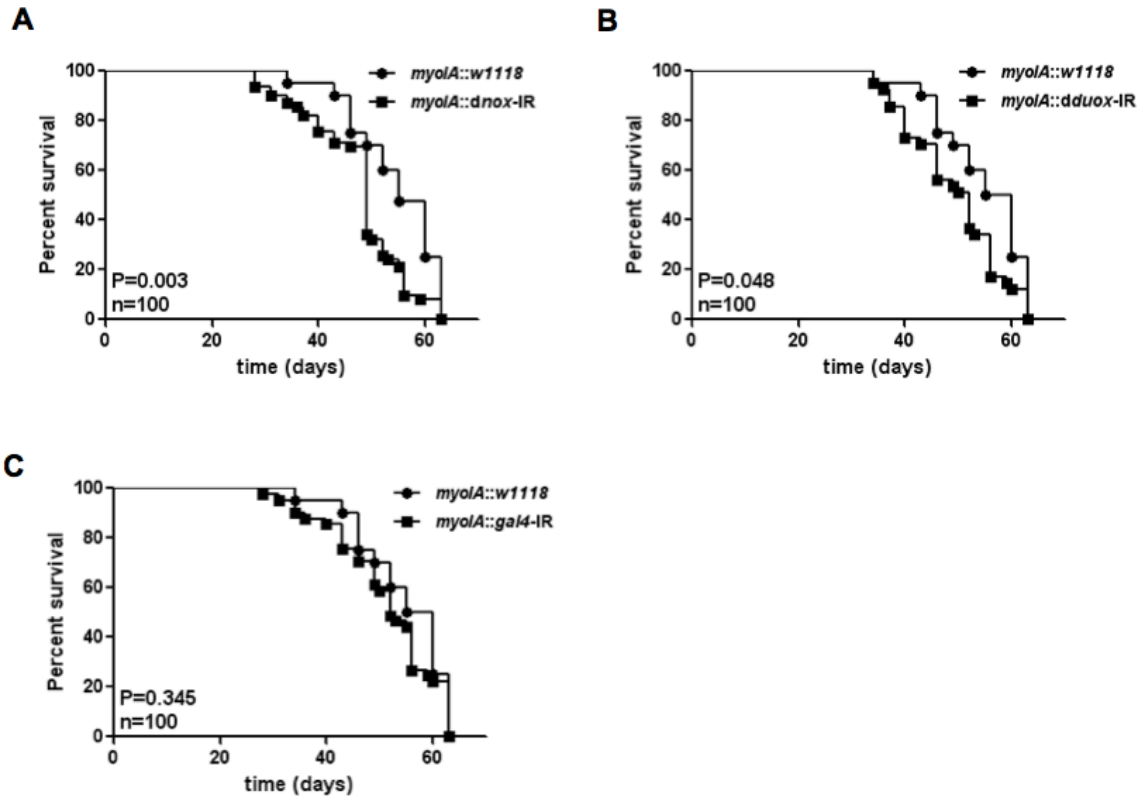

Figure S4. Lifespan of adult *Drosophila* of the indicated phenotypes at 25°C. Note significant decrease in viability of myoIA-GAL4 UAS-dnoxIR (panel A) compared to myoIA-GAL4 UASdduoxIR or myoIA-GAL4 UAS-gal4IR controls.

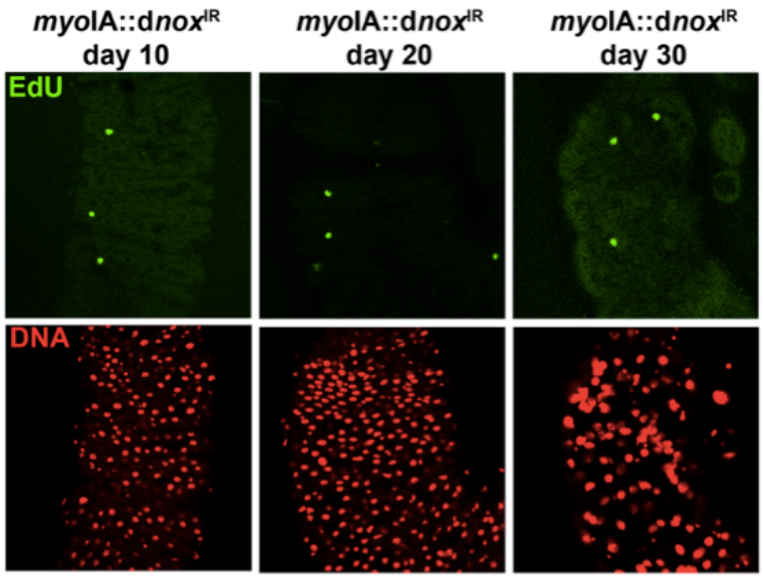

Figure S5. Detection of EdU positive cells, and DNA counter stain in the midgut of adult Drosophila where the levels of Nox are diminished (myoIA-GAL4 UAS-dnoxIR). Note marked changes in histological architecture of the myoIA-GAL4 UAS-dnoxIR up to 30 days after eclosure.

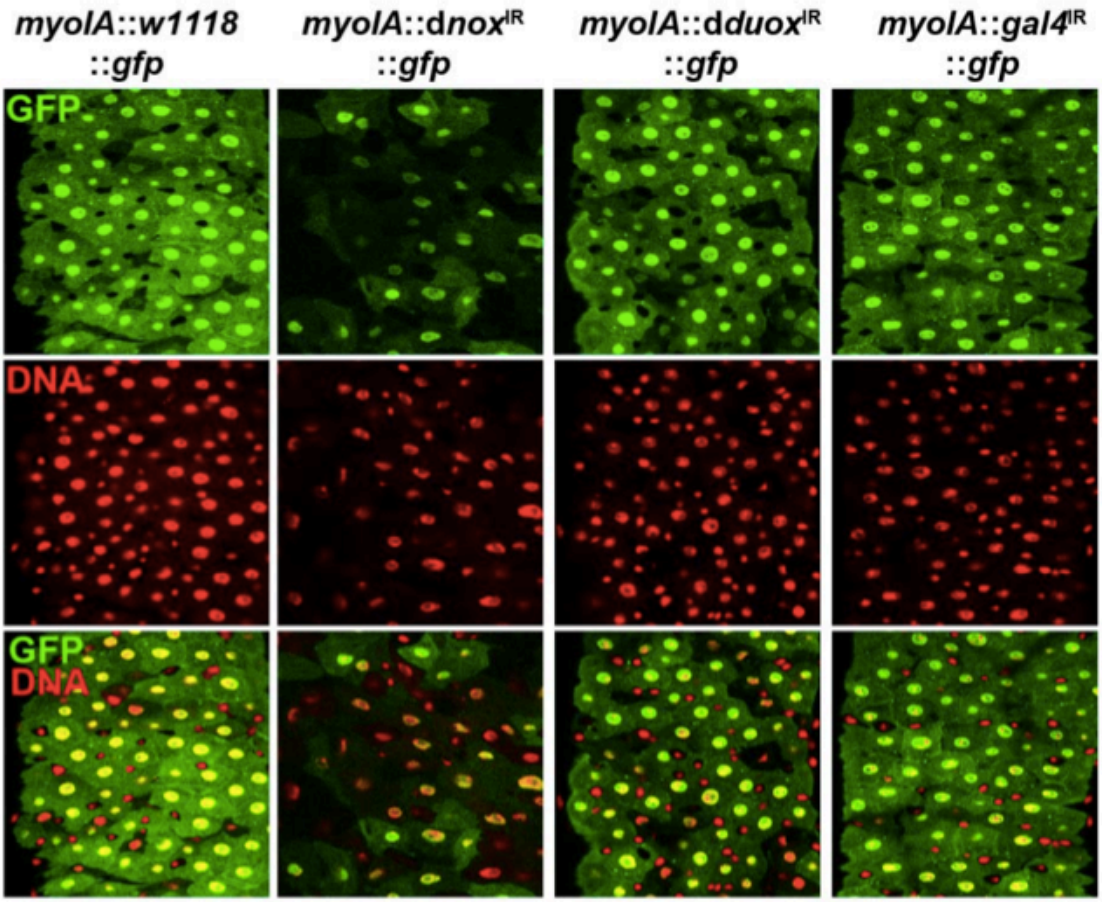

Figure S6. Detection of enterocyte architecture in the midgut of 20-day-old adult *Drosophila* where the levels in the genotypes myoIA-GAL4 UAS-gfp UAS-dnoxIR, myoIA-GAL4 UASgfp UAS-dduoxIR , and myoIA-GAL4 UAS-gfp UAS-gal4IR. Note marked changes in histological architecture of the myoIA-GAL4 UAS-dnoxIR midgut enterocytes compared to control flies.

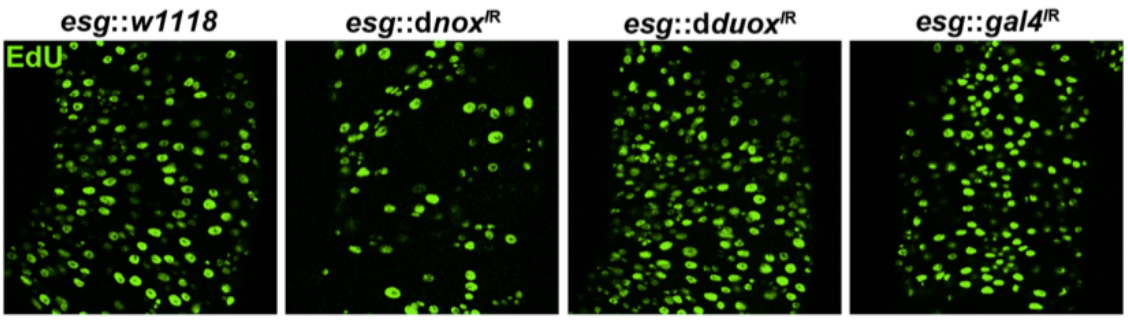

Figure S7. Detection of EdU positive cells in the midgut of adult *Drosophila* where the of genotypes esg-GAL4 UAS-dnoxIR , esg-GAL4 UAS-dduoxIR , and esg-GAL4 UAS-gal4IR. Note the numbers of EdU-positive cells were not diminished to the same extent as detected when Nox levels are diminished in enterocytes (Figure 3).

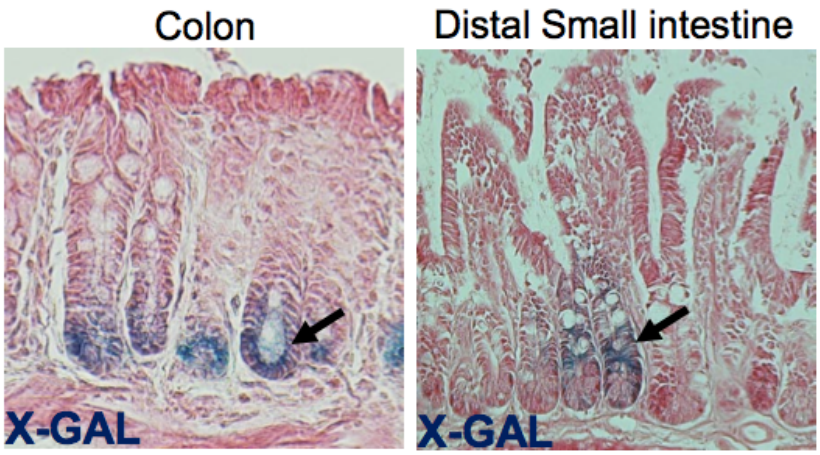

Figure S8. Detection of LacZ activity in the small intestine of B6.Nox1ΔIEC mice. Details of mating regimes and genetics of Nox1 null mice are included in our previous publication (Leoni et al. 2013). Arrows highlight tissue regions stained positive for LacZ actvity.

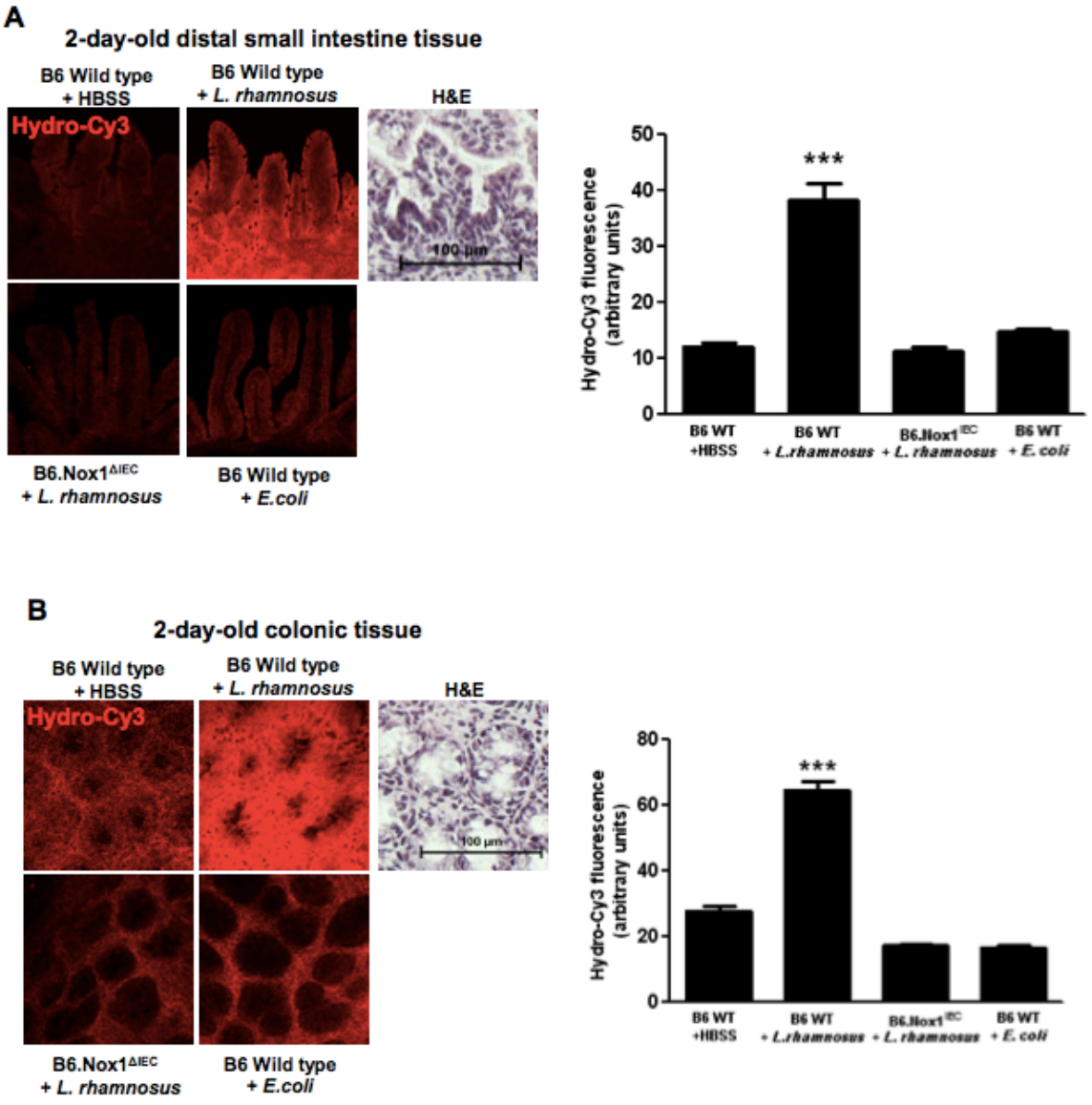

Figure S9. *L. rhamnosus* GG ingestion induces Nox1-dependent generation of cellular ROS in the 2-day-old murine distal small intestine. (A) Detection and quantification of ROS generation in the distal small intestine of B6. wild type or B6.Nox1ΔIEC 2-day-old mice at 1 hour following oral gavage feeding of 3×10^8 cfu of L. rhamnosus GG or E. coli. Mice were administered 5µl of 200 µM hydro-Cy3 at 15 minutes before feeding. (B) Detection and quantification of ROS

generation in the colon of 2-day-old mice treated as described in (A). In each figure, Hematoxylin and eosin (H&E) stain is included for tissue orientation and scale. Scale bar = 100μm. Histograms report densitometric analysis (arbitrary units) of hydro-Cy3 oxidation, using ImageJ software. The densitometry of 10 identically sized areas within an image were measured. Results are an average for 3 mice for each treatment. n=30. Error bars indicate S.E.M.

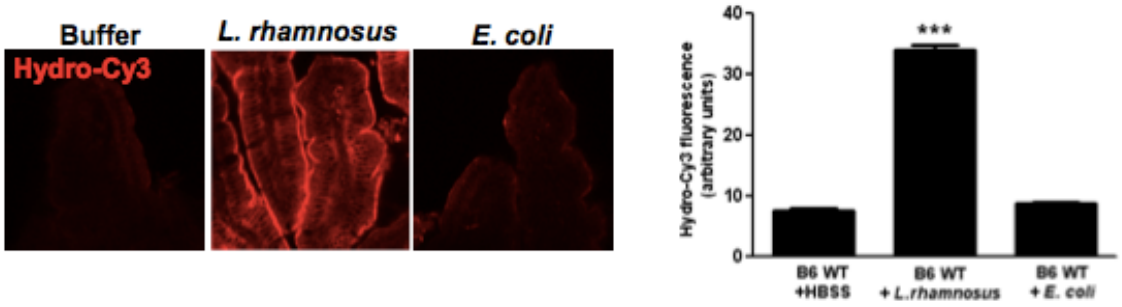

Figure S10. Detection of ROS in the intestine of 6-week-old male germ-free mice at 1 hour following oral gavage feeding of 3×10^8 cfu *L. rhamnosus* GG or *E. coli*. Mice were administered 100µl of 200 µM hydro-Cy3 at 30 minutes before feeding. Histogram reports densitometric analysis (arbitrary units) of hydro-Cy3 oxidation, using ImageJ software. Histograms report densitometric analysis (arbitrary units) of hydro-Cy3 oxidation, using ImageJ software. The densitometry of 10 identically sized areas within an image were measured. Results are an average for 3 mice for each treatment. n=30. Error bars indicate S.E.M.

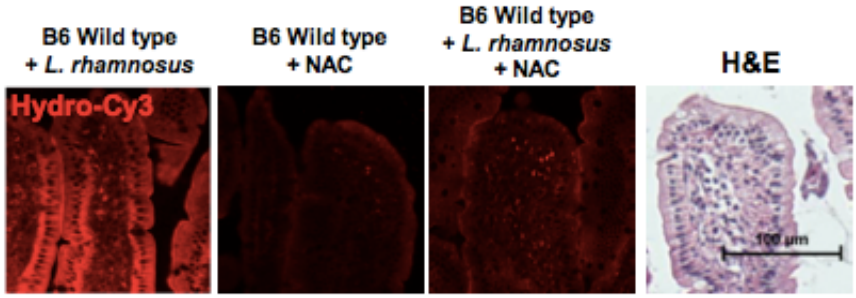

Figure S11. Detection of ROS levels in the distal small intestine of 6-week old B6. wild type mice at 1 hour following oral gavage feeding of 3×10^8 cfu *L. rhamnosus* GG. Mice were administered 100µl of 200 µM hydro-Cy3 by IP at 30 minutes before feeding. Some mice (as noted by label) were pre-treated with N-acetylcysteine (NAC), (a glutathione precursor and direct antioxidant) by IP at 1 hour before oral gavage. H&E stained section is included for tissue orientation and scale.

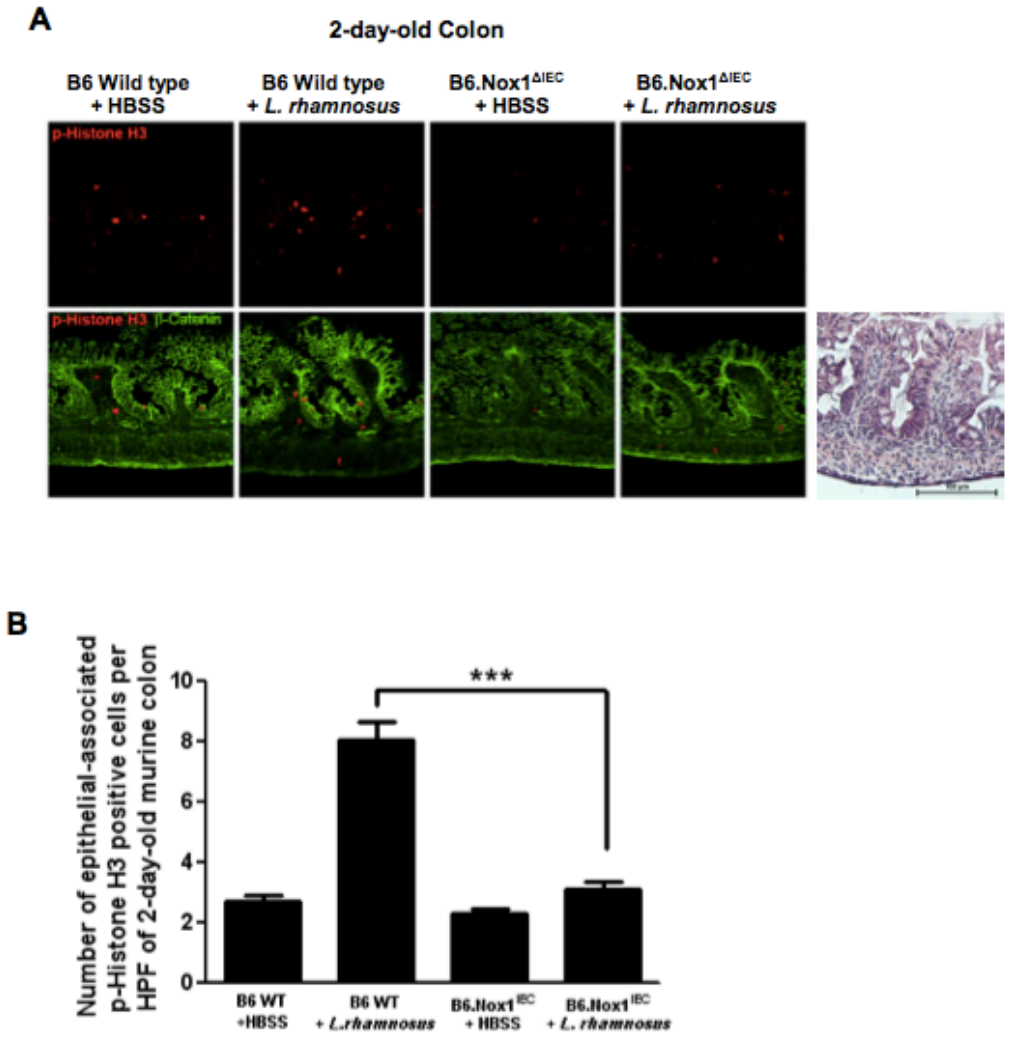

Figure S12. *L. rhamnosus* GG ingestion induces Nox1-dependent cellular proliferation in the 2-day-old murine colon. (A) Detection of p-Histone H3 in cells within the colon of 2-day-old w.t. or B6.Nox1ΔIEC mice at 2 hour following oral gavage feeding of 1×10^8 cfu of HBSS or *L. rhamnosus* GG. (B) Numeration of epithelial-associated p-Histone H3 positive cells per 20X field of 2-day-old murine colon in (a). Forty 20X fields were counted in three mice for each treatment. ***= $P < 0.001$.

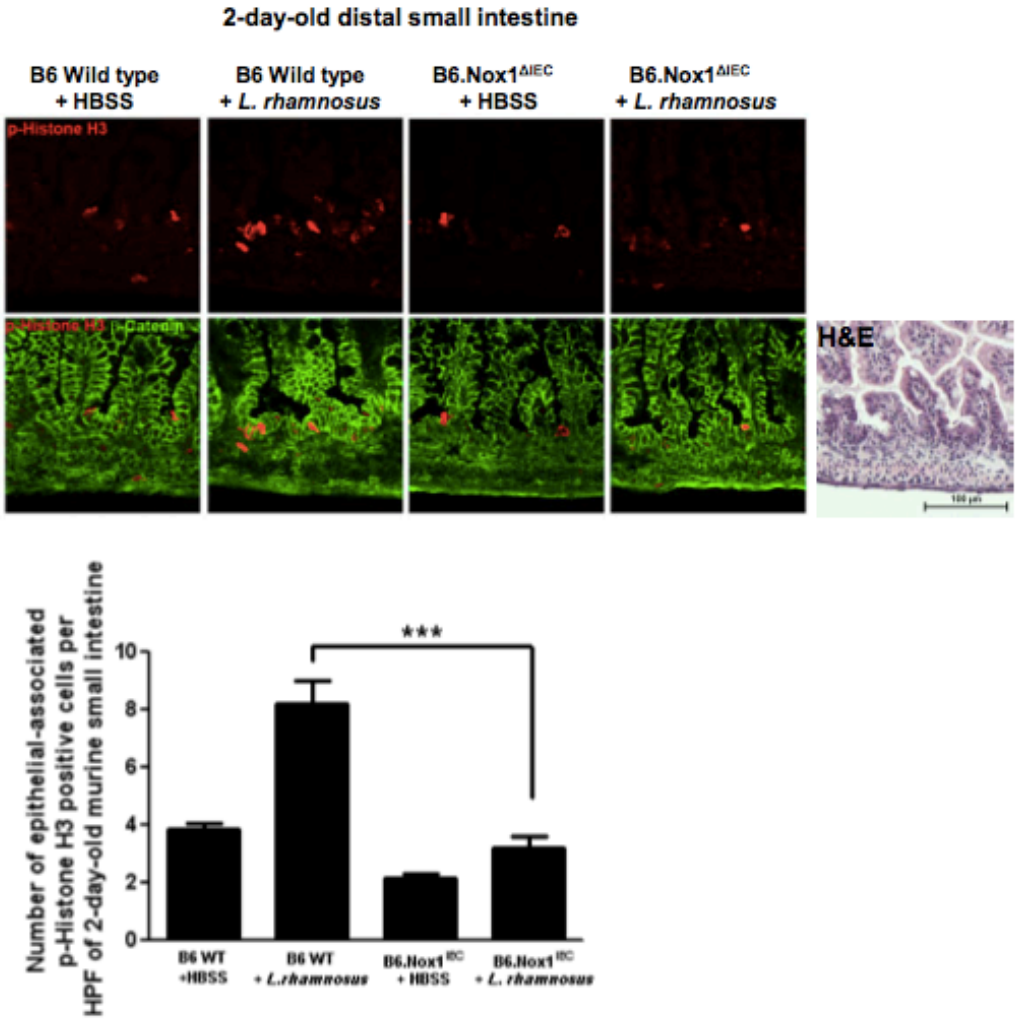

Figure S13. *L. rhamnosus* GG ingestion induces Nox1-dependent cellular proliferation in the 2-day-old murine distal small intestine (A) Detection of p-Histone H3 in cells within the colon of 2-day-old w.t. or B6.Nox1ΔIEC mice at 2 hour following oral gavage feeding of 1×10^8 cfu of HBSS or *L. rhamnosus* GG. (B) Numeration of epithelial-associated p-Histone H3 positive cells per 20X field of 2-day-old murine colon in (a). Forty 20X fields were counted in three mice for each treatment. ***= $P < 0.001$.

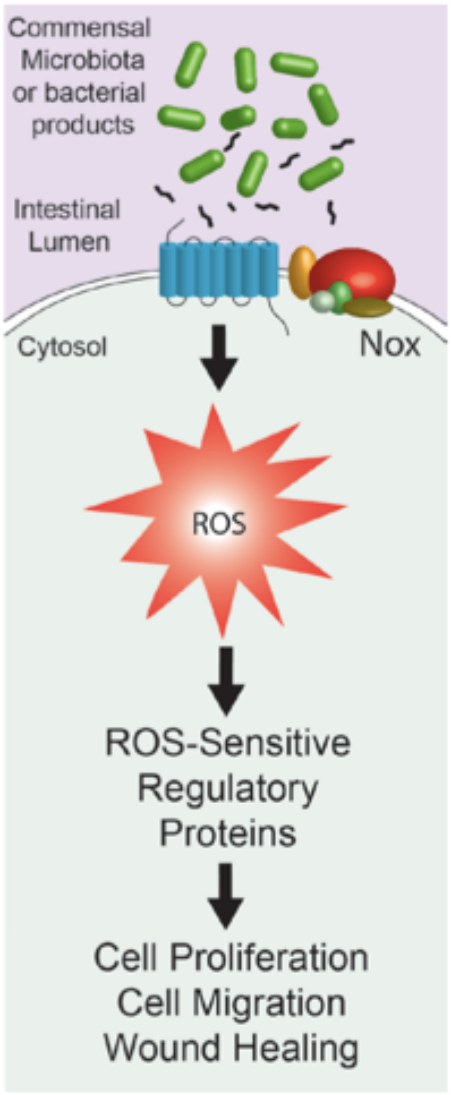

Figure S14. *L. rhamnosus* GG is a potent inducer of Nox1-dependent ROS generation, and of ROS-dependent cellular proliferation in enterocytes.

Chapter 2 Acknowledgements

RMJ is supported by NIH Grant K01DK081481, and ASN is supported, in part, by National Institutes of Health Grant R01DK071604 and RO1AI064462. PWD is supported by R01HD059122.

Chapter 2 References

1. **Neish AS.** 2009. Microbes in gastrointestinal health and disease. Gastroenterology **136:**65-80.
2. **Hooper LV, Littman DR, Macpherson AJ.** 2012. Interactions between the microbiota and the immune system. Science **336:**1268-1273.
3. **Nicholson JK, Holmes E, Kinross J, Burcelin R, Gibson G, Jia W, Pettersson S.** 2012. Host-gut microbiota metabolic interactions. Science **336:**1262-1267.
4. **Sartor RB.** 2008. Microbial influences in inflammatory bowel diseases. Gastroenterology **134:**577-594.
5. **Park J, Floch MH.** 2007. Prebiotics, probiotics, and dietary fiber in gastrointestinal disease. Gastroenterology clinics of North America **36:**47-63, v.
6. **Rakoff-Nahoum S, Paglino J, Eslami-Varzaneh F, Edberg S, Medzhitov R.** 2004. Recognition of commensal microflora by toll-like receptors is required for intestinal homeostasis. Cell **118:**229-241.
7. **Kumar A, Wu H, Collier-Hyams LS, Hansen JM, Li T, Yamoah K, Pan ZQ, Jones DP, Neish AS.** 2007. Commensal bacteria modulate

cullin-dependent signaling via generation of reactive oxygen species. EMBO J. **26:**4457-4466.

8. **Kumar A, Wu H, Collier-Hyams LS, Kwon YM, Hanson JM, Neish AS.** 2009. The bacterial fermentation product butyrate influences epithelial signaling via reactive oxygen species-mediated changes in cullin-1 neddylation. J. Immunol. **182:**538-546.

9. **Swanson PA, 2nd, Kumar A, Samarin S, Vijay-Kumar M, Kundu K, Murthy N, Hansen J, Nusrat A, Neish AS.** 2011. Enteric commensal bacteria potentiate epithelial restitution via reactive oxygen species-mediated inactivation of focal adhesion kinase phosphatases. Proc. Natl. Acad. Sci. U. S. A. **108:**8803-8808.

10. **Wentworth CC, Alam A, Jones RM, Nusrat A, Neish AS.** 2011. Enteric commensal bacteria induce extracellular signal-regulated kinase pathway signaling via formyl peptide receptor-dependent redox modulation of dual specific phosphatase 3. J. Biol. Chem. **286:**38448-38455.

11. **Wentworth CC, Jones RM, Kwon YM, Nusrat A, Neish AS.** 2010. Commensal-epithelial signaling mediated via formyl peptide receptors. Am. J. Pathol. **177:**2782-2790.

12. **Micchelli CA, Perrimon N.** 2006. Evidence that stem cells reside in the adult Drosophila midgut epithelium. Nature **439:**475-479.

13. **Ohlstein B, Spradling A.** 2006. The adult Drosophila posterior midgut is maintained by pluripotent stem cells. Nature **439:**470-474.

14. **van der Flier LG, Clevers H.** 2009. Stem cells, self-renewal, and differentiation in the intestinal epithelium. Annual review of physiology **71:**241-260.

15. **Mathur D, Bost A, Driver I, Ohlstein B.** 2010. A transient niche regulates the specification of Drosophila intestinal stem cells. Science **327:**210-213.

16. **Hernandez-Garcia D, Wood CD, Castro-Obregon S, Covarrubias L.** 2010. Reactive oxygen species: A radical role in development? Free radical biology & medicine **49:**130-143.

17. **Ha EM, Oh CT, Ryu JH, Bae YS, Kang SW, Jang IH, Brey PT, Lee WJ.** 2005. An antioxidant system required for host protection against gut infection in Drosophila. Developmental cell **8:**125-132.

18. **Kotchoni SO, Kuhns C, Ditzer A, Kirch HH, Bartels D.** 2006. Over-expression of different aldehyde dehydrogenase genes in Arabidopsis thaliana confers tolerance to abiotic stress and protects plants against lipid peroxidation and oxidative stress. Plant, cell & environment **29:**1033-1048.

19. **Tsukagoshi H, Busch W, Benfey PN.** 2010. Transcriptional regulation of ROS controls transition from proliferation to differentiation in the root. Cell **143:**606-616.

20. **Owusu-Ansah E, Banerjee U.** 2009. Reactive oxygen species prime Drosophila haematopoietic progenitors for differentiation. Nature **461:**537-541.

21. **Bedard K, Krause KH.** 2007. The NOX family of ROS-generating NADPH oxidases: physiology and pathophysiology. Physiological reviews **87:**245-313.

22. **Lambeth JD.** 2004. NOX enzymes and the biology of reactive oxygen. Nat. Rev. Immunol. **4:**181-189.

23. **Ogier-Denis E, Mkaddem SB, Vandewalle A.** 2008. NOX enzymes and Toll-like receptor signaling. Seminars in immunopathology **30:**291-300.

24. **Takashima S, Mkrtchyan M, Younossi-Hartenstein A, Merriam JR, Hartenstein V.** 2008. The behaviour of Drosophila adult hindgut stem cells is controlled by Wnt and Hh signalling. Nature **454:**651-655.

25. **Kundu K, Knight SF, Willett N, Lee S, Taylor WR, Murthy N.** 2009. Hydrocyanines: a class of fluorescent sensors that can image reactive oxygen species in cell culture, tissue, and in vivo. Angew. Chem. Int. Ed. Engl. **48:**299-303.

26. **Wong CN, Ng P, Douglas AE.** 2011. Low-diversity bacterial community in the gut of the fruitfly Drosophila melanogaster. Environmental microbiology **13:**1889-1900.

27. **Ha EM, Oh CT, Bae YS, Lee WJ.** 2005. A direct role for dual oxidase in Drosophila gut immunity. Science **310:**847-850.

28. **Quinn MT, Gauss KA.** 2004. Structure and regulation of the neutrophil respiratory burst oxidase: comparison with nonphagocyte oxidases. Journal of leukocyte biology **76:**760-781.

29. **Morgan NS, Skovronsky DM, Artavanis-Tsakonas S, Mooseker MS.** 1994. The molecular cloning and characterization of Drosophila melanogaster myosin-IA and myosin-IB. Journal of molecular biology **239:**347-356.

30. **Jiang H, Patel PH, Kohlmaier A, Grenley MO, McEwen DG, Edgar BA.** 2009. Cytokine/Jak/Stat signaling mediates regeneration and homeostasis in the Drosophila midgut. Cell **137:**1343-1355.

31. **Leoni G, Alam A, Neumann PA, Lambeth JD, Cheng G, McCoy J, Hilgarth RS, Kundu K, Murthy N, Kusters D, Reutelingsperger C, Perretti M, Parkos CA, Neish AS, Nusrat A.** 2013. Annexin A1, formyl peptide receptor, and NOX1 orchestrate epithelial repair. The Journal of clinical investigation **123:**443-454.

32. **Geiszt M, Lekstrom K, Brenner S, Hewitt SM, Dana R, Malech HL, Leto TL.** 2003. NAD(P)H oxidase 1, a product of differentiated colon epithelial cells, can partially replace glycoprotein 91phox in the regulated production of superoxide by phagocytes. J. Immunol. **171:**299-306.

33. **Suh YA, Arnold RS, Lassegue B, Shi J, Xu X, Sorescu D, Chung AB, Griendling KK, Lambeth JD.** 1999. Cell transformation by the superoxide-generating oxidase Mox1. Nature **401:**79-82.

34. **Preidis GA, Saulnier DM, Blutt SE, Mistretta TA, Riehle KP, Major AM, Venable SF, Finegold MJ, Petrosino JF, Conner ME, Versalovic J.** 2012. Probiotics stimulate enterocyte migration and microbial diversity in the neonatal mouse intestine. FASEB journal :

official publication of the Federation of American Societies for Experimental Biology **26:**1960-1969.

35. **Jones RM, Mercante JW, Neish AS.** 2012. Reactive oxygen production induced by the gut microbiota: pharmacotherapeutic implications. Current medicinal chemistry **19:**1519-1529.

36. **Ray PD, Huang BW, Tsuji Y.** 2012. Reactive oxygen species (ROS) homeostasis and redox regulation in cellular signaling. Cellular signalling **24:**981-990.

37. **O'Callaghan J, O'Toole PW.** 2013. Lactobacillus: host-microbe relationships. Curr. Top. Microbiol. Immunol. **358:**119-154.

38. **Storelli G, Defaye A, Erkosar B, Hols P, Royet J, Leulier F.** 2011. Lactobacillus plantarum promotes Drosophila systemic growth by modulating hormonal signals through TOR-dependent nutrient sensing. Cell metabolism **14:**403-414.

39. **Mitsuishi Y, Motohashi H, Yamamoto M.** 2012. The Keap1-Nrf2 system in cancers: stress response and anabolic metabolism. Frontiers in oncology **2:**200.

40. **Sadok A, Bourgarel-Rey V, Gattacceca F, Penel C, Lehmann M, Kovacic H.** 2008. Nox1-dependent superoxide production controls colon adenocarcinoma cell migration. Biochimica et biophysica acta **1783:**23-33.

41. **Coant N, Ben Mkaddem S, Pedruzzi E, Guichard C, Treton X, Ducroc R, Freund JN, Cazals-Hatem D, Bouhnik Y, Woerther PL, Skurnik D, Grodet A, Fay M, Biard D, Lesuffleur T, Deffert**

C, Moreau R, Groyer A, Krause KH, Daniel F, Ogier-Denis E. 2010. NADPH oxidase 1 modulates WNT and NOTCH1 signaling to control the fate of proliferative progenitor cells in the colon. Mol. Cell. Biol. **30:**2636-2650.

42. **Chakrabarti S, Liehl P, Buchon N, Lemaitre B.** 2012. Infection-induced host translational blockage inhibits immune responses and epithelial renewal in the Drosophila gut. Cell host & microbe **12:**60-70.

43. **Buchon N, Broderick NA, Poidevin M, Pradervand S, Lemaitre B.** 2009. Drosophila intestinal response to bacterial infection: activation of host defense and stem cell proliferation. Cell host & microbe **5:**200-211.

44. **Lee KA, Kim SH, Kim EK, Ha EM, You H, Kim B, Kim MJ, Kwon Y, Ryu JH, Lee WJ.** 2013. Bacterial-derived uracil as a modulator of mucosal immunity and gut-microbe homeostasis in Drosophila. Cell **153:**797-811.

45. **Chen X, Lee KA, Ha EM, Lee KM, Seo YY, Choi HK, Kim HN, Kim MJ, Cho CS, Lee SY, Lee WJ, Yoon J.** 2011. A specific and sensitive method for detection of hypochlorous acid for the imaging of microbe-induced HOCl production. Chemical communications **47:**4373-4375.

Chapter 2 Epithelial adhesion mediated by pilin SpaC is required for *Lactobacillus rhamnosus* GG-induced probiotic effects

Courtney S. Ardita,[a] Jeffrey W. Mercante,[a*] Young Man Kwon,[a**] Liping Luo,[a] Madelyn E. Crawford,[a] Domonica N. Powell,[a] Rheinallt M. Jones,[a] Andrew S. Neish [a]

Epithelial Pathobiology Unit, Department of Pathology and Laboratory Medicine, Emory University School of Medicine, Atlanta, Georgia, USA[a]

C.S.A. and J.W.M contributed equally to this work.

Chapter 3 Abstract

Lactobacillus rhamnosus GG (LGG) is a widely used probiotic, and the strain's salutary effects on the intestine have been extensively documented. We previously reported that LGG can modulate inflammatory signaling, as well as epithelial migration and proliferation by activating NADPH oxidase 1-catalyzed generation of reactive oxygen species (ROS). However, how LGG induces these responses is unknown. Here, we report that LGG's probiotic benefits are dependent on bacterial-epithelial interaction mediated by the SpaC pilin subunit. By comparing LGG to an isogenic mutant that lacks SpaC (LGGΩ*spaC*), we establish that SpaC is necessary for LGG to adhere to gut mucosa, that SpaC contributes to LGG-induced epithelial generation of ROS, and that SpaC plays a role in LGG's capacity to stimulate ERK MAPK signaling in enterocytes. In addition, we show that SpaC is required for LGG-mediated stimulation of cell proliferation and protection against radiologically-inflicted intestinal injury. The identification of a critical surface protein required for LGG to mediate its probiotic influence advances our understanding of the molecular basis for the symbiotic relationship between some commensal bacteria of the gut lumen and enterocytes. Further insights into this relationship are critical for the development of novel approaches to treat intestinal diseases.

Chapter 3 Introduction

The mammalian intestinal microbiota is a complex and diverse community that normally thrives in a symbiotic relationship with the host. The intestinal lumen provides a temperature controlled and nutrient rich environment, while the

resident microbial population contributes to host well-being by several means, including competitive exclusion of pathogens by occupying mucosal attachment sites, extraction of calories from indigestible complex carbohydrates, activation of epithelial transcriptional programs that stimulate mucosal development, stimulation of adaptive immune functions, and activation of cytoprotective pathways (1-3). Experiments in germ-free animals have verified a compelling role for the microbiota in epithelial proliferation, migration, and wound recovery post-injury (4). Thus, an appropriate reciprocal dialog between host and the gut microbiota has been implicated in a wide variety of host functions. Conversely, a disturbed or "dysbiotic" relationship is thought to be central to the pathogenesis of inflammatory bowel disease (IBD), certain enteric infections, and likely a variety of systemic immune and metabolic disorders (5). In fact, therapeutic modification of the microbiota has been suggested as a possible solution to the aforementioned health conditions. Probiotics are viable microorganisms, generally representative members of the intestinal microbiota (often strains of *Lactobacillus*, *Bifidobacterium*, and *Streptococcus*), which exert beneficial effects on the health of the host, including enhancement of barrier function and suppression of inflammatory processes (2). While probiotic approaches have shown promise in numerous intestinal and systemic disorders, a plausible mode of action is largely unknown.

Research into the mechanisms by which bacteria influence host epithelial processes is in its infancy, but one clue has come from the study of bacteria-phagocyte interactions. The rapid generation of reactive oxygen species (ROS) is a cardinal feature of the phagocytic response to pathogenic and commensal

bacteria, but evidence is accumulating that physiological levels of ROS are also elicited in other cell types in response to microbial signals (6, 7). Our laboratory has previously shown that mammalian intestinal epithelia generate physiological levels of ROS when contacted by certain strains of commensal bacteria (8, 9). This bacterial-induced ROS generation modulates numerous cellular functions including transient oxidative inactivation of enzymes required for modulating cullin-dependent signaling (10, 11), inducing ERK-specific signaling (12), and potentiating epithelial restitution via redox inactivation of focal adhesion kinase phosphatases (13). We also showed that specific taxa composing the microbiota, especially those within the genus *Lactobacillus*, can directly stimulate intestinal stem cell growth and accelerate epithelial growth during homesostasis (9) or wound healing by redox-dependent mechanisms involving NADPH oxidase 1 (14).

In our investigations, we have used the extensively characterized commensal bacteria *Lactobacillus rhamnosus* GG (LGG) as our probiotic model, and found that this strain is especially potent in stimulating ROS generation in contacted mammalian cells (9). The mechanism for this specific property is unknown, and characterization would provide a paradigm for future identification and characterization of candidate probiotics. One possibility is that commensal bacteria that interact with the host have enhanced binding to the intestinal epithelium. Recent studies have identified surface proteins of LGG that are necessary for binding to intestinal mucus. Specifically, a genetic island within the LGG genome contained genes for three secreted LPxTG-like pilins (*spaCBA*). Of these gene products, SpaC was shown to bind mucus *ex vivo* and was required

for LGG adherence to cultured intestinal epithelial monolayers (15-17). Here, we advance these findings by showing that LGG-induced probiotic effects are SpaC-dependent both *in vitro* and *in vivo*. We found that an isogenic LGG *spaC* mutant (LGGΩ*spaC*) exhibited qualitatively lower adherence to both cultured cells and to murine intestinal mucosa compared to wild-type bacteria. The isogenic *spaC* mutant also induced the generation of markedly lower levels of ROS, induced weaker phosphorylation of ERK, and stimulated less cell proliferation compared to wild-type LGG. In addition, LGG's ability to protect against intestinal damage following radiological insult (18) was abolished in mice treated with the *spaC* mutant. Together, these data are evidence that the SpaC pilin subunit is necessary to maintain intimate contact of LGG with the host intestinal epithelia, and that bacterial-host contact is necessary for LGG to elicit beneficial cellular responses.

Chapter 3 Materials and Methods

Bacterial strains, plasmids, and growth conditions. Bacterial strains used in this study include *Lactobacillus rhamnosus* GG (LGG) (ATCC 53103), an isogenic LGG-*spaC* mutant (Ω*spaC*::Ery^r, CMPG10102) (15), and a laboratory strain of *Escherichia coli* K12 (DH5). For routine culture, lactobacilli were grown in deMann-Ragosa-Sharpe (MRS) or LBS media (Difco) at 37^{o}C under static, microaerophilic conditions, while *E. coli* was grown in Luria-Bertaini (LB) media at 37^{o}C with aeration. GFP-expressing LGG and LGGΩ*spaC* were created by transformation with plasmid pJM09, which harbors the GFPmut3* (19) gene inserted at the EcoRI site of plasmid pGK13 (A kind gift from J. Kok,

unpublished). Plasmid pCM (chloramphenicol resistant) and pEM (erythromycin resistant) were employed for *in vivo* experiments requiring antibiotic selection. Chloramphenicol or erythromycin was added to media as needed at 10 μg/ml and 2.5 μg/ml, respectively. Prior to use, all bacteria were gently washed in HBSS or PBS, and then diluted to the appropriate concentration.

Cell culture. The human intestinal epithelial cell lines Caco-2 and T84 were grown in the presence of high glucose (4.5 g/l) Dulbecco's Modified Eagle Medium (Sigma-Aldrich, St. Louis, MO; cat. no. D6429) supplemented with 2 mM L-glutamine, 1% nonessential amino acids, 10% FBS, 100 units/ml penicillin, 100 μg/ml streptomycin at 37°C in a 4% CO_2 atmosphere.

Mice. Six to ten-week-old C57BL/6 (wild-type) mice used for all experiments were purchased from The Jackson Laboratory (Bar Harbor, ME) or bred in the small animal facility at Emory University. After experimental procedures, mice were anesthetized with CO_2 and euthanized by cervical dislocation. All murine experimental procedures were reviewed and approved by the Institutional Animal Care and Use Committee at Emory University and were performed according to the Emory guidelines for the ethical treatment of animals.

Bacterial adhesion assay. For both *in vitro* and *in vivo* adhesion assays, bacteria were labeled with either CellTrace CFSE or CellTrace Far Red DDOA-SE (Life Technologies, Grand Island, NY; cat. nos. 34554 and 34553, respectively) as per manufacturer's instructions. For quantitation of *in vitro* bacterial adhesion, 200 μl of stained LGG, LGGΩ*spaC*, or *E. coli* at 1×10^8 cfu/ml were applied to confluent Caco-2 monolayers in an 8-well microscopic chamber

slide. Bacteria were incubated with cells for 1 hour at 37°C in a 4% CO_2 atmosphere, then gently washed 4 times with 400 µl of HBSS, and fixed with 4% p-formaldehyde (PFA). Cellular actin was stained with Alexa Flour 633 Phalloidin (Life Technologies; cat. no. A12379) or Alexa Fluor 488 Phalloidin (Life Technologies; cat. no. A22284). Cell-attached bacteria were counted by confocal microscopy (Zeiss LSM 510) at 40X magnification in 20 random fields and averaged. For visualization and quantification of *in vivo* bacterial adhesion, mice were given a single 200 µl dose of LGG/pJM09 (GFP-expressing and conferring erythromycin resistance), LGGΩ*spaC*/pJM02 (GFP-expressing and conferring chloramphenicol resistance), or *E. coli*/pJM02 (GFP-expressing and conferring chloramphenicol resistance) at 1×10^{11} cfu/ml by oral gavage. After 1 hour mice were sacrificed and a 2 cm section of the proximal jejunum was removed, opened longitudinally and washed twice with 0.6 ml of 0.2% TritonX-100 in PBS. For bacterial visualization, washed sections were frozen in OCT medium, cut into 7 µm sections, mounted, fixed with 4% PFA, stained with Alexa Fluor 546 Phalloidin and Lectin HPA Alexa Fluor 647 (Life Technologies; cat. nos. A22283 and L32454, respectively), and visualized at 40X by confocal microscopy. For bacterial quantitation, washed sections were homogenized and plated on MRS or LB media containing either erythromycin (5 µg/ml) or chloramphenicol (10 µg/ml).

FISH probes. Oligonucleotide probes were designed to match the specifications of previously validated FISH probes. The Eub338 (5'-GCTGCCTCCCGTAGGAGT-3') probe binds the bacterial 16S rRNA region of a broad range of bacteria genera (20) and the Lcas467 probe (5'-

CCGTCACGCCGACAACAG-3') binds the 16S region of a few select *Lactobacillus* species including *L. rhamnosus* with high specificity (21). A negative control probe consisting of 5'-ACATCCTACGGGAGGC-3' was used to control for non-specific hybridization. All probes were labeled at the N-terminus with fluorescein isothiocyanate (FITC). Eub338 and the negative control probe were synthesized by Sigma-Aldrich (St. Louis, MO), and Lcas467 was synthesized by Eurofins MWG Operon (Ebersberg, Germany).

Fluorescence *in situ* hybridization. Female wild-type mice were orally gavaged with 200 µl of PBS or LGG, LGGΩ*spaC*, or *E. coli* 1×10^{10} cfu/ml daily for 3 days, from day zero through day two. On day 3, 24 hours after the last feeding, mice were euthanized and segments of the jejunum and colon of were snap frozen in OCT. The tissue was cut into 5 µm sections and mounted on slides. Prepared slides were fixed in 10% formalin for 15 min, rinsed in PBS, and stored at -20°C until use. Before hybridization, tissue sections were incubated with lysozyme buffer (1 mg/ml lysozyme, 5 mM EDTA, 1 M Tris-HCl pH 7.5) for 10 min at room temperature to permeabilize the cell wall of slide-mounted bacteria. To prevent non-specific binding of the oligonucleotide probes, tissue sections were then incubated with 1% BSA in PBS for 30 min. A hybridization buffer (0.9 M NaCl, 20 mM Tris/HCl, 0.01% SDS, 35-40% formamide) was prepared with 35% formamide for the Eub338 and negative control probes and 40% formamide for the Lcas467 probe. The probes were added to the buffer at a final concentration of 2.5 ng/µl for the Eub338 and negative control probes and 5 ng/µl for the Lcas467 probe. Tissue sections were incubated with each probe in buffer at 46°C for 3 hours. Slides were then washed thoroughly to remove excess

probe and the nuclear counterstain, TO-PRO-3 Iodide (Life Technologies; cat. no. T3605), was applied. FISH samples were preserved with VECTASHIELD mounting medium (Vector Laboratories, Burlingame, CA; cat. no. H1000) and imaged at 40X using confocal fluorescent microscopy.

***In vitro* measurements of ROS generation.** ROS generation in cultured cells was measured with the cell membrane permeable hydrocyanine-3 dye (hydro-Cy3), which was kindly provided by Dr. Niren Murthy (Georgia Institute of Technology, Atlanta, GA, USA). Briefly, 100 μm hydro-Cy3 in cell-line-specific media was preloaded into Caco-2 cells grown in black-sided 96 well plates by incubation at 37°C in a 4% CO_2 atmosphere for 1 hour in low light conditions followed by washing with HBSS. 1×10^8 cfu of washed bacteria were then applied apically and cellular ROS generation was measured at various time points by a fluorescence microplate reader (SpectraMax M2; Molecular Devices, Sunnyvale, CA, U.S.A.) using excitation and emission wavelengths of 544 nm and 574 nm, respectively.

Confocal microscopy for *in vitro* and *in vivo* ROS generation. For the detection of ROS generation by laser scanning confocal microscopy in *in vitro* cell culture, Caco-2 cells were grown in multi-chamber slides, hydro-Cy3 was preloaded and bacteria were applied as described above. After a predetermined incubation period, cells were washed with HBSS and a coverslip was applied. Fluorescence images were then immediately captured at 40X by laser scanning confocal microscopy using a Helium-Neon excitation laser at 543 nm and a 505-530 nm band-pass filter set. For the visualization of *in vivo* ROS generation, mice were fasted for 16 hours, and then given 200 μl of 100 μm

hydro-Cy3 by IP injection 15 min before the administration of either 200 μl of HBSS or a bacterial suspension at 1 × 10^{10} cfu/ml by oral gavage. Mice were sacrificed 1 hour post-gavage and the proximal jejunum was prepared by whole-mount, as previously described (12). Fluorescent images were immediately captured at 40X by laser scanning confocal microscopy, as described above. For quantitation of ROS generation from intestinal epithelia, fluorescence was measured at 5 random positions on each slide and processed using the ImageJ software package (http://rsb.info.nih.gov/ij) from the National Institutes of Health. Measurements of both *in vitro* and *in vivo* ROS generation are the average of at least 3 independent experiments and representative confocal images are shown.

Immunoblot analysis for *in vitro* and *in vivo* ERK phosphorylation. ERK phosphorylation in cultured epithelial cells in response to bacterial contact was assessed by western blot analysis. Briefly, 1 × 10^{8} cfu of LGG or LGGΩ*spaC* were applied to polarized epithelial monolayers, incubated for a predetermined period of time, washed once with HBSS and then the cells were lysed in SDS–PAGE loading buffer. For the detection of ERK phosphorylation in the murine colon, mice were fasted for 2 to 4 hours and then 100 μl of PBS or LGG, the LGGΩ*spaC* mutant, or *E. coli* at 1 × 10^{7} cfu/ml was administered intrarectally. After 7 min, the colon was removed and opened along the mesenteric border, epithelial cells were removed from the most distal 5 cm of the colon by scraping and lysed in RIPA buffer at 100 mg tissue/ml. Samples were then sonicated and centrifuged at 21,130 x g for 20 min at 4°C. Cell lysates from both *in vitro* and *in vivo* experiments were separated by SDS-PAGE,

transferred to a nitrocellulose membrane, and probed with a primary antibody specific for phospho-ERK (Cell Signaling, Danvers, MA; cat. no. 4370S) or β-actin (Sigma Aldrich; cat. no. A5441). Protein-specific bands were detected using HRP-conjugated secondary antibodies (GE Healthcare, cat. nos. NA934V and NA931V) together with SuperSignal West Pico Chemiluminescent Substrate (Thermo Scientific; cat. no. 34080).

EdU assay for *in vitro* cellular proliferation. Caco-2 cells were assayed for cellular proliferation by EdU incorporation. Semi-confluent Caco-2 monolayers were grown in a chamber slide format and co-incubated with 1×10^8 cfu LGG or LGGΩ*spaC*. After 4 hours, EdU (Life Technologies, cat. no. C10337), which is incorporated during active DNA synthesis, was added to the culture media and incubated for an additional 30 min. Cells were then fixed, stained for DNA, washed, and visualized at 20X by laser scanning confocal microscopy. The percent of proliferating cells was calculated as a ratio of EdU-positive cells versus all cells in a given visual field.

Phospho-histone H3 assay for *in vivo* cellular proliferation. Mice were gavaged orally with 200 μl of PBS or LGG, LGGΩ*spaC*, or *E. coli* at 1×10^{10} cfu/ml. Two to 4 hours after feeding, a 3 cm section of the proximal jejunum was removed, snap frozen in OCT, cut into 6 μm sections, mounted on a glass slide, fixed, stained and visualized at 20X by confocal laser scanning microscopy. The number of PHH3-positive cells per crypt was counted for 5-10 random fields per mouse and averaged.

Irradiation protection assay *in vivo*. Female C57/B6 mice were orally gavaged with 200 μl of PBS or LGG, LGGΩ*spaC*, or *E. coli* at 1×10^{10}

cfu/ml daily for 4 days, beginning at day zero through day three. After feeding on day three, mice were subjected to 12 Gy whole body irradiation, or 0.631 Gy/min for 19.01 min, in a γ Cell 40 ^{137}Cs irradiator. Six hours after irradiation, mice were euthanized via cervical dislocation and dissected. The small bowel was opened along the mesenteric border, prepared as a Swiss roll, and fixed in 10% formalin while shaking overnight. The tissue was processed and embedded in paraffin before being cut for histological analysis. Slides were stained for TUNEL using the Apoptag Plus Peroxidase *In Situ* Apoptosis Detection Kit (Millipore, Billerica, MA; cat. no. S7101) according to the manufacturer's instruction with the exception of using hematoxylin as a counterstain. The number of apoptosis-positive cells per jejunal crypt was determined in 50 crypts per mouse at 40X magnification and averaged.

Statistical analyses and data presentation. Differences between groups of at least $p \leq 0.05$ by a standard two-tailed Student's t-test were considered significant. Error bars represent the standard error of the mean (SEM). Graphpad Prism 6 was used for all graphing and statistical analyses.

Chapter 3 Results

SpaC is necessary for *L. rhamnosus GG* adhesion to cultured cells and to the murine intestinal epithelia. Previous studies investigating LGG adherence employed an *ex vivo* approach where mucus was isolated from the human intestine and binding was assessed *in vitro* (15, 16). As an improvement to this approach, we investigated LGG adherence by direct visualization of fluorescent bacteria both *in vitro* and *in vivo* as well as by plate count. Bacteria

were applied to cultured Caco-2 cells for 1 hour. After several washes to remove unattached bacteria, the treated cells were then fixed, mounted, and visualized by confocal microscopy. Similar to previous reports using purified mucus, we detected significantly higher numbers of wild-type LGG adhered to cultured cells compared to the isogenic *spaC* mutant or *E. coli* K12 control (Figure 1A and B). LGG has the capacity to bind intestinal mucus of disparate species; therefore, to further assess the binding properties of LGG *in vivo,* we assayed bacterial adhesion within the mouse small intestine (22). For this purpose, GFP-expressing strains of LGG, its isogenic *spaC* mutant, or *E. coli* were fed to wild-type mice and then the number of adherent bacteria was measured by both confocal microscopy and direct plating as detailed in Materials and Methods. Both methods detected significantly higher numbers of LGG adhering to the murine small intestinal mucosa (by at least 2 orders of magnitude) compared to the isogenic *spaC* mutant or *E. coli* control (Figure 2A and B). Finally, fluorescence *in situ* hybridization (FISH) was performed to visually determine the effects of the *spaC* mutation on the ability of LGG to adhere and persist in the intestine. Wild type mice were fed a daily dose of LGG, its isogenic *spaC* mutant, or *E. coli* for three days and sacrificed 24 hours after the last dose. Intestinal sections were subjected to FISH using a *Lactobacillus*-specific probe Lcas467. Confocal analysis of the tissue revealed that LGG, but not the *spaC* mutant, formed a layer directly luminal of the intestinal epithelial cells in both colon and small intestine samples (Figure 2C). Together, these data show that the SpaC pilin subunit is required for stable adherence of LGG to the intestinal mucosa.

***L. rhamnosus GG* Ω*spaC* is a less potent inducer of ROS generation in cultured epithelial cells and the murine intestine.** Our research group recently reported that contact of cultured cells with LGG induces the generation of physiological levels of ROS (9). Here, we examine whether LGG must be in physical contact with intestinal enterocytes to induce ROS generation. Cultured Caco-2 cells were treated with the cell-permeant ROS-indicator hydrocyanine-3 dye (hydro-Cy3) before being overlaid with bacteria (23). Confocal analysis revealed markedly lower induction of cellular ROS in cells contacted by the *spaC* mutant compared to wild-type LGG (Figure 3A). In addition, fluorometric quantification confirmed significantly reduced levels of ROS generation induced by the pilin mutant (Figure 3B). An increase in ROS generation was not observed when cells were treated with LGG-conditioned media (data not shown). We also recapitulated these observations *in vivo*. Mice were intraperitoneally administered hydro-Cy3 and subsequently fed LGG, its isogenic *spaC* mutant, or *E. coli* by gavage. Microscopic analysis of whole mounted sections of the jejunum revealed a near total loss of ROS generation following feeding of the *spaC* mutant compared to wild-type LGG (Figure 4A and B). These data indicate that SpaC–mediated adhesion of LGG to cultured cells and to epithelial cells in the jejunum is required to elicit maximal generation of cellular ROS.

***L. rhamnosus GG* SpaC is required for efficient ERK phosphorylation in polarized cultured cells and the murine small intestine.** Previous studies from our laboratory have shown that contact of LGG with the apical surface of polarized, cultured epithelial cells induces rapid ERK

phosphorylation without provoking the pro-inflammatory NF-κB or the pro-apoptotic JNK signaling pathways (12). Additionally, we demonstrated ERK induction occurs by a redox-sensitive mechanism (8). Therefore, we examined the extent to which LGG-induced phosphorylation of ERK is dependent on SpaC-mediated bacterial contact. Polarized T84 cells were overlaid with LGG or the *spaC* mutant for up to 30 minutes before analysis of cellular lysates by immunoblot. Contact with wild-type LGG induced significantly higher levels of ERK phosphorylation compared to the isogenic *spaC* mutant (Figure 5A). Notably, inclusion of the anti-oxidant *N*-acetyl-cysteine virtually abolished bacterial-dependent ERK phosphorylation, confirming that LGG-stimulated activation of this MAPK requires intracellular ROS generation as described previously (8). These events were also studied *in vivo*; intrarectal administration of wild-type LGG induced significantly higher levels of ERK phosphorylation in colonic epithelial cells compared to the *spaC* mutant or controls (Figure 5B and C). These data indicate that SpaC-mediated contact of LGG with cells is essential for activation of the ERK signaling pathway *in vitro* as well as *in vivo*.

***L. rhamnosus GG* SpaC contributes to bacterial-dependent cellular proliferation.** The ERK1/2 MAP kinase is involved in diverse, critical cellular functions, including differentiation, motility, and proliferation (24, 25). We have previously demonstrated that LGG applied directly to cultured epithelial cells can induce cellular proliferation (8). Thus, we next considered whether direct, SpaC-mediated contact of LGG with intestinal cells is necessary to induce a pro-proliferative response. After incubation of cultured Caco-2 cells with LGG or the *spaC* mutant, the thymidine nucleoside analog, EdU, was added to

measure active DNA synthesis. Consistent with our previous report, the application of LGG significantly increased the ratio of proliferating cells within the population, whereas no significant difference from media control was detected following treatment with the *spaC* mutant (Figure 6A and B).

Our group has recently reported that LGG, when administered orally, increases proliferative cell numbers in the murine small intestinal crypts in intact gut (9), while transrectal administration of LGG can stimulate colonic epithelial proliferation and migration post-injury (14). In order to investigate the importance of SpaC for LGG-induced cellular proliferation, we quantified phospho-histone H3 (PHH3) in the proximal murine small intestine after oral administration of LGG, its isogenic *spaC* mutant, or *E. coli*. As previously demonstrated, feeding of LGG leads to a significant increase in epithelial cell proliferation; however, mice fed either the *spaC* mutant or *E. coli* did not exhibit significantly increased numbers of PHH3-positive cells compared to buffer alone (Figure 7A and B). Taken together, these data indicate that the SpaC pilin subunit of wild-type LGG is necessary to stimulate robust cellular proliferation both in cultured epithelial cells and in the murine small intestine.

The *L. rhamnosus GG* SpaC pilin subunit contributes to cellular protection from radiation-induced intestinal injury. Previous research has established that LGG can protect small intestines from radiation-induced injury and reduces the amount of cellular apoptosis observed in intestinal crypts after exposure to gamma irradiation (18). To investigate whether the SpaC subunit is required for this protection, mice were orally gavaged with PBS, LGG, its isogenic *spaC* mutant, or *E. coli* prior to whole body irradiation. Staining for

broken DNA by the TUNEL method in histological sections revealed that mice treated with LGG, but not the *spaC* mutant, had markedly reduced amounts of apoptosis in their jejunal crypts when compared to controls (Figure 8A and B). These data indicate that the SpaC pilin is essential for LGG's protective effect against radiation-induced injury.

Chapter 2 Discussion

The taxonomic, anatomic, and functional characterization of the mammalian intestinal microbiota has become a subject of increasing interest. Nucleic acid-based techniques have allowed detailed descriptions of this microbial community structure in both spatial and temporal distribution, while identifying intriguing correlations with normal intestinal functions as well as in disease conditions. One specific realization from this body of work is that the intestinal microbiota can exist in a luminal, planktonic state or can occupy a mucosal-associated niche. While the former are often bacteria with fermentative capacity, recent work suggests that mucosal-associated microbes are responsible for many of the physiological functions normally attributed to the entire population. These taxa, which include *Lactobacillus*, *Bifidobacterium*, and *Bacteroides*, have a wide variety of functions ascribed to them; for example, *Lactobacillus reuteri* can inhibit Western-diet-associated obesity (26), *Bifidobacterium infantis*-conditioned medium enhances intestinal epithelial cell barrier function (27), *Bacteroides thetaiotaomicron* is known to induce gene regulatory events in the upper GI tract (28), and *Bacteroides fragilis* has been shown to influence immune development and enhance barrier function (29). Studies from our

research group and others have shown that lactobacilli stimulate epithelial ROS generation and activate motility and proliferation events. Thus, an emerging paradigm of host-commensal interactions suggests key roles for specific mucosal-associated taxa.

As the mucosal epithelial membrane is insulated from direct contact with the microbiota by a glycocalyx and layers of secreted mucins, the study of commensal interactions with these complex carbohydrates has become a topic of considerable interest. Pathogens, such as *Helicobacter pylori*, typically reside within this mucous layer, and a functional class of bacteria, often with mucolytic capacity, has also been identified in this environment (30). The mucous layer not only provides a constant and renewable energy source, but also forms a substrate for adhesion, and may play a role in bacterial persistence.

The recent discovery of a sortase-dependent pili *spaCBA* gene cluster in the well-characterized probiotic LGG, which is required for mucus attachment, may be indicative of a wider phylogenetic distribution of such genes in commensal bacteria (15). Here, we advance the functional characterization of the SpaC protein by showing that 1) SpaC is necessary for LGG to maintain contact with the host mucous layer overlaying the intestinal epithelia *in vivo*, and 2) that SpaC-mediated bacterial-host contact is essential for LGG to elicit its cellular modulatory responses. Specifically, we show that LGG, but not its isogenic *spaC* mutant, efficiently elicits cellular ROS generation at physiological levels, potentiates ERK MAPK signaling, stimulates cellular proliferation, and protects against radiation-induced injury. Together, these data are direct functional evidence for the role of SpaC in mediating the probiotic effects of LGG.

While Gram-positive bacterial pili were first studied in pathogens, they are increasingly being recognized as important components of Gram-positive commensal biology. These pili are formed by subunits encoded in gene clusters that typically contain a major and one or more minor pilin genes, and are located in close proximity to a pilin-specific sortase. Following translation, pilin subunits are transported out of the cell via the Sec pathway and remain attached to the membrane through their C-terminal hydrophobic tails. These proteins contain a LPxTG-like domain that is subsequently recognized by the membrane-associated pilin sortase that covalently joins subunits to construct a functional pilus. The shaft of each pilus is primarily composed of major pilin subunits with one minor subunit at the tip. Depending on the type of bacteria, this minor subunit may also be dispersed along the pilus shaft. If multiple minor subunits exist they may be located at the pilus base near the cell wall or found dispersed throughout the structure. Once all subunits have been polymerized, a housekeeping sortase is responsible for covalently attaching the pilus to the cell wall (31, 32).

Unsurprisingly, additional lactobacilli display mucosal adhesive properties, and other species with the capacity to bind mucins are actively being identified, as are the proteins involved in these interactions (33). In 2002, Roos and Jonsson identified a protein in *L. reuteri* 1063 that could bind pig and hen mucus. This protein, named Mub due to its mucus binding capacity, contained a LPQTG domain and displayed robust mucus adhesion at pH's below neutral, potentially indicating that its capacity to bind mucus was most important under the acidic conditions that would be encountered during passage through a digestive tract (34). *Lactobacillus plantarum* contains a gene that has been

designated mannose-specific adhesion (*msa*) due it is ability to bind the common epithelial sugar mannose. The Msa protein is homologous to Mub and also contains an LPxTG-like domain. *L. plantarum* strains expressing Msa can agglutinate the yeast *Saccharomyces cerevisiae*, a finding that might explain how these strains competitively inhibit intestinal pathogens (35). *L. plantarum* Lp6 has the capacity to bind rat mucus and can also agglutinate *S. cerevisiae*; this strain also likely encodes a *msa* gene since the addition of D-mannose inhibits the aforementioned properties (36). GroEL, identified in *Lactobacillus johnsonii* La1, binds mucus and HT29 cells in a pH-dependent manner and, similar to Msa, has the ability to agglutinate *H. pylori* (37).

Until recently, it was widely held that commensal bacteria elicited their positive influences on the intestine solely by mechanisms such as competitive exclusion of pathogens or the fermentation of complex dietary carbohydrates. However, recent reports by our research group and others show that commensal microbes are actively involved in modulating host cellular signaling processes. Genes that initially evolved to facilitate gastrointestinal colonization through physical attachment may have subsequently adapted to ensure persistence through more complex interactions. Experiments comparing the binding capacities between wild-type *L. plantarum* 299v and a *msa*-deficient mutant showed that Msa is not required for binding jejunal mucosa in pigs. While the wild-type lactobacilli had a slight competitive advantage over the *msa* mutant in direct competition, the study indicated that Msa was more important for host gene regulation than physical adhesion (38). Two secreted LGG proteins, p40 and p70, can contribute to intestinal epithelial homoeostasis by preventing

apoptosis as well as promoting proliferation (39, 40). Interestingly, the *Lactobacillus casei* BL23 homologues of these factors, known as CmuA or CmuB, can hydrolyze muropeptides and bind mucin in addition to their homeostatic capacity (41).

In our past studies, we showed that the bacterial product, *N*-formyl-Met-Leu-Phe (fMLF) is a ligand for the Formyl Peptide Receptor (FPR) located on the apical side of epithelial cells, interfacing with the microbiota. Moreover, fMLF binding to FPR potentiated the specific and ROS-dependent activation of the ERK MAPK signaling pathway. The elevated capacity of commensal bacteria to bind the mucous layer may result in more frequent and sustained contact of fMLF peptides with cell surface-localized FPRs. However, fMLF-FPR binding is certainly only one example of a commensal bacterial-host ligand-receptor interaction. Additional interactions between bacterial proteins/products and cellular pattern recognition receptors, such as Toll-like or Nod-like receptors, clearly influence host signaling. Importantly, whether LGG displays specific surface decorations that can directly bind host cellular receptors remains an open question.

Abnormal composition of the microbiota, known as a “dysbiotic flora,” has been implicated in the pathogenesis of inflammatory bowel diseases and some systemic immune disorders (5). We show here that the beneficial effects of LGG, a well-established probiotic, and, by extension, the effects of a normal microbiota, are potentiated by intimate and persistent bacterial contact with the intestinal mucous layer. The appearance of mucus binding proteins in gut commensal inhabitants facilitates a mutualistic relationship where the bacteria

benefit by securing a stable niche, and the host benefits from a wide range of activities provided by the microbiota. Importantly, the abundance of mucus binding proteins, such as SpaC, in the intestinal microbiota may be an indicator of the condition of this microbial population and its potential to elicit beneficial influences on host health. Conversely, the absence of mucus binding genes may be a hallmark of a dysbiotic flora. The development of meta-genomic and deep sequencing techniques will facilitate the identification of these genes. Moreover, application of these techniques will advance the spatial and temporal characterization of these indicator genes along the entire gastrointestinal tract and will provide insights into the establishment of a healthy microbiota in the mammalian gut.

Chapter 3 Figures

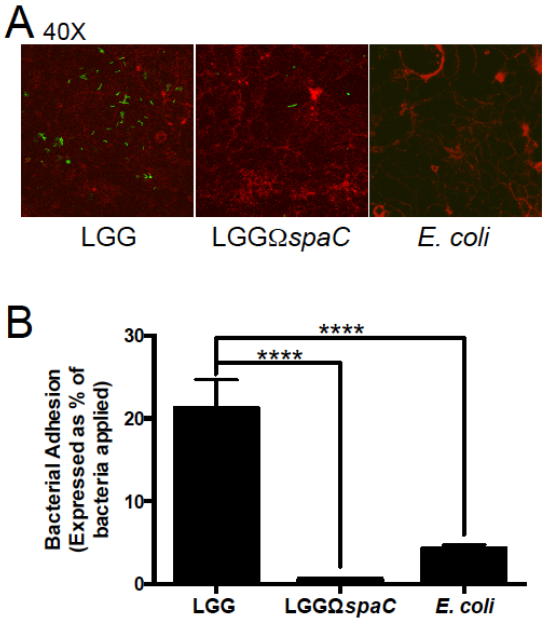

Figure 1. The *L. rhamnosus* GG SpaC pilin protein is required for adherence to cultured intestinal epithelial cells. (A) Adhesion of LGG, LGGΩ*spaC*, and *E. coli* to cultured, confluent Caco-2 intestinal epithelial cells. 2×10^7 cfu bacteria were stained with a fluorescent, cell-permeant dye, co-incubated with epithelial cells in a chamber slide format for 1 hour, gently washed with HBSS and then prepared for confocal microscopy as described in Materials and Methods. Green, bacteria; red, cellular actin. Representative results shown. (B) Quantification of cell-adherent bacteria from confocal images averaged from 20 random fields. Experiments were repeated at least 3 times with similar results. ****= $p < 0.0001$.

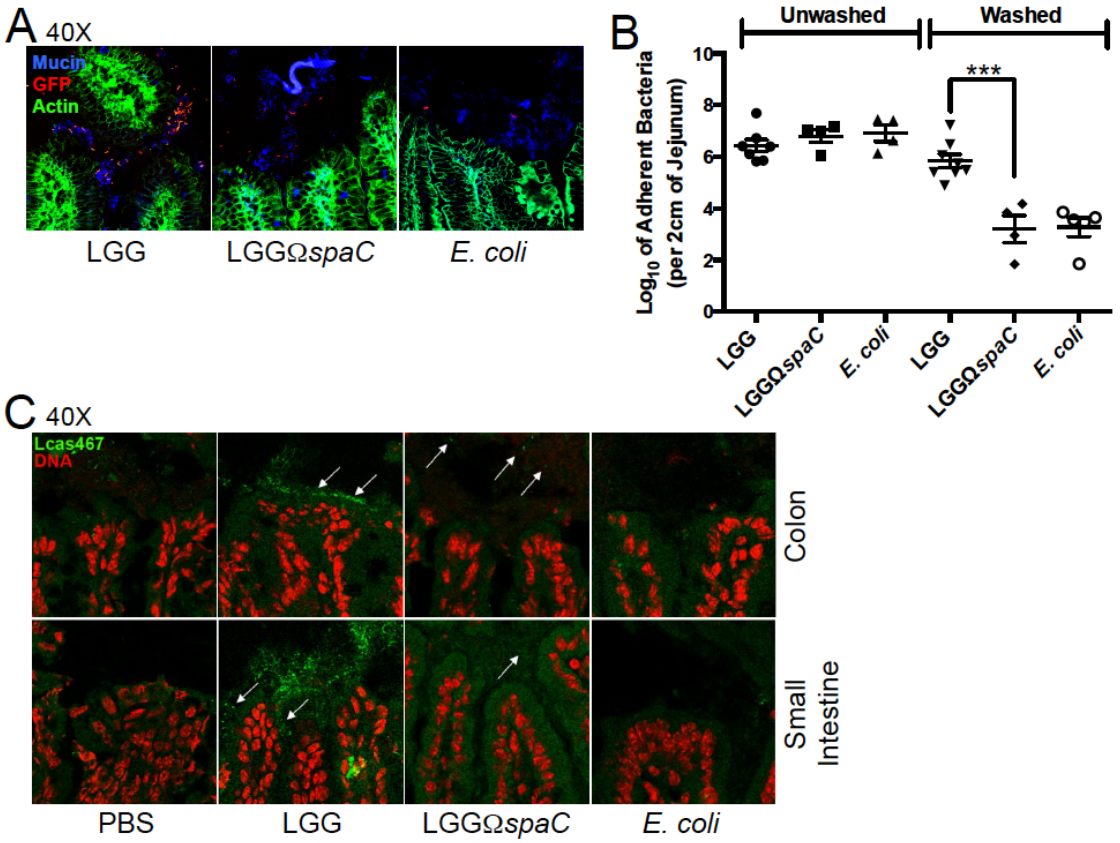

Figure 2. The *L. rhamnosus GG* SpaC pilin protein is required for robust adherence to murine intestinal mucosa. (A) Adhesion of GFP-expressing LGG, LGGΩ*spaC*, and *E. coli* to murine intestinal mucosa. 2 × 10^{10} cfu of bacteria were fed by oral gavage, 1 hour after which a 2 cm section of the proximal jejunum was removed, washed, and frozen in OCT media, mounted and stained for confocal microscopy. Blue, mucus; red, GFP expressing bacteria; green, cellular actin. (B) Quantification of mucosa-attached bacteria. 2 cm sections of proximal jejunum tissue were obtained from mice treated as in "A." This tissue was then washed, homogenized and plated on antibiotic-containing media. Experiments were repeated at least 4 times with similar results. ***= $p < 0.001$. (C) FISH of murine

intestines using a *Lactobacillus* specific probe, Lcas467 (white arrows). Samples were taken 24 hours after mice were given the final of 3 daily doses of 2×10^9 cfu of bacteria and prepared as described in Materials and Methods.

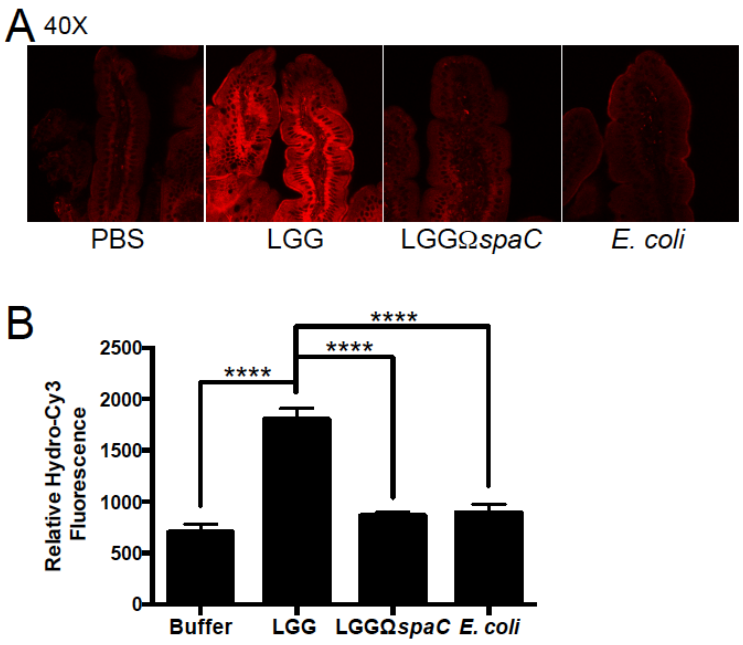

Figure 3. *L. rhamnosus* GG Ω*spaC* is compromised for bacterial-induced cellular ROS generation. (A) Cellular ROS generation induced by LGG, LGGΩ*spaC*, and *E. coli* within Caco-2 intestinal epithelial cells. Cell monolayers were preloaded with hydro-Cy3, washed, and incubated with 1×10^8 cfu bacteria in a chamber slide format for 1 hour, after which the slide was mounted and visualized by confocal microscopy. Representative results shown. Red, ROS; Blue, DNA (B) Quantification of cellular ROS induction in Caco-2 cells by LGG, LGGΩ*spaC*, or *E. coli*. Cell monolayers grown in 96-well microplates were preloaded with hydro-Cy3, washed, and incubated with 1×10^8 cfu bacteria. ROS was measured at various time points up to 1 hour in a fluorescence microplate reader. Experiments were repeated at least 3 times.

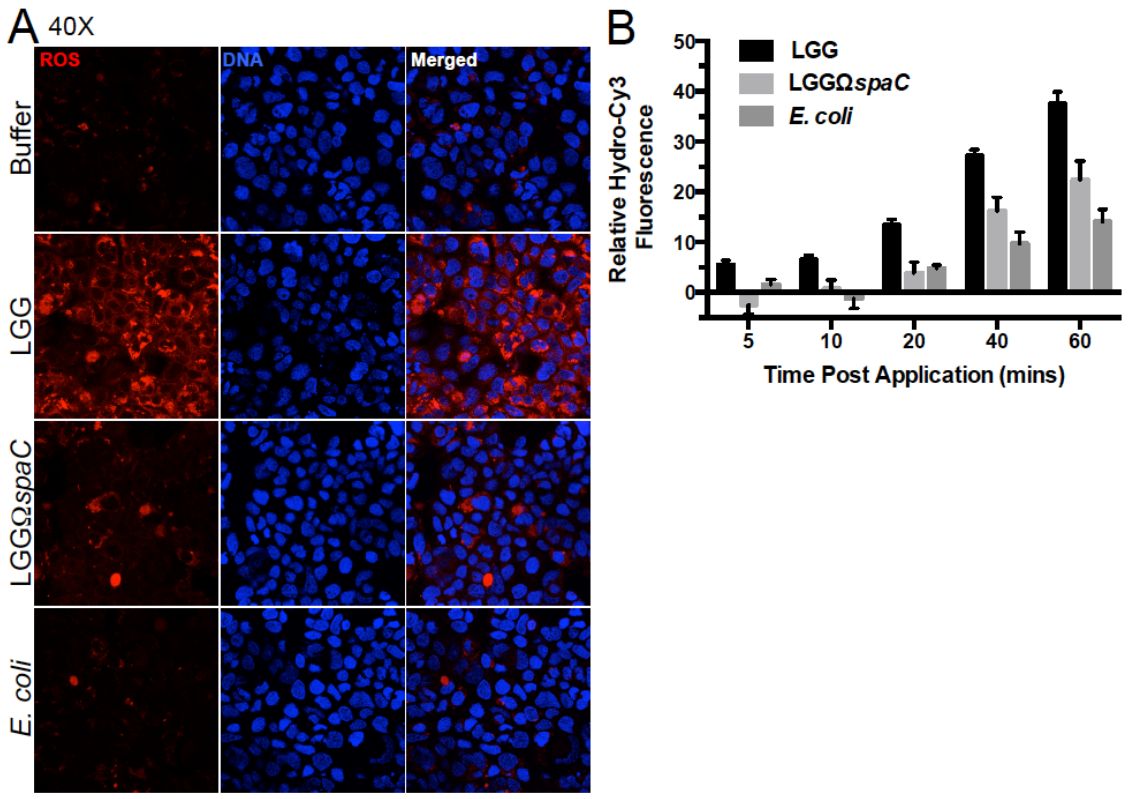

Figure 4. The *L. rhamnosus* GG SpaC pilin contributes to bacterial-induced cellular ROS generation in the murine intestine. (A) Cellular ROS generation in the murine intestine induced by LGG, LGGΩ*spaC*, or *E. coli*. Hydro-Cy3 was administered IP 15 minutes before oral gavage of 2 × 10^9 cfu bacteria. The proximal jejunum was prepared by whole mount as described in Materials and Methods and examined by confocal microscopy. Representative images at 40x magnification shown. Red, ROS (B) Quantification of ROS in the murine intestine induced by LGG, LGGΩ*spaC*, or *E. coli* as shown in "A". Average ROS fluorescence intensity was measured at 5 random fields within the epithelia and averaged. ****= $p < 0.0001$. Experiments were repeated at least 3 times.

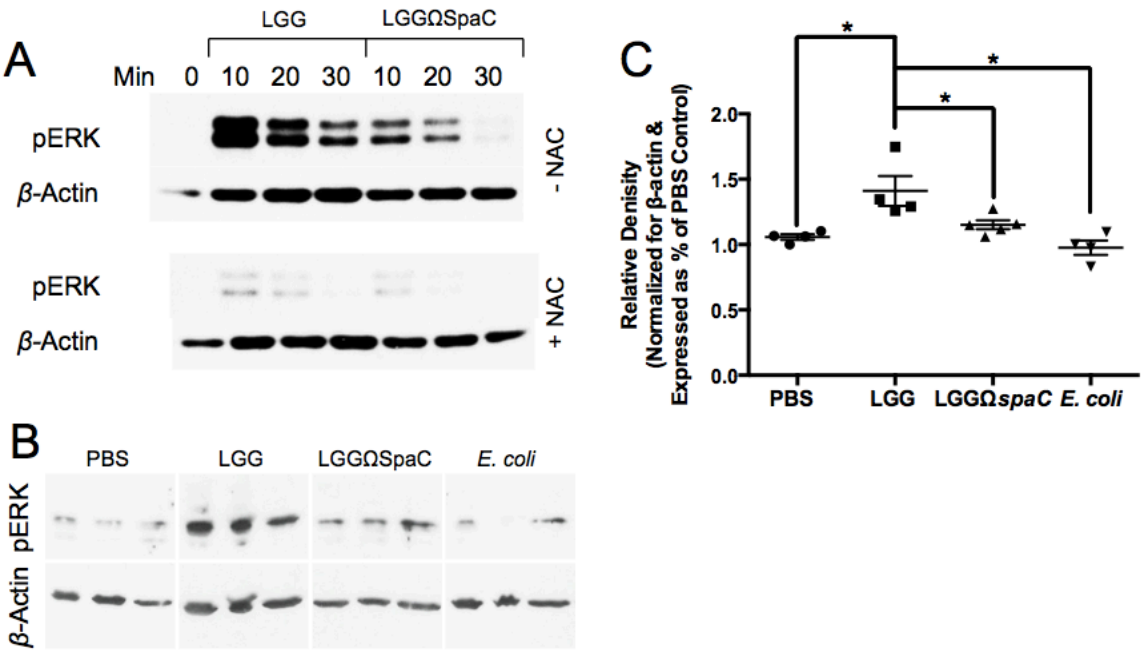

Figure 5. The SpaC pilin subunit is required for efficient *L. rhamnosus* GG-dependent ERK phosphorylation. (A) Phosphorylation of cellular ERK within cultured epithelial cells after contact by LGG or LGGΩ*spaC*. 1 × 10^8 cfu bacteria were applied apically to polarized T84 cell monolayers grown on transwell inserts and incubated for various times before immunobloting for phospho-ERK and *β*-actin (as described in Material and Methods). NAC, *N*-acetyl-cysteine (B) Phosphorylation of cellular ERK in murine colonic epithelial cells after treatment with LGG, LGGΩ*spaC*, or *E. coli*. Colon epithelial cells were harvested from mice 7 minutes after intrarectal injections with 1 × 10^6 cfu bacteria. Images were taken from the same blot but rearranged for clarity. (C) Quantification of ERK phosphorylation as shown in "B". The amount of phosphorylated ERK was normalized for *β*-actin and compared to a sample treated with PBS. n ≥ 4, * = $p < 0.05$

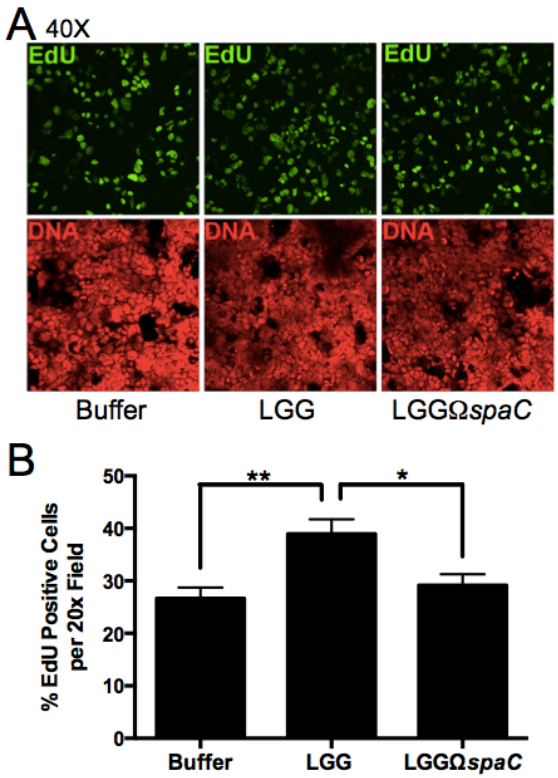

Figure 6. *L. rhamnosus* GG-induced *in vitro* cellular proliferation is SpaC-dependent. (A) Detection of EdU-positive cells in cultured epithelial cells following contact by either LGG or LGGΩ*spaC*. 1×10^8 cfu bacteria were applied to semi-confluent Caco-2 cell monolayers and assayed for proliferation as described in Materials and Methods. Representative results shown. (B) Quantification of cellular proliferation after contact of Caco-2 cell monolayers by LGG or LGGΩ*spaC* as shown in "A". The average number of EdU-positive cells was quantified as a ratio of the total number of cells counted at 10 random fields. Experiments were repeated at least 3 times. * = $p < 0.05$; ** = $p < 0.01$.

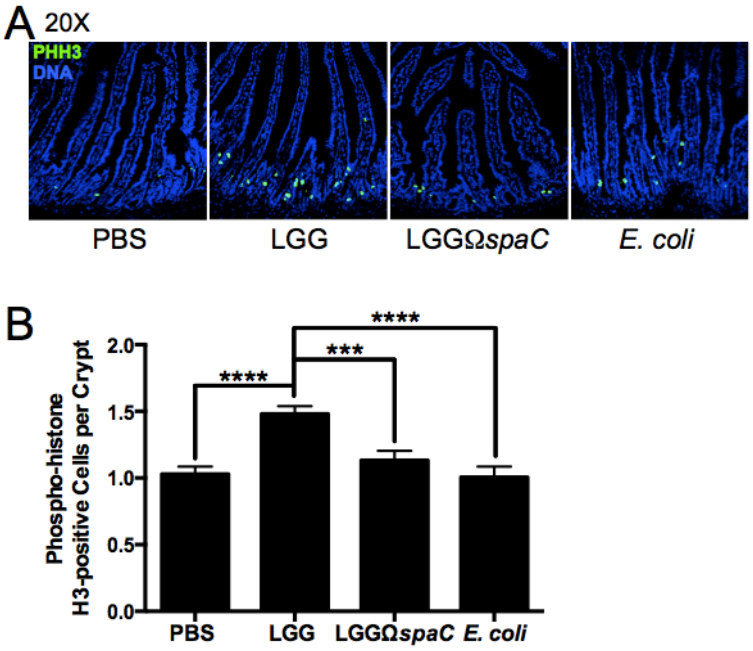

Figure 7. *L. rhamnosus* GG-induced *in vivo* cellular proliferation is SpaC-dependent. (A) Visualization of phospho-histone H3 (PHH3)-positive proliferating epithelial cells in the murine proximal small intestine following administration of LGG, LGGΩ*spaC*, or *E. coli*. 2 × 10^9 cfu bacteria were given by oral gavage and cell staining was performed as described in Materials and Methods. (B) Quantification of small intestinal epithelial proliferation as shown in "A". The average number of PHH3-positive cells is expressed as a ratio of the number of crypts counted in 5-10 random fields for each mouse. n=5, *** = $p < 0.001$; **** = $p < 0.0001$.

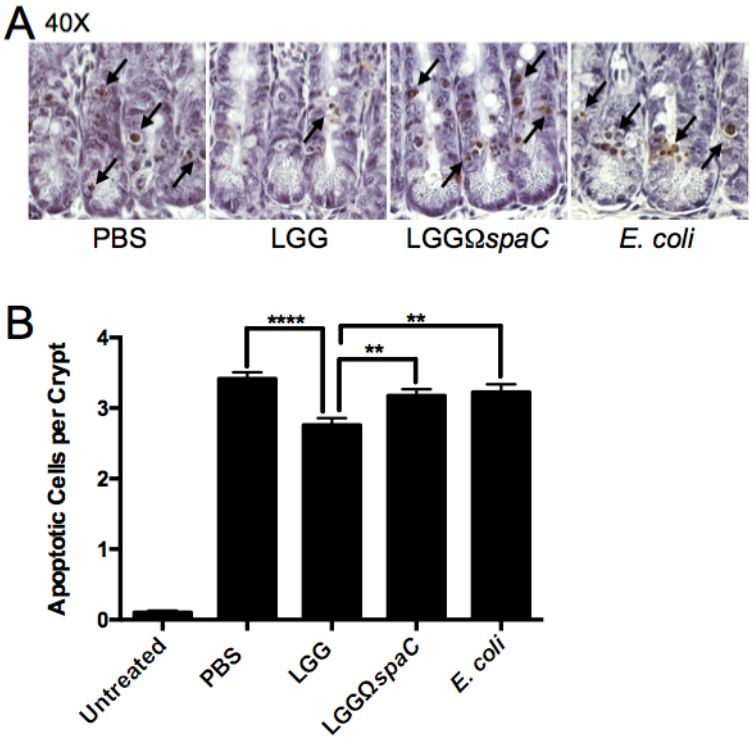

Figure 8. *L. rhamnosus* GG-induced *in vivo* cellular protection is SpaC-dependent. (A) Visualization of TUNEL positive apoptotic cells (black arrows) in murine jejunum following administration of LGG, LGGΩ*spaC*, or *E. coli* and irradiation treatment. Mice were orally gavaged with 2 × 10^9 cfu bacteria once daily for 4 days and then exposed to 12 Gy whole body irradiation. Cell staining was performed as described in Materials and Methods. (B) Quantification of apoptosis in the jejunum as shown in "A" and expressed as average number of apoptotic cells per jejunal crypt. 50 crypts per mouse, n=4, ** = $p < 0.01$; **** = $p < 0.0001$.

Chapter 3 Acknowledgements

We would like to thank Dr. Soile Tykkynen for providing the *L. rhamnosus* GG Ω*spaC* strain and Dr. Niren Murthy for providing the hydrocyanine-3 dye.

This work was supported by NIH Grants RO1AL64462 (to A.S.N.), K12GM000680 (to J.W.M.), and R01DK098391 (to R.M.J.).

Chapter 3 References

1. **Hooper LV, Gordon JI.** 2001. Commensal host-bacterial relationships in the gut. Science **292:**1115-1118.
2. **Neish AS.** 2009. Microbes in gastrointestinal health and disease. Gastroenterology **136:**65-80.
3. **Thomas CM, Versalovic J.** 2010. Probiotics-host communication: Modulation of signaling pathways in the intestine. Gut microbes **1:**148-163.
4. **Pull SL, Doherty JM, Mills JC, Gordon JI, Stappenbeck TS.** 2005. Activated macrophages are an adaptive element of the colonic epithelial progenitor niche necessary for regenerative responses to injury. Proc. Natl. Acad. Sci. U. S. A. **102:**99-104.
5. **Sartor RB.** 2008. Microbial influences in inflammatory bowel diseases. Gastroenterology **134:**577-594.
6. **Neish AS.** 2013. Redox signaling mediated by the gut microbiota. Free Radic. Res. **47:**950-957.
7. **Lambeth JD.** 2004. NOX enzymes and the biology of reactive oxygen. Nat. Rev. Immunol. **4:**181-189.

8. **Wentworth CC, Alam A, Jones RM, Nusrat A, Neish AS.** 2011. Enteric commensal bacteria induce extracellular signal-regulated kinase pathway signaling via formyl peptide receptor-dependent redox modulation of dual specific phosphatase 3. J. Biol. Chem. **286:**38448-38455.

9. **Jones RM, Luo L, Ardita CS, Richardson AN, Kwon YM, Mercante JW, Alam A, Gates CL, Wu H, Swanson PA, Lambeth JD, Denning PW, Neish AS.** 2013. Symbiotic lactobacilli stimulate gut epithelial proliferation via Nox-mediated generation of reactive oxygen species. EMBO J.

10. **Kumar A, Wu H, Collier-Hyams LS, Hansen JM, Li T, Yamoah K, Pan ZQ, Jones DP, Neish AS.** 2007. Commensal bacteria modulate cullin-dependent signaling via generation of reactive oxygen species. EMBO J. **26:**4457-4466.

11. **Kumar A, Wu H, Collier-Hyams LS, Kwon YM, Hanson JM, Neish AS.** 2009. The bacterial fermentation product butyrate influences epithelial signaling via reactive oxygen species-mediated changes in cullin-1 neddylation. J. Immunol. **182:**538-546.

12. **Wentworth CC, Jones RM, Kwon YM, Nusrat A, Neish AS.** 2010. Commensal-epithelial signaling mediated via formyl peptide receptors. Am. J. Pathol. **177:**2782-2790.

13. **Swanson PA, 2nd, Kumar A, Samarin S, Vijay-Kumar M, Kundu K, Murthy N, Hansen J, Nusrat A, Neish AS.** 2011. Enteric commensal bacteria potentiate epithelial restitution via reactive oxygen

species-mediated inactivation of focal adhesion kinase phosphatases. Proc. Natl. Acad. Sci. U. S. A. **108:**8803-8808.

14. **Alam A, Leoni G, Wentworth CC, Kwal JM, Wu H, Ardita CS, Swanson PA, Lambeth JD, Jones RM, Nusrat A, Neish AS.** 2013. Redox signaling regulates commensal-mediated mucosal homeostasis and restitution and requires formyl peptide receptor 1. Mucosal Immunol.

15. **Kankainen M, Paulin L, Tynkkynen S, von Ossowski I, Reunanen J, Partanen P, Satokari R, Vesterlund S, Hendrickx AP, Lebeer S, De Keersmaecker SC, Vanderleyden J, Hamalainen T, Laukkanen S, Salovuori N, Ritari J, Alatalo E, Korpela R, Mattila-Sandholm T, Lassig A, Hatakka K, Kinnunen KT, Karjalainen H, Saxelin M, Laakso K, Surakka A, Palva A, Salusjarvi T, Auvinen P, de Vos WM.** 2009. Comparative genomic analysis of Lactobacillus rhamnosus GG reveals pili containing a human-mucus binding protein. Proc. Natl. Acad. Sci. U. S. A. **106:**17193-17198.

16. **von Ossowski I, Reunanen J, Satokari R, Vesterlund S, Kankainen M, Huhtinen H, Tynkkynen S, Salminen S, de Vos WM, Palva A.** 2010. Mucosal adhesion properties of the probiotic Lactobacillus rhamnosus GG SpaCBA and SpaFED pilin subunits. Appl. Environ. Microbiol. **76:**2049-2057.

17. **Lebeer S, Claes I, Tytgat HL, Verhoeven TL, Marien E, von Ossowski I, Reunanen J, Palva A, Vos WM, Keersmaecker SC, Vanderleyden J.** 2012. Functional analysis of Lactobacillus rhamnosus

GG pili in relation to adhesion and immunomodulatory interactions with intestinal epithelial cells. Appl. Environ. Microbiol. **78:**185-193.

18. **Ciorba MA, Riehl TE, Rao MS, Moon C, Ee X, Nava GM, Walker MR, Marinshaw JM, Stappenbeck TS, Stenson WF.** 2012. Lactobacillus probiotic protects intestinal epithelium from radiation injury in a TLR-2/cyclo-oxygenase-2-dependent manner. Gut **61:**829-838.
19. **Cormack BP, Valdivia RH, Falkow S.** 1996. FACS-optimized mutants of the green fluorescent protein (GFP). Gene **173:**33-38.
20. **Amann RI, Binder BJ, Olson RJ, Chisholm SW, Devereux R, Stahl DA.** 1990. Combination of 16S rRNA-targeted oligonucleotide probes with flow cytometry for analyzing mixed microbial populations. Appl. Environ. Microbiol. **56:**1919-1925.
21. **Quevedo B, Giertsen E, Zijnge V, Luthi-Schaller H, Guggenheim B, Thurnheer T, Gmur R.** 2011. Phylogenetic group- and species-specific oligonucleotide probes for single-cell detection of lactic acid bacteria in oral biofilms. BMC Microbiol. **11:**14.
22. **Rinkinen M, Westermarck E, Salminen S, Ouwehand AC.** 2003. Absence of host specificity for in vitro adhesion of probiotic lactic acid bacteria to intestinal mucus. Vet. Microbiol. **97:**55-61.
23. **Kundu K, Knight SF, Willett N, Lee S, Taylor WR, Murthy N.** 2009. Hydrocyanines: a class of fluorescent sensors that can image reactive oxygen species in cell culture, tissue, and in vivo. Angew. Chem. Int. Ed. Engl. **48:**299-303.

24. **Manning G, Plowman GD, Hunter T, Sudarsanam S.** 2002. Evolution of protein kinase signaling from yeast to man. Trends Biochem. Sci. **27:**514-520.

25. **Ramos JW.** 2008. The regulation of extracellular signal-regulated kinase (ERK) in mammalian cells. Int. J. Biochem. Cell Biol. **40:**2707-2719.

26. **Poutahidis T, Kleinewietfeld M, Smillie C, Levkovich T, Perrotta A, Bhela S, Varian BJ, Ibrahim YM, Lakritz JR, Kearney SM, Chatzigiagkos A, Hafler DA, Alm EJ, Erdman SE.** 2013. Microbial reprogramming inhibits Western diet-associated obesity. PLoS One **8:**e68596.

27. **Ewaschuk JB, Diaz H, Meddings L, Diederichs B, Dmytrash A, Backer J, Looijer-van Langen M, Madsen KL.** 2008. Secreted bioactive factors from Bifidobacterium infantis enhance epithelial cell barrier function. Am. J. Physiol. Gastrointest. Liver Physiol. **295:**G1025-1034.

28. **Hooper LV, Wong MH, Thelin A, Hansson L, Falk PG, Gordon JI.** 2001. Molecular analysis of commensal host-microbial relationships in the intestine. Science **291:**881-884.

29. **Mazmanian SK, Liu CH, Tzianabos AO, Kasper DL.** 2005. An immunomodulatory molecule of symbiotic bacteria directs maturation of the host immune system. Cell **122:**107-118.

30. **Ouwerkerk JP, de Vos WM, Belzer C.** 2013. Glycobiome: bacteria and mucus at the epithelial interface. Best Pract. Res. Clin. Gastroenterol. **27:**25-38.

31. **Scott JR, Zahner D.** 2006. Pili with strong attachments: Gram-positive bacteria do it differently. Mol. Microbiol. **62:**320-330.

32. **Marraffini LA, Dedent AC, Schneewind O.** 2006. Sortases and the art of anchoring proteins to the envelopes of gram-positive bacteria. Microbiol. Mol. Biol. Rev. **70:**192-221.

33. **O'Callaghan J, O'Toole PW.** 2013. Lactobacillus: host-microbe relationships. Curr. Top. Microbiol. Immunol. **358:**119-154.

34. **Roos S, Jonsson H.** 2002. A high-molecular-mass cell-surface protein from Lactobacillus reuteri 1063 adheres to mucus components. Microbiology **148:**433-442.

35. **Pretzer G, Snel J, Molenaar D, Wiersma A, Bron PA, Lambert J, de Vos WM, van der Meer R, Smits MA, Kleerebezem M.** 2005. Biodiversity-based identification and functional characterization of the mannose-specific adhesin of Lactobacillus plantarum. J. Bacteriol. **187:**6128-6136.

36. **Sun J, Le GW, Shi YH, Su GW.** 2007. Factors involved in binding of Lactobacillus plantarum Lp6 to rat small intestinal mucus. Lett. Appl. Microbiol. **44:**79-85.

37. **Bergonzelli GE, Granato D, Pridmore RD, Marvin-Guy LF, Donnicola D, Corthesy-Theulaz IE.** 2006. GroEL of Lactobacillus johnsonii La1 (NCC 533) is cell surface associated: potential role in interactions with the host and the gastric pathogen Helicobacter pylori. Infect. Immun. **74:**425-434.

38. **Gross G, van der Meulen J, Snel J, van der Meer R, Kleerebezem M, Niewold TA, Hulst MM, Smits MA.** 2008. Mannose-specific interaction of Lactobacillus plantarum with porcine jejunal epithelium. FEMS Immunol. Med. Microbiol. **54:**215-223.

39. **Yan F, Cao H, Cover TL, Washington MK, Shi Y, Liu L, Chaturvedi R, Peek RM, Jr., Wilson KT, Polk DB.** 2011. Colon-specific delivery of a probiotic-derived soluble protein ameliorates intestinal inflammation in mice through an EGFR-dependent mechanism. J. Clin. Invest. **121:**2242-2253.

40. **Yan F, Cao H, Cover TL, Whitehead R, Washington MK, Polk DB.** 2007. Soluble proteins produced by probiotic bacteria regulate intestinal epithelial cell survival and growth. Gastroenterology **132:**562-575.

41. **Bauerl C, Perez-Martinez G, Yan F, Polk DB, Monedero V.** 2010. Functional analysis of the p40 and p75 proteins from Lactobacillus casei BL23. J Mol Microbiol Biotechnol **19:**231-241.

Chapter 4 Discussion

The intestinal microbiota is intimately involved in the development and homeostasis of the mammalian intestines. Over the course of evolution, the prokaryotic inhabitants of the gastrointestinal system have evolved into the "forgotten organ" that provides its host with benefits including additional metabolic capabilities, stimulation of innate and adaptive immune system, and competitive exclusion of pathogens (1). The relatively recent development of germ free animals systems and improvement of nucleic acid based technologies that allow the study of this complex microbial ecosystem in a culture free manner has provided new insights of the relationship between the mammals and their intestinal microbiota. Our appreciation of the complexity involved in this association increases with our knowledge of the mechanism involved in the relationship. In fact, this relationship is so complex that some scientists are even referring the humans and their microbiotas as a "metaorganisms" (2). In addition, the increasing prevalence of inflammatory bowel disease has highlighted the need for increased efforts to elucidate the molecular mechanisms behind this complex relationship in order to harness and focus the microbiota's salutary effects through the use of probiotic treatments. This work establishes how symbiotic lactobacilli stimulate intestinal epithelial proliferation though Nox1-mediated generation of reactive oxygen species. In addition, it demonstrates that the intimate contact between *Lactobacillus rhamnosus* GG (LGG) and intestinal epithelial cells is dependent on SpaC and that this contact is necessary for LGG to elicit its probiotic effects.

The role of ROS in cellular signaling and how it contributes to homeostasis and protection is becoming increasingly well established despite the fact that ROS was traditionally viewed as harmful byproducts of mitochondrial respiratory that aerobic organisms have had to evolve mechanisms to cope with in order to survive. In Chapter 2 of this study we established a link between Nox-mediated generation of ROS and gut epithelial proliferation induced by symbiotic lactobacilli. We isolated *L. plantarum* from the luminal contents of adult Drosophila gut and therefore established its presence as a natural commensal of Drosophila. When *L. plantarum* was fed to axenic Drosophila, it induced the generation of ROS in first instar larvae, third instar larvae, and adult flies. This ROS inducing capacity was unique to lactobacilli as other commensals isolated from the fly gut as well as known a known fly pathogen did not share this ROS-eliciting property. This phenomenon seems to be shared among the lactobacilli that inhabit other metazoans, however, because we found lactobacilli can induce ROS production in human epithelial cells and murine intestines. In these model systems, the known human commensal *L. rhamnosus* GG induced the greatest amount of ROS production. Interestingly, like in the fly system, this ROS induction in mice occurs throughout the life cycle as ROS production was seen in the small intestines and colon of 2 day old as well as adult mice exposed to *L. rhamnosus* GG.

Furthermore, we established that this ROS generation was dependent on cellular expression of NADPH oxidase enzymes. Drosophila lacking dNox in enterocytes as well as mice lacking Nox1 in their intestinal epithelial cells showed reduced amounts of ROS generation after exposure to lactobacilli. In addition,

we demonstrate that cellular ROS generation contributes to gut epithelial cell proliferation. The midguts germ free Drosophila fed food mixed with *L. plantarum* have more proliferating cells than those fed food alone or food mixed with the pathogen *Erwinia carotovora*. However, this increase in proliferation is abolished in *Drosophila* that do not express enterocytic dNox or *Drosophila* that have been pretreated with the antioxidant N-acetylcysteine (NAC) indicating that this process is dependent on Nox expression as well as ROS, respectively. Exposure to lactobacilli induced intestinal proliferation in the mammalian system as well; mice fed *L. rhamnosus* GG had more proliferation in their small intestines and colon than mice fed HBSS. And, like in the fly system, this increased proliferation was dependent on Nox expression and the presence of ROS since increase proliferation was not observed in mice lacking intestinal epithelial cell expressed Nox1 or mice treated with NAC.

Chapter 3 of this work further explores the mechanisms behind *L. rhamnosus* GG-induce ROS generation in the murine system. *L. rhamnosus* contains SpaC, a pilin adhesion protein, which has been previously shown to contribute to *L. rhamnosus* GG's ability to bind intestinal mucus. Here, we used an isogenic *L. rhamnosus* GG mutant that lacks SpaC (LGGΩ*spaC*) to further characterize SpaC's function. We establish that SpaC is necessary for *L. rhamnosus* to maintain contact with the host mucous layer overlaying the intestinal epithelia *in vivo*, and that SpaC-mediated bacterial-host contact is essential for *L. rhamnosus GG* to elicit its cellular modulatory responses. More specifically, we demonstrate that *L. rhamnosus* GG but not LGGΩ*spaC* induces the production of physiological levels of ROS, potentiates ERK MAPK signaling,

stimulates cellular proliferation, and protects against radiation-induced injury. Together, these data advance our understanding of the molecular basis behind the symbiotic relationship between enterocytes and commensal lactobacilli.

These new findings in *Drosophila* and murine intestines highlight the fact that exposure to commensal bacteria and physiological ROS generation has been a critical part of multicellular life over the course of evolution. The identification of Nox1 as the cellular component that is involved in ROS production after bacterial stimulation helps further understand the probiotic process and may lead to the development of new treatments for intestinal diseases. Drugs that target or bacterial components that stimulate Nox1 provide promising possibilities for the treatment of inflammatory bowel disease. Work to identify them should be started immediately as they would provide beneficial Nox stimulation without the potential negative effects of bacterial overgrowth following treatment with live probiotics.

Here, we have established that the salutary effects of probiotic *L. rhamnosus* GG are dependent on intimate and persistent contact with the intestinal mucous layer. Mucus binding genes present in commensal inhabits of the mammalian intestine allow them to secure a stable niche while simultaneously allowing them to elicit the wide range of host benefits attributed to the microbiota. Several adverse health conditions, including inflammatory bowel disease and some systemic immune disorders, are associated with intestinal dysbiosis or an alteration in the normal composition of the intestinal microbiota. Interestingly, the prevalence of genes, like SpaC, that confer mucus-binding capabilities may be a hallmark of a healthy microbiota; these genes are

probably absent in subjects with a dysbiotic intestinal flora. Future work that identifies more mucus-binding genes and the bacterial strains that possess them will enable scientist and healthcare professionals to assess their important in the establishment and maintenance of a healthy microbiota. Moreover, it will allow the spatial and temporal characterization of these indicator genes within the gastrointestinal tract and may lead to important insights into which type of probiotic effects are needed most at particular location within the gastrointestinal tract. This information, in turn, could lead to more special individualized treatment for people suffering from inflammatory bowel disease.

Chapter 4 References

1. **O'Hara AM, Shanahan F.** 2006. The gut flora as a forgotten organ. EMBO reports **7:**688-693.

2. **Ottaviani E, Ventura N, Mandrioli M, Candela M, Franchini A, Franceschi C.** 2011. Gut microbiota as a candidate for lifespan extension: an ecological/evolutionary perspective targeted on living organisms as metaorganisms. Biogerontology **12:**599-609.

Appendix 1 Probing the Spatial Organization of Measles Virus Fusion Complexes

Courtney S. Ardita,[1] Tanja Paal,[1] Melinda A. Brindley,[1] Andrew Prussia,[2] Dominika Gaus,[1] Stefanie A. Krumm,[1] James P. Synder,[2] and Richard K. Plemper[1]

Department of Pediatrics, Emory University School of Medicine and Children's Healthcare of Atlanta, Atlanta, Georgia, USA[1]; Department of Chemistry, Emory University, Atlanta, Georgia, USA[2]

C.S.A, T.P., M.A.B. and A.P. contributed equally to this work.

Appendix 1 Abstract

The spatial organization of metastable paramyxovirus fusion (F) and attachment glycoprotein hetero-oligomers is largely unknown. To further elucidate the organization of functional fusion complexes of measles virus (MeV), an archetype of the paramyxovirus family, we subjected central predictions of alternative docking models to experimental testing using three distinct approaches. Carbohydrate shielding through engineered N-glycans indicates close proximity of a membrane-distal, but not membrane-proximal, section of the MeV attachment (H) protein stalk domain to F. Directed mutagenesis of this section identified residues 111, 114, and 118 as modulators of avidity of glycoprotein interactions and determinants of F triggering. Stalk-length variation through deletion or insertion of HR elements at positions flanking this section demonstrates that the location of the stalk segment containing these residues cannot be altered in functional fusion complexes. In contrast, increasing the distance between the H head domains harboring the receptor binding sites and this section through insertion of structurally rigid α-helical domains with a pitch of up to approximately 75 Å downstream of stalk position 118 partially maintains functionality in transient expression assays and supports efficient growth of recombinant virions. In aggregate, these findings argue against specific protein-protein contacts between the H head and F head domains but instead support a docking model that is characterized by short-range contacts between the prefusion F head and the attachment protein stalk, possibly involving H residues 111, 114, and 118, and extension of the head domain of the attachment protein above prefusion F.

Appendix 1 Introduction

Paramyxoviruses infect cells through fusion of the viral envelope with target cell membranes. For all members of the *Paramyxovirinae* subfamily, this involves the concerted action of two envelope glycoproteins, the fusion (F) and attachment (H, HN, or G, depending on the *Paramyxovirinae* genus) proteins. Both proteins feature short lumenal tails, a single transmembrane domain, and large ectodomains. The F protein, in type I orientation, forms homotrimers, while homodimers or homotetramers have been suggested as functional units for attachment proteins of different *Paramyxovirinae* subfamily members (7, 14, 28, 41, 49, 50, 66). For entry, upon receptor binding, the attachment protein is considered to initiate a series of conformational rearrangements in the metastable prefusion F protein (15, 77), which ultimately brings together transmembrane domains and fusion peptides and, thus, donor and target membranes (3, 32, 45, 53, 80).

Multiple studies have demonstrated that specific interactions between compatible F and attachment proteins of paramyxovirinae are imperative for the formation of functional fusion complexes (6, 29, 36, 42, 43, 56, 75). However, the molecular nature of these interactions and the spatial organization of functional glycoprotein hetero-oligomers remain largely unknown. Individual ectodomain and partial ectodomain crystal structures have been obtained for different paramyxovirus F (13, 76, 77) and attachment (8, 14, 17, 28, 35, 79) proteins, respectively. For F, a stabilized human parainfluenza virus type 5 (HPIV5) ectodomain that is believed to represent a prefusion conformation folds into a

globular head structure that is attached to the transmembrane domains through a helical stalk consisting of the membrane-proximal heptad repeat B (HR-B) domains (77). For the attachment protein, a globular head that harbors the receptor binding sites is considered to be connected to the transmembrane region through extended stalk domains (34, 78). Crystal structures of isolated head domains have been solved for several paramyxovirus attachment proteins, including measles virus (MeV) H, and reveal the six-blade propeller fold typical of sialidase structures (8, 14, 17, 28, 79). However, morbilliviruses recognize proteinaceous receptors (for MeV, the regulator of complement activation [CD46] and/or signaling lymphocytic activation molecule [SLAM], depending on the virus strain) (21, 40, 46, 51, 64, 65). X-ray data do not extend to the stalk domains, but circular dichroism analysis (78) and structure predictions (36, 78) support an α-helical coiled-coil configuration of the stalk.

The nature of individual residues that engage in specific intermolecular interactions between glycoproteins of paramyxovirinae prior to refolding has been studied most extensively for the attachment protein. The stalk domains of several paramyxovirus HN proteins have been implicated in mediating specificity for their homotypic F proteins (18, 20, 43, 63, 70, 72). We have found that this extends to MeV and canine distemper virus H and, thus, to paramyxovirinae recognizing proteinaceous receptors (36), supporting the general hypothesis that F-interacting residues may reside in the stalk region of the attachment protein (30, 78).

Considerably less information concerning the nature of F microdomains that mediate attachment protein specificity is available. Among the few

exceptions are peptides derived from Newcastle disease virus (NDV) and Sendai virus F HR-B domains, which interact with soluble variants of the respective HN proteins in vitro (25, 67). Multiple domains have been suggested to mediate specificity of HPIV2 F for its HN (69). However, a conclusive N-glycan shielding study (44) and structural information (77, 78) argue against direct contacts between NDV F HR-B domains and HN in native glycoprotein complexes. Thus, the role of individual HPIV2 F residues in HN binding is unclear (25, 44).

Building on the observation that MeV H is able to engage in productive heterotypic interactions with F proteins derived from some but not all isolates of closely related canine distemper virus, we have recently identified residues in morbillivirus F (MeV F residue 121) and H (H stalk residues 110 to 114) that interdependently contribute to physical MeV glycoprotein interaction and F triggering for fusion (36). While these residues could mediate reciprocal glycoprotein specificity through long-range effects, molecular modeling of the MeV H stalk in an α-helical conformation has posited F residue 121 at the same level above the viral envelope as H residues 110 to 114, making direct contacts structurally conceivable (36). This spatial organization of functional fusion complexes furthermore provides a comprehensive explanation for previous demonstrations of a specific role for attachment protein stalk domains of paramyxovirinae in functional and physical interactions with F (18, 44, 63, 70, 72). However, this “staggered-head” model mandates positioning the globular head of the attachment protein above the prefusion F trimer (36), as opposed to a suggested “parallel-head” alignment of the glycoproteins (31, 47). The latter is mostly based on transmission electron microscopy micrographs of viral particles

apparently showing glycoprotein spikes of equal length (33). Unfortunately, these images lack the resolution for an identification of the molecular nature of the spikes (attachment or F protein) or the distinguishing between densely packaged H and F head domains of different heights and laterally aligned head domains. Indeed, a recent single-particle reconstruction based on cryo-electron microscopy images of HPIV5 particles revealed that defined spikes correspond to F in a postfusion conformation, which was interpreted as a product of possible premature F refolding (38). These two-dimensional images of heavy-metal-stained particles did not reveal F spikes in a prefusion conformation. Rather, a dense surface layer was considered to correspond to prefusion glycoprotein hetero-oligomers (38). In addition to further-advanced image reconstructions, biochemical assessment of alternative docking modes is imperative for the elucidation of the organization of functional fusion complexes of paramyxovirinae.

In this study, we subjected central predictions of the hypothetical alignment models to experimental analysis. By employing carbohydrate shielding, directed mutagenesis, and variation of the length of the H stalk domain, we examined the proximity of different regions of the H stalk to F, probed a role of individual residues around the previously identified H stalk section from positions 110 to 114 in the formation of functional fusion complexes, tested the effect of varying the length of the H stalk membrane proximal and membrane distal to this section, and explored the general possibility of whether specific contacts between the prefusion F and H head domains are required for F triggering. Experimental data were interpreted in the light of a working model of

MeV glycoprotein hetero-oligomers prior to receptor binding.

Appendix 1 Materials and Methods

Cell culture, transfection, and production of virus stocks. All cell lines were maintained at 37°C and 5% CO2 in Dulbecco's modified Eagle's medium supplemented with 10% fetal bovine serum. Vero (African green monkey kidney epithelial) cells (ATCC CCL-81) stably expressing human SLAM (Vero-SLAM cells) (52), and baby hamster kidney (BHK-21) cells stably expressing T7 polymerase (BSR-T7/5 [BHK-T7] cells) (10) were incubated at every third passage in the presence of G-418 (Geneticin) at a concentration of 100 μg/ml. Lipofectamine 2000 (Invitrogen) was used for all cell transfections. To prepare MeV stocks, Vero-SLAM cells were infected at a multiplicity of infection (MOI) of 0.001 PFU/cell and incubated at 37°C. Cells were scraped in Opti-MEM (Invitrogen), virus was released by two freeze-thaw cycles, and titers were determined by 50% tissue culture infective dose (TCID50) titration according to the Spearman-Karber method (59) as described previously (56). To prepare stocks of modified vaccinia virus Ankara expressing T7 polymerase (60), DF-1 (chicken embryo fibroblast) cells (ATCC CRL-12203) were infected at an MOI of 1.0 PFU/cell, and cell-associated viral particles were harvested 40 h postinfection.

Site-directed mutagenesis, random staggered-priming mutagenesis, and generation of recombinant MeV genomes. Base vectors for all transient MeV glycoprotein expression experiments and directed-mutagenesis approaches were plasmids pCG-F and pCG-H, encoding

glycoproteins derived from the MeV Edmonston strain under the control of the constitutive cytomegalovirus promoter (12). For point mutations, heptamer insertions, or heptamer deletions, directed mutagenesis following the QuikChange protocol (Stratagene) was employed using appropriate primers (individual sequences are available upon request). All changes were confirmed by DNA sequencing, and expression of mutagenized proteins was verified by immunoblotting. To generate different-length tandem repeats of the H stalk downstream of stalk nucleotide 351, a staggered-priming mutagenesis strategy was developed. Using a pCG-H variant harboring an additional copy of stalk residues 84 to 90 at residue 118 (H-118▽7x) as the template, mutagenesis was carried out with primer 5′-**cactgacctagtgaaattc**ATAGAACACCAAGTGAAAGAT**atcgagcatcaggtcaagg**, which consists of H stalk nucleotides 333 to 351 (boldface), the HR insertion (uppercase letters), and, for the H-118▽7x template, stalk nucleotides 250 to 268 and 352 to 370 (boldface and underlined), corresponding to amino acids 84 to 90 and the additional copy of this HR inserted at residue 118, respectively. This reaction efficiently (approximately 25 to 50% of clones analyzed) yielded H constructs with extended-length tandem stalk insertions at stalk position 118 (see Figure 6B for individual sequences). To transfer an H variant harboring a 41-residue stalk elongation (H-118▽41x) into a full-length cDNA copy of the MeV Edmonston genome, a PacI/SpeI fragment containing the H-encoding open reading frame (ORF) was replaced in p(+)MeV-NSe (58) with this variant, resulting in plasmid p(+)MeV-H 118▽41x. An additional stop codon was added to the H-118▽41x ORF to render the resulting genome compatible to the rule-of-six

that applies to many members of the paramyxovirus family, including MeV (26). An enhanced green fluorescent protein (eGFP)-encoding ORF was furthermore inserted as an additional transcription unit upstream of the nucleocapsid-encoding ORF through replacement of a PacI/NotI fragment with that derived from p(+)MeV-eGFP (22), resulting in plasmid p(+)MeV- eGFP-H 118▽41x.

Quantification of envelope glycoprotein surface expression. Vero cells were transfected with 2 μg of plasmid DNA encoding MeV H constructs as indicated. After being washed in cold phosphate-buffered saline (PBS), cells were incubated in PBS with 0.5 mg/ml sulfosuccinimidyl-2-(biotinamido)ethyl-1,3-dithiopropionate (Pierce) for 20 min at 4°C, followed by washing and quenching for 10 min at 4°C in Dulbecco's modified Eagle's medium. Samples were lysed in immunoprecipitation buffer, and lysates were cleared by centrifugation for 45 min at 20,000 × *g* and 4°C. Biotinylated proteins were adsorbed to immobilized streptavidin for 120 min at 4°C, washed two times in buffer A (100 mM Tris, pH 7.6, 500 mM lithium chloride, 0.1% Triton X-100) and then buffer B (20 mM HEPES, pH 7.2, 2 mM EGTA, 10 mM magnesium chloride, 0.1% Triton X-100), and incubated in urea buffer (200 mM Tris, pH 6.8, 8 M urea, 5% sodium dodecyl sulfate [SDS], 0.1 mM EDTA, 0.03% bromphenol blue, 1.5% dithiothreitol) for 30 min at 50°C. Samples were then subjected to SDS-polyacrylamide gel electrophoresis (PAGE) and immunoblotting using a polyclonal antiserum directed against the H cytosolic tail (54). For densitometric quantification, immunoblots were decorated with anti-rabbit IRDye 800CW conjugate (LI-COR) and analyzed using an Odyssey infrared imager and Odyssey software (LI-COR). Amounts of surface steady-state levels of cellular transferrin

receptor that were analyzed in parallel using a monoclonal anti-human transferrin antiserum (Zymed) served as an internal standard.

Enzymatic deglycosylation. For PNGase F-catalyzed deglycosylation, H variants were expressed and subjected to surface biotinylation as described above. Following streptavidin pull-down, samples were split into two equal aliquots, proteins were denatured (0.5% SDS, 400 mM dithiothreitol; 95°C for 10 min), and aliquots were subjected to PNGase F deglycosylation (50 mM sodium phosphate, pH 7.5, 1% NP-40; 1 h at 37°C) or mock treatment. All samples were then analyzed by SDS-PAGE and immunoblotting using antiserum directed against the cytosolic H tail.

Expression and purification of soluble SLAM molecules. For expression of a soluble SLAM-murine immunoglobulin G (sSLAM-mIgG) fusion protein, a cDNA sequence encoding the first 233 amino acids of the SLAM ectodomain was isolated through reverse transcription-PCR from Vero-SLAM cells, and the sequence was confirmed. This fragment was subcloned in frame to the 5′ end of an ORF encoding murine IgG heavy chains that is present in the RCASBP(A) vector, a replication-competent retrovirus vector derived from avian leukosis virus (23). After transfection of the RCASBP(A) construct into permissive DF-1 cells, sSLAM-mIgG was purified from culture supernatants (2.5 liters, total volume) through affinity chromatography using immobilized protein G, ultrafiltration, and dialysis against PBS. The final purity of sSLAM-mIgG determined by SDS-PAGE and Coomassie blue staining was ≥90%, and concentrations of purified material were adjusted to 1 mg/ml.

Flow cytometry for analysis of receptor binding capacity. To

determine the ability of MeV H variants to bind the SLAM receptor, SLAM- and CD46-negative CHO cells were transfected in a six-well plate format with MeV H constructs (5 μg) and an eGFP expression plasmid (1 μg) as a marker for transfection. Thirty-six hours posttransfection, cells were lifted off and washed twice in PBS supplemented with 3% fetal calf serum. Cell populations were split into two equal aliquots and incubated with either sSLAM-mIgG or a monoclonal antibody mix directed against epitopes in the MeV H ectodomain (Millipore) for 1 h on ice. Following decoration of cells with anti-mouse Fc-specific allophycocyanin conjugate (Jackson Immunoresearch) for 30 min on ice, samples were analyzed using a FACSCanto II cytometer and FlowJo software. Fluorescence intensity was determined for the GFP-positive cell population.

Quantitative cell-to-cell fusion assays. To quantify fusion activity, an effector Vero-SLAM cell population (3×10^5 cells/well) was cotransfected with 2 μg each of H and F expression plasmids, and target Vero-SLAM cells (2×10^5 cells/well) were transfected with 2 μg of the reporter plasmid encoding firefly luciferase under the control of the T7 promoter. Single transfections of plasmids encoding MeV F served as controls. Two hours posttransfection, the effector cells were infected with modified vaccinia virus Ankara expressing T7 polymerase at an MOI of 1.0 PFU/cell. Following incubation for 16 h at 37°C, in the case of effector cells in the presence of 100 μM fusion inhibitory peptide (Bachem), target cells were detached and overlaid on washed effector cells at a 1:1 ratio and incubated at 37°C. Five hours postoverlay, cells were lysed using Bright Glo lysis buffer (Promega), and the luciferase activity was determined using a luminescence counter (PerkinElmer) and the Britelite reporter gene assay system

(PerkinElmer). The instrument's arbitrary values were analyzed by subtracting the relative background provided by values of the controls, and these values were normalized against the reference constructs indicated in the figure legends. On average, background values were <1.5% of the values obtained for reference constructs.

Envelope glycoprotein cross-linking and immunoprecipitation. Vero-SLAM cells were transfected with 4 μg each of plasmid DNA encoding MeV F and H variants as specified for the individual experiments and incubated in the presence of 100 μM fusion inhibitory peptide. At 36 h posttransfection, cells were washed three times with cold PBS and treated with DTSSP (1 mM final concentration in PBS) for two hours at 4°C, followed by the addition of Tris, pH 7.5, to a final concentration of 20 mM for quenching (15 min, 4°C). Cells were then lysed in radioimmunoprecipitation assay buffer (1% sodium deoxycholate, 1% NP-40, 150 mM NaCl, 50 mM Tris-Cl, pH 7.2, 10 mM EDTA, 50 mM NaF, 0.05% SDS, protease inhibitors [Roche], 1 mM phenylmethylsulfonyl fluoride), and cleared lysates (20,000 × *g*; 30 min at 4°C) were incubated with specific antibodies directed against epitopes in the MeV H ectodomain (Millipore) at 4°C. After precipitation with immobilized protein G at 4°C, samples were washed two times each in buffers A and B as described above, eluted in urea buffer, and subjected to SDS-PAGE and immunoblotting. Coprecipitated F was visualized in a ChemiDoc XRS digital imaging system (Bio-Rad) using a polyclonal antiserum against the F cytosolic tail (37) and rabbit IgG light chain-specific horseradish peroxidase conjugate. For densitometry, signals were quantified using the QuantityOne software package (Bio-Rad).

Recovery of recombinant MeV. Recombinant MeV was generated as described previously (58) with the following modifications: BHK-T7 cells were cotransfected by calcium phosphate precipitation with a plasmid carrying a cDNA copy of the recombinant MeV genome and plasmids encoding the MeV L, N, or P protein. All constructs were under the control of the T7 promoter. Helper cells were overlaid on Vero-SLAM cells 76 h posttransfection, and emerging virus particles were transferred to fresh Vero-SLAM cells. The integrity of recombinant MeV particles was then confirmed by reverse transcription-PCR and DNA sequencing of the modified area using Superscript II reverse transcriptase and random hexamer primers for first-strand synthesis.

Virus growth curves. For multistep growth curves, cells were infected in a six-well-plate format with recombinant MeV Edmonston (recMeV-Edm) variants as specified at an MOI of 0.001 PFU/cell. To ensure equal MOIs for each variant analyzed, all input stocks were prediluted to approximately 10^4 TCID50/ml in Opti-MEM (Invitrogen) prior to infection, and titers were reconfirmed by TCID50 titration. Sixty minutes postinfection, inocula were replaced with fresh growth medium. Cell-associated viral particles were harvested every 12 h as described above and subjected to TCID50 titration. For documentation of the viral cytopathic effect (CPE), plates were photographed at a magnification of ×200.

Molecular modeling. Previously described structural models of MeV F and H proteins were used in this analysis (36, 57). Briefly, a homology model of the MeV F protein was built on the basis of the coordinates reported for the prefusion HPIV5 F X-ray crystal structure (77). The MeV H structural model was

built by connecting the X-ray coordinates available for residues 154 to 607 forming the head domain (14, 28) to a coiled-coil model of the MeV H stalk (residues 58 to 153), which was generated by mapping these residues on the α-helical scaffold of cortexillin I (11) as described previously (36). In the present study, a slightly different mapping of the stalk residues was used to better accommodate the stutter in the HR sequence at residues I99 and L105. A single-residue gap was introduced in the alignment after P108, placing this residue in "a" position of the helical wheel. Proline residues 94 and 127 are also expected to introduce kinks in the helix structure in agreement with electron microphotographs of the related HPIV5 HN (78). Due to the lack of native X-ray information, however, these are not represented in the schematic models. For the modeling of N-glycan additions, a sugar with the following structure was prepared in three dimensions by using Maestro software (Schrodinger, LLC, New York, NY): asparagine-GlcNAc-β(1,4)-GlcNAc-β(1,4)-Man[-α(1,3)-Man-β(1,2)-GlcNAc-β(1,4)-Gal-α(2,6)-NeuNAc] [-α(1,6)-Man-β(1,2)-GlcNAc-β(1,4)-Gal-α(2,6)-NeuNAc]. For a reasonable low-energy conformation of the carbohydrate, a Monte Carlo conformational search of 1,000 steps was performed with MacroModel 9.5 software (Schrodinger, LLC, New York, NY) using the OPLS2005 force field with generalized Born/surface area water solvation. The low-energy conformation was attached to the proteins by superimposing the backbone atoms of asparagine to the target glycosylation position on the MeV H stalk. Structural models of MeV H stalk deletion mutants were generated by removing HR regions from the stalk model, save for one flanking residue on either side of the deletion (residues 85 to 89 for HR 84 to 90 and residues 119 to

123 for HR 118 to 124). The flanking residues were then used to superimpose the backbone atoms of the downstream structure to the upstream structure, generating one construct (H-Δ84-90) with residues 58 to 83 attached to residues 91 to 607 and another construct (H-Δ118-124) with residues 58 to 117 attached to residues 125 to 607. MeV H stalk insertions were generated by duplicating the desired section of the stalk plus one flanking residue on either side for superimposing (residues 83 to 91, 117 to 125, and 83 to 118). These duplicate sections were inserted into the downstream structure and aligned by superimposing the backbone atoms of the overlapping residues. The upstream structure was then superimposed in the same manner to the C-terminal end of the newly extended stalk, generating the constructs H-84▽7x, H-118▽7x, and H-118▽41x.

Appendix 1 Results

With the overarching goal of further elucidating the spatial organization of paramyxovirus envelope glycoproteins in a prefusion state, we subjected key predictions of hypothetical docking models to experimental testing.

Engineering of N glycosylation sites into the H stalk. Independently of the lateral arrangement of the head domains, schematic juxtapositions of F and H structures predict that membrane-proximal regions of the H stalk are not in direct contact with the F trimer. For membrane-distal stalk sections, however, the staggered-head (Figure 1A, left panel), but not the parallel-head model (Figure 1A, right panel), implies close proximity of the prefusion F head domain.

Carbohydrate shielding through insertion of additional N-glycosylation sites is reportedly capable of examining the contribution of protein domains to activity (24, 68) and has been used in a conclusive study to test candidate contact zones between NDV HN and F (43). We employed this strategy to probe the proximity of F from the H stalk domain at a membrane-proximal and membrane-distal position. Since the exact rotational orientation of the H stalk is unknown, N-glycosylation sites were introduced separately for each position at three consecutive residues: residues 70 to 72 were chosen as targets for membrane-proximal N-glycans guided by the prediction of the staggered-head model that carbohydrates at these positions will not impair the interaction of H with F, and residues 110 to 112 were chosen for membrane-distal N-glycans based on our previous identification of the role of MeV H section 110 to 114 in mediating F specificity (36).

Of the membrane-proximal set, only the engineered site at position 72 was recognized efficiently without affecting intracellular transport competence, as demonstrated by comparing the electrophoretic mobilities of these H variants with that of standard H before and after PNGase F deglycosylation of cell surface-exposed material (Figure 1B). Subsequent full characterization was therefore limited to the corresponding variant, H-72-Nglyc. Equivalent analysis of the electrophoretic mobility of the membrane-distal set confirmed glycosylation at each of the targeted positions, 110, 111, and 112 (Figure 1C). Recognition of the engineered glycosylation sites was highly efficient for all four constructs, since immunoblotting revealed homotypic mobility patterns that lacked subspecies with Edmonston H (H-Edm)-like mobility prior to PNGase F treatment.

Carbohydrate shielding at a membrane-distal, but not membrane-proximal, position of the H stalk interferes with the formation of functional fusion complexes. Assessments of plasma membrane steady-state levels through surface biotinylation and of SLAM binding through flow cytometry demonstrated essentially unchanged intracellular transport competence and ability to interact with SLAM receptor for all four H variants with engineered N-glycans (Figure 2A). To establish a receptor binding assay, we generated an sSLAM-mIgG fusion protein that specifically blocks MeV entry, confirming its ability to bind MeV H (Figure 2B). Figure 2C exemplifies that, following binding of this sSLAM-IgG construct to H-expressing cells by flow cytometry, the ratios of SLAM-specific mean fluorescence intensity to H-specific mean fluorescence intensity provide an assessment of receptor (SLAM) binding competence. For a control, an I194S mutant (H-I194S) that reportedly is unable to bind to SLAM was assessed (48). This construct returned a SLAM-to-H signal ratio of 0.03, compared to 1.07 obtained for standard H (Figure 2C) confirming specificity of the assay. Quantification of cell-to-cell fusion using a luciferase reporter-based content mixing assay demonstrated that fusion activity and, thus, F triggering were virtually unaffected by the additional N-glycan at H stalk position 72 (Figure 2A). In contrast, N-glycans at position 110, 111, or 112 completely blocked F triggering (Figure 2A), as implied by Figure 1A.

To assess whether this lack of functionality extends to altered physical interaction of the glycoproteins, we further advanced a coimmunoprecipitation (co-IP) assay that we have previously developed for MeV H and F (36, 55, 56). The general strategy of coprecipitating one envelope glycoprotein with antibodies

directed against the other after lysis of the producer cells has been applied to multiple members of the paramyxovirus family (2, 5, 19, 43, 75). However, in this setup, the possibility that removal of the stabilizing lipid bilayer induces conformational changes in the metastable prefusion F trimer (76) prior to co-IP, potentially distorting results, cannot be excluded. To assess envelope glycoprotein hetero-oligomers in situ prior to membrane lysis, we examined membrane-impermeable chemical cross-linkers. Covalently linking surface-expressed MeV glycoprotein hetero-oligomers with membrane-impermeable, reducible DTSSP prior to membrane extraction, immunoprecipitation of H under stringent conditions, and detection of coprecipitated F allowed specific analysis of plasma membrane-embedded envelope glycoprotein complexes (Figure 2D). Having established this assay, we found that N-glycans at stalk position 111 (representative of N-glycan-mediated shielding of membrane-distal stalk positions) essentially block the formation of functional fusion complexes (<10% of those observed for unchanged H and F). This observation underscores the concept that DTSSP-mediated MeV glycoprotein cross-linking does not generate artificial H and F complexes. In contrast, N-glycans at position 72 still allow glycoprotein interaction, although at a reduced level compared to standard complexes (Figure 2E).

These data demonstrate that insertion of additional N-glycans at a membrane-proximal or -distal position of the H stalk does not result in a loss of receptor binding capacity or intracellular protein retention through gross H misfolding. The block of F triggering and glycoprotein hetero-oligomerization by membrane-distal, but not membrane-proximal, N-glycans indicates close

proximity of this H stalk section to F.

H residues 111, 114, and 118 are determinants for F triggering. To assess whether a specific subset of residues in the previously identified linear H stalk segment from positions 110 to 114 determines effective F triggering, we next subjected this domain to alanine-scanning mutagenesis. In a first round, all five residues or only the first three or last two residues were mutagenized. The surface expression and SLAM binding ability of these H variants were unchanged, but none was capable of triggering F in cell-to-cell fusion assays (Figure 3). This extends the essential role of the segment in F triggering to homotypic MeV glycoprotein pairs and indicates that residues in both subsections examined individually (positions 110 to 112 and positions 113 and 114) are required for the formation of functional fusion complexes.

Subsequent single-residue mutagenesis revealed a complete loss of F triggering by H-F111A and a significant reduction by H-L114A, while changes at each of the other three positions (110, 112, and 113) did not affect fusion activity (≥85% of F triggering by standard H; Figure 4A). We note that H-F111A and H-L114A showed essentially unaltered surface expression, while approximately 20% (H-T112A and H-D113A) to 30% (H-R110A) reductions were observed for the F triggering-competent mutants (Figure 4A). SLAM binding levels of all variants were equivalent to that of standard H (Figure 4A).

A three-residue distance between individual positions determining F triggering supports the predicted helical character of the attachment protein stalk domains of paramyxovirinae (36, 44, 78), since an α-helical configuration positions residues 111 and 114 in immediate proximity on consecutive turns of the

helix (Figure 4B). To explore whether neighboring residues on preceding or subsequent turns likewise contribute to F triggering, we extended the alanine mutagenesis to stalk positions 108, 117, 118, and 122, which are predicted to be located at the same face of the helix as residues 111 and 114 (Figure 4B). Of these, an I118A mutation likewise abolished fusion activity but did not reduce surface expression or SLAM binding capacity (Figure 4A). None of the other changes resulted in major reductions of F triggering or SLAM binding, although the proline-to-alanine change at position 108 caused an approximately 50% reduction in surface expression (Figure 4A). In addition to affecting F triggering, the individual mutation of residue 114 or, in particular, 111 or 118 to alanine impaired physical glycoprotein interaction at the plasma membrane (Figure 4C).

Taken together, these data identify H stalk positions 111, 114, and 118, but not intermittent or flanking residues 108, 112, 113, 117, or 122, as determinants for the formation of functional fusion complexes between MeV H and F. This is consistent with an α-helical configuration of the stalk domains in situ, supporting previous results derived from secondary structure predictions and in vitro analysis of soluble attachment protein ectodomain fragments (36, 44, 78).

H variants with a stalk elongation downstream of residue 118 functionally interact with F. The N-glycan shielding and cross-linking results are compatible with close proximity between F and the H stalk section including residues 111, 114, and 118. The corresponding alignment of F and H (staggered-head model) shown in Figure 5A implies that shortening the stalk domain will likely disturb glycoprotein hetero-oligomerization due to steric interference of a lowered H head with F. In contrast to the parallel-head model, the staggered-

head alignment furthermore predicts that stalk elongation distal, but not proximal, to residues 111/114/118 should be tolerated, since the relative positions of contacting domains proximal to residue 118 would likely be preserved (Figure 5A). Deleting or inserting complete HR domains is anticipated to minimally compromise the predicted overall helical conformation of the stalk while altering its length by approximately 11 Å per HR domain.

To test these predictions, we identified two HRs (residues 84 to 90 and residues 118 to 124) (Figure 5A; for amino acid sequences, see Figure 6B) that flank the 111/114/118 section and are distinct from H residues 91 to 105. Introducing mutations in the latter section was avoided, since this reportedly affects F triggering either through long-range effects or a shared role of this segment and other segments in the formation of functional fusion complexes (16). Our approach furthermore preserved the hydrophobic nature of residue 84, which was likewise identified by Corey and Iorio in the same study to be required for F triggering (16).

Four constructs were generated: constructs with a deletion of the HR from positions 84 to 90 [H-Δ(84-90)] or 118 to 124 [H-Δ(118-124)] or an insertion of an additional copy of the HR from positions 118 to 124 at residue 84 (H-84▽7x) or the HR from positions 84 to 90 at residue 118 (H-118▽7x). The isoleucine residue at position 118 was conserved in all of these, with the exception of H-Δ(118-124), in which, however, an I118L change maintained the hydrophobic nature at position 118. All H variants reached the surface, although plasma membrane steady-state levels of H-118▽7x and H-Δ(84-90) were reduced by approximately 30 and 50%, respectively (Figure 5B). All four constructs were

fully capable of SLAM binding (Figure 5B). However, microscopic analysis (data not shown) and quantitative fusion assays revealed that both HR deletions and the membrane-proximal HR insertion completely abrogated F triggering. In contrast, stalk elongation membrane-distal of the 111/114/118 section still allowed the formation of functional fusion complexes, since coexpression of H-118▽7x with F resulted in approximately 50% fusion activity of standard H and F (Figure 5B). Likewise, only stalk elongation downstream of 111/114 (H-118▽7x) was compatible with glycoprotein hetero-oligomerization, whereas membrane-proximal insertion (H-84▽7x) and HR deletions at either position essentially abolished glycoprotein interactions (Figure 5C).

These results demonstrate that the overall stalk lengths can be increased, but the distance between the transmembrane domain and stalk section from positions 91 to 118 must be preserved for effective hetero-oligomerization and F triggering.

Extensive stalk insertions argue against specific contacts between H and F head domains. F triggering by H-118▽7x suggests that H domains downstream of residue 118 do not engage in functional protein-protein contacts in prefusion hetero-oligomers, thus, further arguing against a parallel-head alignment and indicating a lack of functional contacts between the base of the H and the top of the F head in staggered alignment. Alternatively, structural flexibility of the carboxy-terminal third of the stalk (residues 118 to 154) could compensate for the single HR insertion of the H-118▽7x variant.

To probe these alternatives, we further extended the stalk domain membrane distal to position 118. Insertion of a second additional HR domain

generated variant H-118▽14x, with a predicted added stalk length of approximately 22 Å. Compared to H-118▽7x, the second HR domain addition returned very similar surface expression (approximately 70%) of H-Edm, was fully capable of SLAM binding, and improved F triggering to approximately 80% of the standard H value in cell-to-cell fusion assays (Figure 6A). In parallel to our study of stalk extensions of defined length, we developed a staggered-priming mutagenesis strategy to create different-length tandem repeats of H stalk section 84 to 117, always inserted at position 118. This convenient approach yielded two additional H variants (sequences shown in Figure 6B) that harbor 41-residue (H-118▽41x) and 55-residue (H-118▽55x) stalk elongations. The two constructs were fully capable of SLAM binding and showed plasma membrane steady-state levels of approximately 65% and 45% of standard H, respectively (Figure 6A). Remarkably, coexpression of F with H-118▽41x, featuring stalk extensions of nearly 50% of the original lengths (depicted in Figure 6C), returned approximately 50% fusion activity of standard H. A drastic reduction in F triggering was found for H-118▽55x. However, microphotographs of cells coexpressing this variant and F (Figure 6D) and cell-to-cell fusion assays confirmed some residual activity, equivalent to approximately 10% of the standard H value (Figure 6A). As suggested by these findings, all three H variants are capable of physically engaging F. While an approximately 70% reduction of hetero-oligomer formation was observed for H-118▽55x, co-IP efficiencies of H-118▽14x and H-118▽41x with F were similar (nearly 80%) to that observed for H-Edm (Figure 6E).

In aggregate, these findings demonstrate that membrane-distal insertion

into the H stalk of a structurally rigid 41-amino-acid domain composed of consecutive HRs, which is equivalent to a pitch of approximately 75 Å in an α-helical configuration, is largely compatible with the formation of functional fusion complexes.

H variants with a large stalk insertion are functional in the context of virus infection. The remarkable nature of these findings raised the question of whether tolerance of the 41-residue insertion is limited to inducing cell-to-cell fusion in a transient glycoprotein expression setting or extends to sustaining viral entry and efficient production of infectious particles. To test this, we generated a cDNA copy of the MeV Edmonston genome that harbored the H-118▽41x gene in place of the standard H gene and, to facilitate detection of recombinant virions, an eGFP gene as an additional transcription unit.

recMeV-eGFP-(H-118▽41x) virions were recovered successfully and subjected to analysis of CPE in cell monolayers and growth in comparison to standard recMeV-eGFP. Figure 7A shows that cell-to-cell fusion was also the predominant CPE associated with the recMeV-eGFP-(H-118▽41x) variant. However, final syncytial sizes were reduced, and the incubation time until syncytial disintegration was increased compared to that for the recMeV-eGFP variant. These observations were corroborated by multiple-step viral growth curves. The recMeV-eGFP-(H-118▽41x) variant grew efficiently to final titers equivalent to those reached by the recMeV-eGFP variant (Figure 7B). However, presumably due to reduced lateral spread and, hence, less-rapid breakdown of syncytia in cell culture, recMeV-eGFP-(H-118▽41x) growth curves showed an extended plateau phase of high virus titers, as opposed to the sharp drop from the

peak titer observed for the recMeV-eGFP variant (Figure 7B).

These data confirm that our observations based on transient expression of H-118▽41x and F are fully transferable to the context of virus infection. Thus, they underscore that an H stalk elongation of approximately 50%, inserted membrane distal to residue 118, is compatible with productive interaction of H with the prefusion F trimer and the efficient formation of infectious particles.

Appendix 1 Discussion

With an increasing number of high-resolution X-ray structures of envelope glycoproteins of paramyxovirinae at hand, elucidating the spatial organization of functional fusion complexes in situ has emerged as a major task in better understanding the molecular mechanism of infection by paramyxovirinae. In this study, we subjected key predictions derived from hypothetical glycoprotein interaction models that were generated on the basis of crystallographic and biochemical data (14, 16, 28, 36, 44, 77) to experimental evaluation. In aggregate, our results suggest a spatial ectodomain organization in which the prefusion F head domain contacts a membrane-distal section of the H stalk. This requires positioning of the H head domain above prefusion F in a staggered-head alignment. Several lines of evidence support these conclusions.

First, N-glycan shielding at H stalk position 111 blocks both functional and physical glycoprotein interactions, suggesting close proximity of F to this section of the H stalk. While these results could alternatively derive from a long-range, indirect effect of the added glycans, efficient H-111-Nglyc surface expression, unchanged receptor binding capacity, and a rigid α-helical configuration of the

stalk supported by secondary structure predictions (36, 44) and circular dichroism analysis of the related HPIV5 HN stalk (78) render this unlikely. Nearly unperturbed physical interaction and F triggering capacity of H-72-Nglyc underscore this conclusion. It is noteworthy in this context that additional N-glycosylation sites are efficiently recognized at three consecutive positions starting with residue 110 but only at position 72 of the more-membrane-proximal 70-to-72 triplet. This suggests that rotational flexibility within the postulated α-helical coiled coils is limited in proximity to the transmembrane domains but increases toward membrane-distal positions. Bulky N-glycans at any of the three membrane-distal positions and/or glycan-induced slight rotation of the stalk helix in the *z* axis may interrupt precise protein-protein contacts at the H and F interface.

Second, mutagenesis of individual residues around the previously identified H stalk section from positions 110 to 114 (36) has highlighted three residues (111, 114, and 118), predicted to be located on consecutive turns of the MeV H stalk α-helix as determinants of both effective F triggering and, in particular, in the case of residues 111 and 118, glycoprotein interaction. Previously, Corey and Iorio demonstrated that mutation of MeV H stalk residue I84, L92, I98, or I99 likewise affects F triggering (16). Based on very efficient coprecipitation of these mutants with F, they concluded that these residues likely contribute to F triggering through indirect effects or form one of several interaction domains. Since it is likely a requirement that the F trimer separates at some stage in fusion from the attachment protein for F refolding to proceed (73, 74), increased strength of hetero-oligomer interaction might be sufficient to

reduce or block fusion. While indirect effects could likewise result when an alanine point mutation is inserted at position 111, 114, or 118, the block of F triggering by these H variants combined with a strong reduction of glycoprotein interactions in situ makes it alternatively conceivable that these residues engage in short-range functional contacts required for the initiation of F refolding.

Lastly, shortening the MeV H stalk by either membrane-proximal or membrane-distal residues 84 to 117 blocks both hetero-oligomerization and triggering. This is compatible with both the parallel (required protein-protein contacts are disrupted)- and staggered (steric constraints between F head and a lowered H head)-alignment hypotheses of glycoprotein head domains. Importantly, though, increasing the length of the H stalk membrane proximal to residue 84 by only ~11 Å disrupts hetero-oligomerization and F triggering, while an insertion of the same length membrane distal to residue 118 still allows the formation of functional fusion complexes. This demonstrates that the position of the section from positions 84 to 118 relative to the donor membrane, and thus relative to the F trimer, is critical for productive hetero-oligomerization. Tolerance to stalk elongation at position 118 renders specific protein-protein contacts between the H head and F unlikely, in particular, since structurally rigid insertions with a predicted pitch of approximately 75 Å in an α-helical configuration are compatible with the formation of functional fusion complexes in the context of both transient glycoprotein expression and recombinant virus particles. This finding furthermore supports the idea that H and F oligomers separate after successful initiation of F rearrangements, given that in the case of continued hetero-oligomer interaction, the 75-Å H extension would likely keep

the target membrane outside the range of the F fusion peptide.

The fact that large stalk insertions with very strong α-helical propensity are tolerated membrane distal to residue 118 furthermore lends support to secondary structure predictions (36) extending a rigid, helical configuration found for the PIV5 HN stalk (78) to MeV H. Insertions equivalent to 1.9 (7 residues), 3.9 (14 residues), or 11.4 (41 residues) helix turns are compatible with the formation of functional fusion complexes. This again suggests some rotational flexibility within the H stalk as considered above on the basis of successful insertion of N-glycans at positions 110, 111, and 112. A drop in F triggering and surface expression as a consequence of a 55-residue insertion supports, however, the idea that stalk insertions of progressive length eventually have a destabilizing effect on H.

If H stalks enjoy some rotational flexibility and residues in stalk section 84 to 118 (presumably residues 111, 114, and 118) engage in short-range contacts for F triggering, how is receptor binding by the H head domain (48, 71) signaled to the contact zone despite the presence of a long (41-residue) stalk insertion? Interestingly, no major conformational changes between crystal structures of PIV5 HN, HPIV3 HN, and henipavirus G, solved alone or in complex with their receptors, were observed (8, 9, 74). Although receptor binding was originally proposed to initiate major changes in the NDV HN protein (17, 61, 62), subsequent work has demonstrated that major HN rearrangements are unlikely to be required for NDV F triggering (39). Since the dimer-of-dimer interface of PIV5 HN is substantially smaller than that within the dimer interaction, it has been hypothesized as a possible mechanism for F triggering that receptor binding

may result in partial disassembly of the tetrameric head of the HN attachment protein, in turn changing the interaction with F and inducing triggering (78). Some conformational changes upon receptor binding have also been implicated for Nipah virus and Hendra virus G (1, 4). For the latter, it was proposed that these changes may affect the dimer-of-dimer interface (6).

By analogy, partial or complete disintegration of hypothetical MeV H homotetramers upon receptor binding would not require complex signaling through the stalk domain and, thus, be reconcilable with the partially maintained functionality of the H-118▽41x variant. However, isolated MeV H head domain fragments have crystallized as monomers (14) and homodimers (28). In this context, it should be noted that similarly soluble head domains of henipavirus G attachment proteins are also monomeric in solution and crystals (8, 74). Nevertheless, native G is predicted to exist in a tetrameric dimer-of-dimers configuration (7). Elucidating the order of physiological, membrane-embedded MeV H oligomers before and after receptor binding therefore emerges as a central task in understanding the mechanism of MeV F triggering. While we represent H structures as homodimers in this study for simplicity and in light of the available X-ray data, we remain open to the hypothesis that the tetramer constitutes the physiological oligomer of MeV H. Certainly, reorganization of a hypothetical dimer-of-dimer oligomer rather than an intricate signaling mechanism could provide a straightforward explanation as to how engagement of distinct binding sites in the H-Edm head domain by CD46 or SLAM (48, 71), and even of single-chain antibody moieties carboxy-terminally attached to MeV H through flexible linkers (27), results in effective F triggering.

Appendix 1 Figures

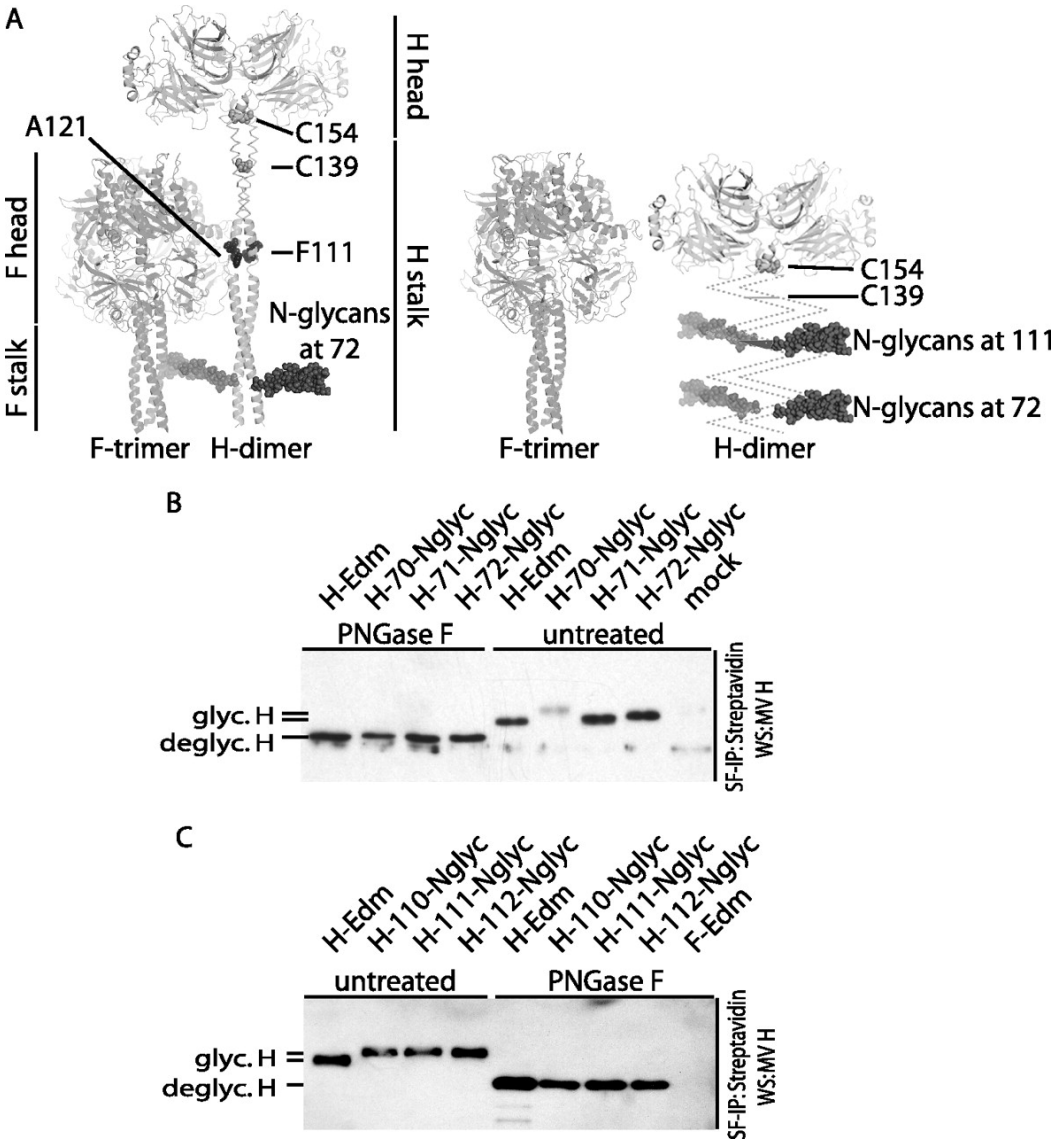

Figure 1. Insertion of additional N-glycans into the MeV H stalk domain at membrane-proximal and membrane-distal positions. glyc., glycosylated; deglyc., deglycosylated. (A) Ribbon representation of hypothetical envelope glycoprotein interaction modes and the positions of additional N-glycans engineered to probe the proximity of the F trimer to H. Staggered alignment (left panel) predicts that only N-glycans added at a membrane-proximal position (shown as dark spheres

for H residue 72) but not a membrane-distal position (highlighted residue 111; engineered N-glycan not shown for spatial constraints) are compatible with the formation of functional fusion complexes. Parallel alignment of the head domains (right panel) permits H and F hetero-oligomerization with added N-glycans at either position in the H stalk (shown for residues 72 and 111 as dark spheres). Prefusion F and H head and stalk domains, F residue A121 (previously identified to contribute to MeV H and F interaction) (36), and cysteine residues in the H stalk (C139 and C154) engaged in disulfide bonds for covalent H dimerization are shown. H is represented as a dimer in accordance with available X-ray information, although a tetramer (dimer-of-dimers) may in fact be the physiological oligomer. Either order is predicted to tolerate additional N-glycans at position 72. (B) Of three N-glycosylation sites engineered at positions 70, 71, and 72, only that at position 72 is efficiently glycosylated and surface expressed. Surface-exposed proteins were biotinylated, precipitated with immobilized streptavidin, and subjected to PNGase F treatment for deglycosylation or mock treated in equal aliquots. Electrophoretic mobility of MeV H species was determined by SDS-PAGE and decoration of immunoblots with a specific antiserum directed against the cytosolic tail of MeV H. (C) Engineered N-glycans at positions 110, 111, and 112 are efficiently recognized. Treatment of samples was as described for panel B.

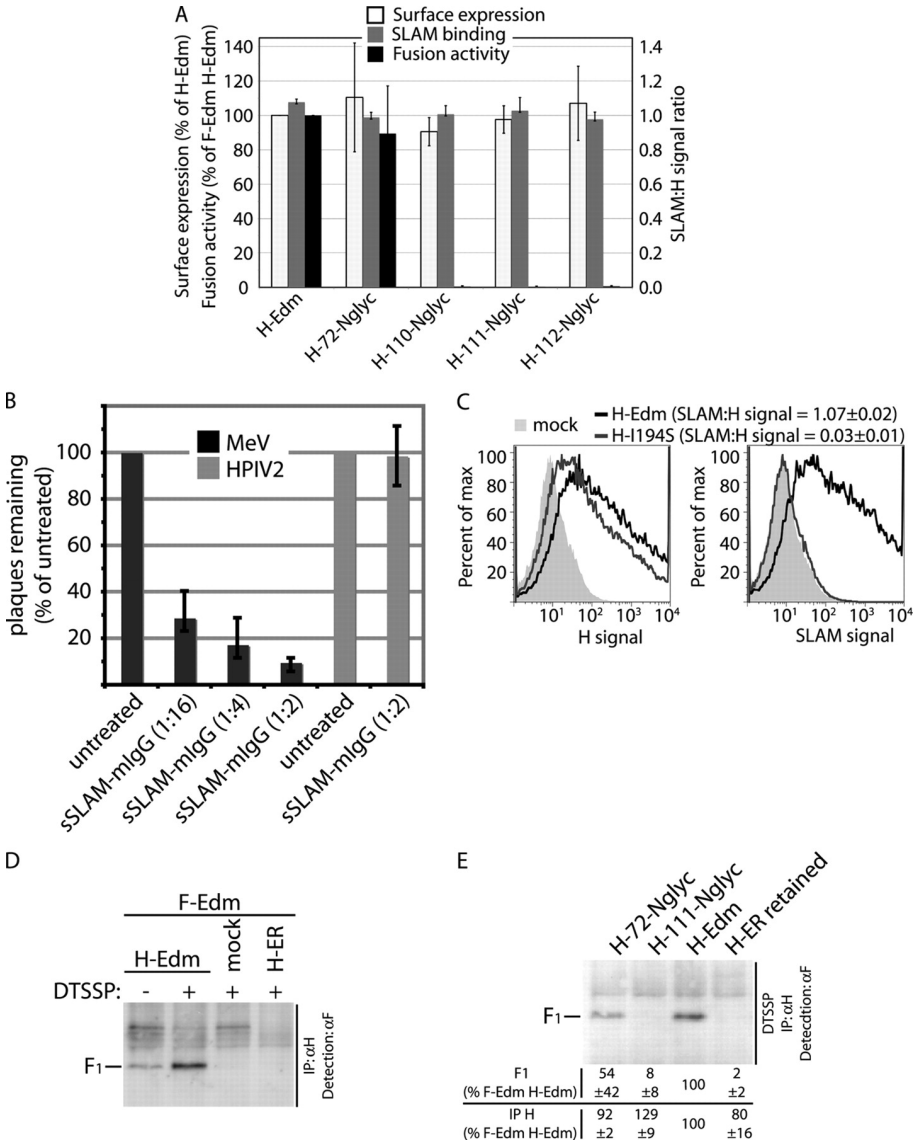

Figure 2. Additional N-glycans at H stalk position 72, but not 110, 111, or 112, allow the formation of functional H-F fusion complexes. (A) Assessment of surface expression, SLAM binding capacity, and cell-to-cell fusion activity of H variants. Surface expression was determined through surface biotinylation using transferrin receptor as an internal standard. SLAM binding was monitored as detailed for panel B. Flow cytometry values are expressed as ratios of SLAM signal to H signal. Fusion activity was determined in a firefly luciferase-based

quantitative fusion assay upon coexpression of H variants with Edmonston F (F-Edm). In all cases, values are expressed relative to unmodified H-Edm and represent the averages from at least three independent experiments ± SEMs. (B) Virus neutralization assay confirming specific interaction of purified, sSLAM, C-terminally fused to mIgG heavy chains (sSLAM-mIgG), with MeV. Virus particles were incubated with dilutions of purified sSLAM-mIgG as specified for 30 min at 25°C, followed by transfer to Vero-SLAM target cells and agar overlay. Plaque counts were determined 72 h postinfection. Counts of equally sSLAM-mIgG-treated HPIV2-induced plaques were not altered by sSLAM-mIgG, confirming specificity of the interaction. Values show plaque counts relative to vehicle (PBS)-treated controls and reflect averages from three independent experiments ± SDs. (C) Assessment of SLAM binding capacity. MeV receptor-negative CHO cells expressing H variants were analyzed by flow cytometry using an sSLAM-mIgG fusion protein or mouse monoclonal antibodies directed against epitopes in the MeV H ectodomain and a mouse-specific allophycocyanin conjugate. Numbers represent the ratios of mean fluorescence intensities obtained after decoration of cells with sSLAM-IgG (SLAM signal) or anti-H antibodies (H signal). Averages from three independent experiments ± SEMs are shown. max, maximum. (D) Chemical cross-linking stabilizes surface-exposed H-Edm/F-Edm hetero-oligomers in situ prior to cell lysis. Cells transfected with equal amounts of H-Edm- and F-Edm-expressing plasmids were treated with the membrane-impermeable, reducible cross-linker DTSSP, followed by quenching and lysis with stringent radioimmunoprecipitation assay buffer. For controls, DTSSP was omitted, cells were transfected with F-Edm-expressing plasmids only or cells

were cotransfected with F-Edm and an H-Edm variant harboring a cytosolic endoplasmic reticulum retention motif (H-ER) (55). For immunoprecipitation (IP), a monoclonal antibody cocktail directed against epitopes in the MeV H ectodomain (αH) was used, followed by cleavage of the linker through reducing denaturation buffer, SDS-PAGE, and detection of coprecipitated F protein on immunoblots with a specific antiserum directed against the F protein cytosolic tail. In the absence of DTSSP, the majority of hetero-oligomers dissociates during cell lysis and immunoprecipitation. Cross-linking of proteolytically matured F material and lack of F cross-linking with the ER-retained H variants confirm membrane impermeability of the linker and analysis of surface-exposed complexes. (E) Co-IP of surface-exposed, proteolytically matured MeV F with MeV H with a monoclonal antibody cocktail directed against the MeV H ectodomain after treatment of cotransfected cells with the membrane-impermeable cross-linker DTSSP. For a control, an H variant carrying a cytosolic ER retention motif (H-ER retained) (55) was included. Values show efficiencies of F co-IP (top row) and, for a control, direct H immunoprecipitation (IP; bottom row). They are expressed relative to H-Edm and represent averages from four (co-IP) or at least three (direct immunoprecipitation) independent experiments ± SEMs.

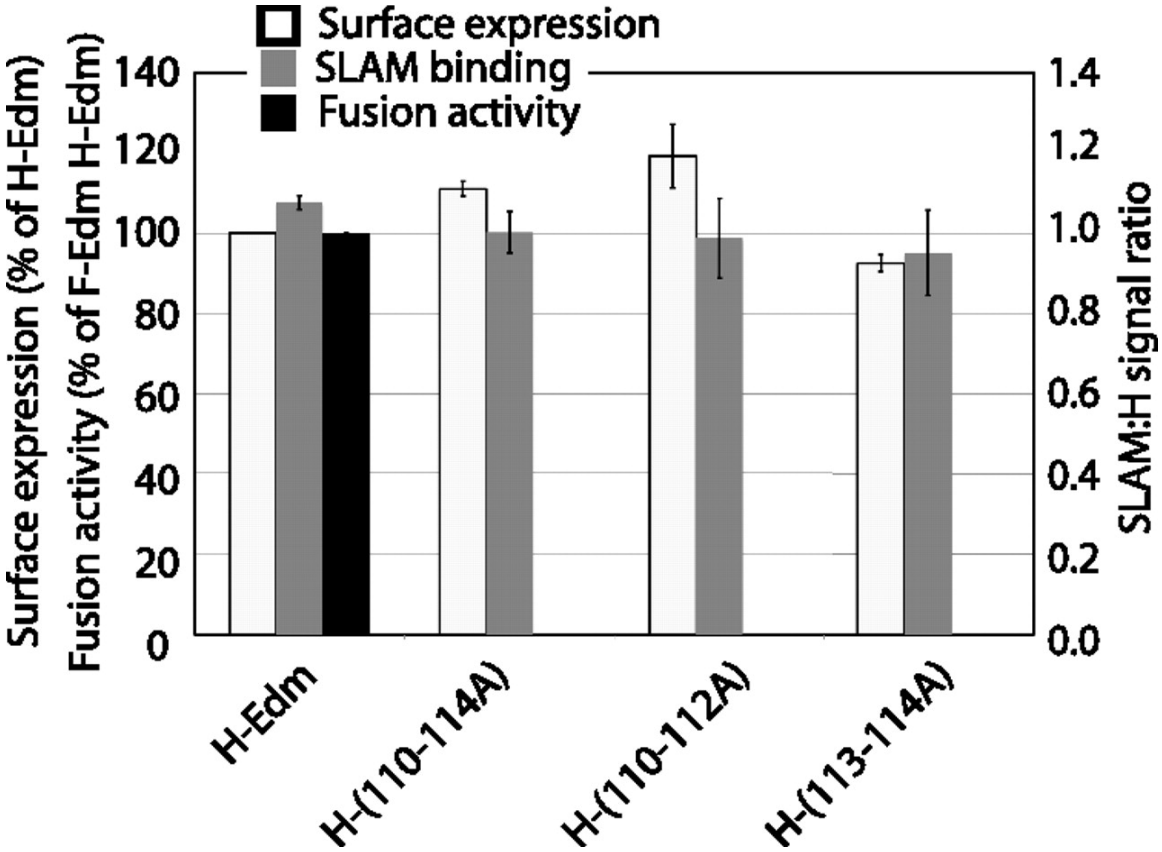

Figure 3. Integrity of the MeV H stalk microdomain from positions 110 to 114 is required for the formation of functional fusion complexes but not H surface expression or SLAM binding. Alanine-scanning mutagenesis was followed by sample analysis as described in the legend to Fig. 2A. Values represent the averages from at least three independent experiments ± SEMs.

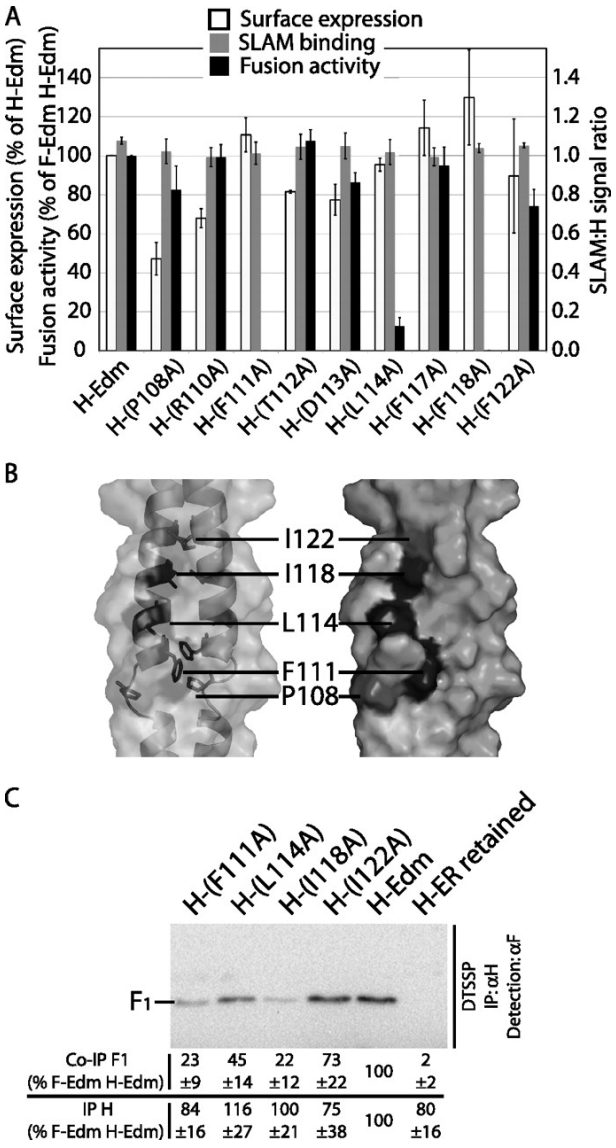

Figure 4. H stalk residues 111, 114, and 118 are determinants for physical and functional interaction of MeV H and F. F-Edm, MeV Edmonston F. (A) Characterization of H variants harboring individual alanine point mutations as in Fig. 2A. Values represent the averages from at least three independent experiments ± SEMs. Only mutation of residue 111, 114, or 118 substantially reduces F triggering activity. (B) In an α-helical configuration of the H stalk, residues 111, 114, and 118 are predicted to be located adjacent to each other on

consecutive turns of the helix. Solvent-accessible surface models of H stalk dimers cover positions 103 to 125. Side chains of residues 111, 114, and 118 are shown in dark gray, and side chains of residues 108 and 122 are shown in light gray. The translucent surface with a ribbon trace (left panel) reveals a possible helix break at P108, making residue 111 accessible (orientation toward the viewer). The opaque surface (right panel) reveals that side chains of residues 111, 114, and 118 form a continuous patch. (C) Co-IP of surface-exposed, matured MeV F with MeV H after DTSSP cross-linking as in Fig. 2E. Values represent averages from four independent experiments ± SEMs. H-ER retained, an H variant carrying a cytosolic endoplasmic reticulum retention motif; IP, immunoprecipitation; αH and αF, antibodies to H and F, respectively.

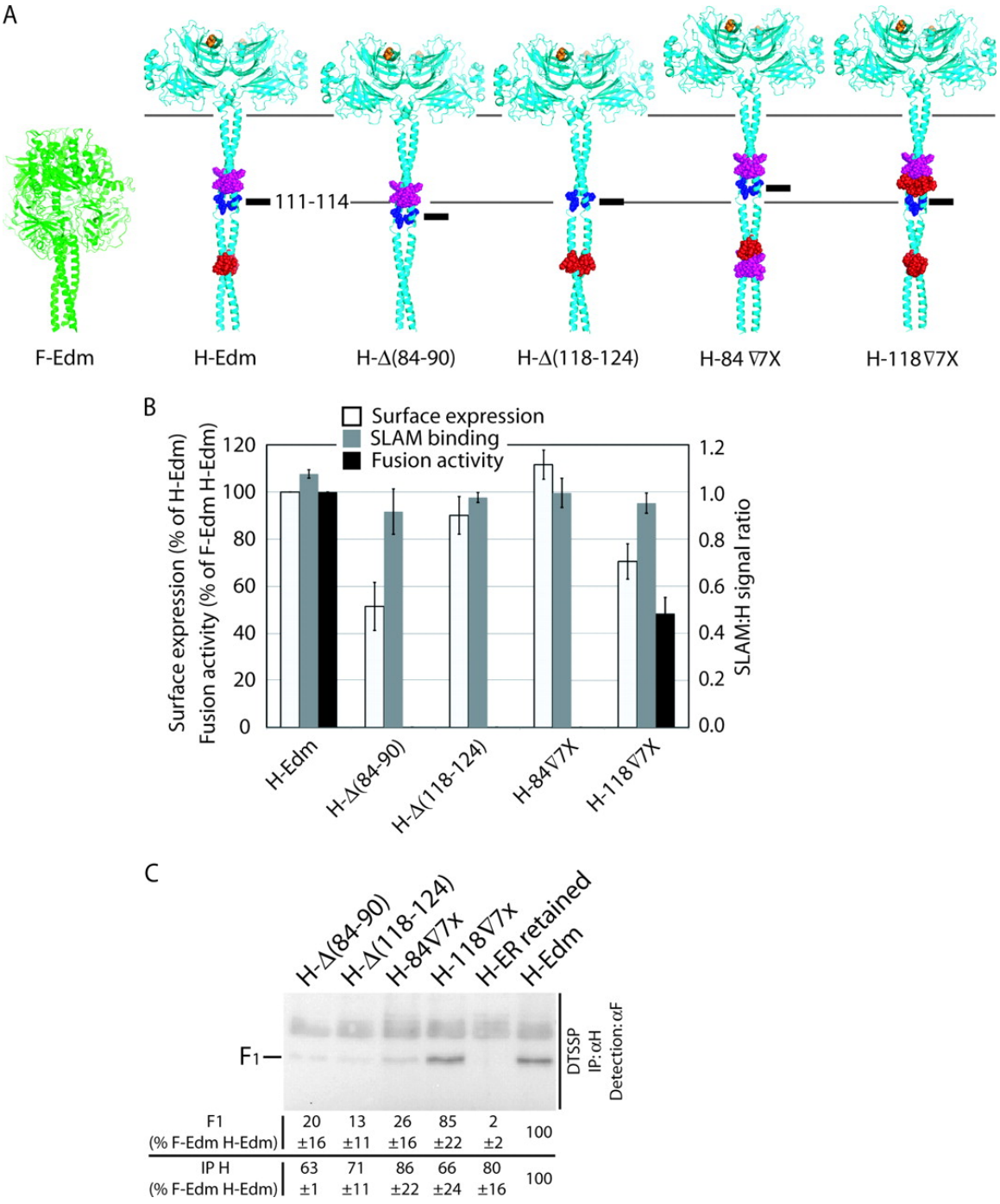

Figure 5. Insertion of a HR element into the H stalk downstream of position 118 is compatible with functional glycoprotein interaction. F-Edm, MeV Edmonston F. (A) Graphic representation of predicted consequences of H stalk deletions or

insertions in a hypothetical hetero-oligomer organization that involves short-range contacts between the prefusion F head and the H stalk. Ribbon models of prefusion MeV F and H (stalk residues 58 to 122 in an α-helical configuration) were aligned at the transmembrane domains as previously described (36). HR elements 118 to 124 (magenta) and 84 to 90 (red) were either individually deleted [H-Δ(118-124) or H-Δ(84-90)] or inserted as an additional copy at residue 84 (H-84▽7x) or 118 (H-118▽7x). The position of residues 111 to 114 (blue; black alignment bars) and alignment guides for this section and the H head domains (horizontal gray lines) are shown. (B) Characterization of the stalk deletion and insertion variants as in Fig. 2A. Values represent the averages from at least three independent experiments ± SEMs. Only the construct with a membrane-distal insertion (H-118▽7x) shows F triggering activity. (C) Co-IP of surface-exposed, matured MeV F with MeV H after DTSSP cross-linking as in Fig. 2E. Values represent averages from four independent experiments ± SEMs. H-ER retained, an H variant carrying a cytosolic endoplasmic reticulum retention motif; IP, immunoprecipitation; αH, antibody to H.

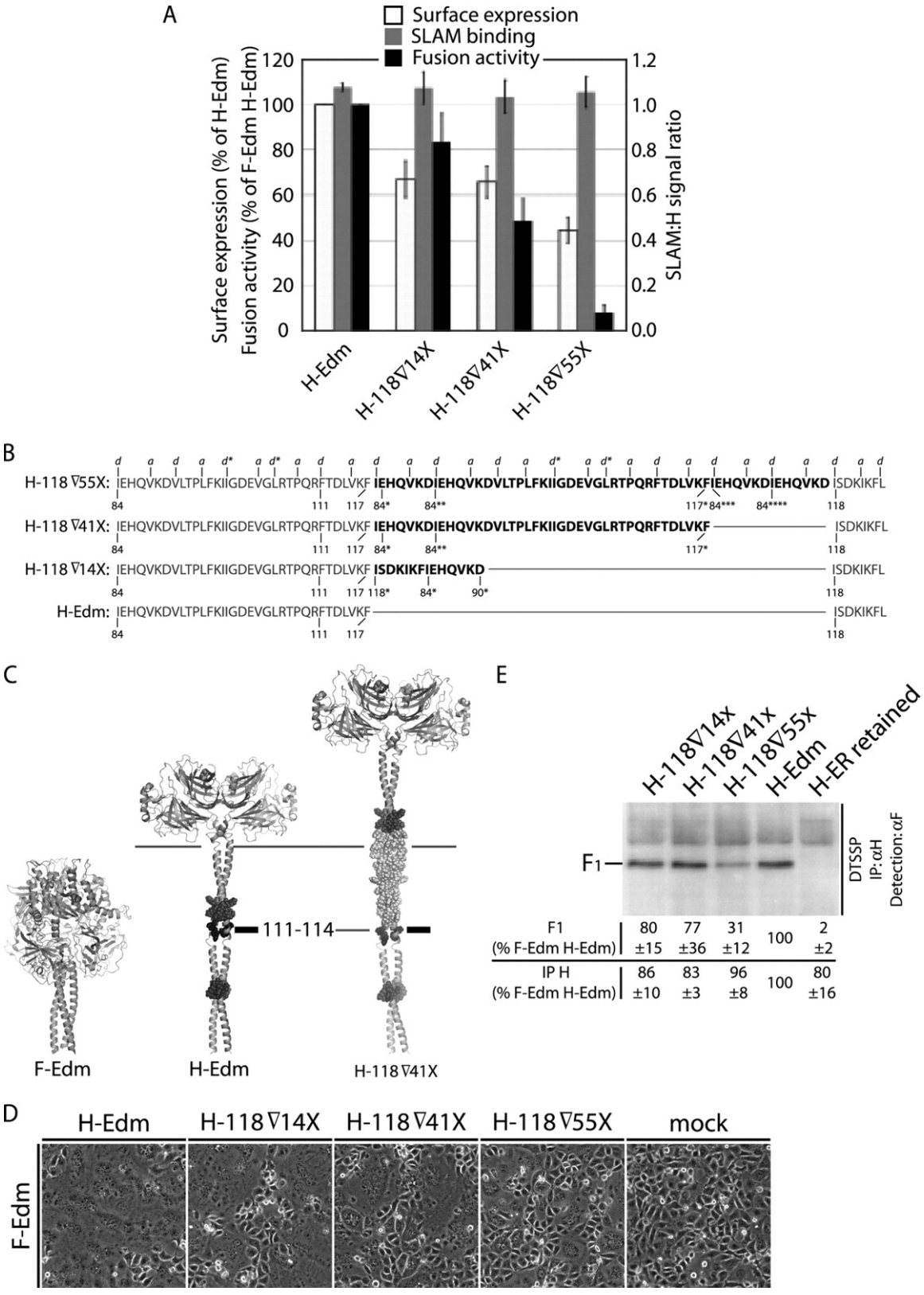
A
Surface expression
SLAM binding
Fusion activity
Surface expression (% of H-Edm)
Fusion activity (% of F-Edm H-Edm)
SLAM:H signal ratio
H-Edm
H-118∇14X
H-118∇41X
H-118∇55X
B
H-118∇55X:
H-118∇41X:
H-118∇14X:
H-Edm:
C
111-114
F-Edm
H-Edm
H-118∇41X
D
H-Edm
H-118∇14X
H-118∇41X
H-118∇55X
mock
F-Edm
E
H-118∇14x
H-118∇41x
H-118∇55x
H-Edm
H-ER retained
F1
DTSP
IP: αH
Detection: αF
F1 (% F-Edm H-Edm) 80 ±15 77 ±36 31 ±12 100 2 ±2
IP H (% F-Edm H-Edm) 86 ±10 83 ±3 96 ±8 100 80 ±16

Figure 6. Membrane-distal insertion of multiple HR elements is compatible with F triggering. F-Edm, MeV Edmonston F. (A) Characterization of H variants harboring stalk insertions at position 118 of 14 (H-84▽14x)-, 41 (H-84▽41x)-, or 55 (H-84▽55x) -residue-insertion variants as in Fig. 2A. Values represent the averages from at least three independent experiments ± SEMs. All constructs show F triggering activity, albeit at a substantially reduced rate in the case of H-84▽55x, harboring the 55-residue insertion. (B) Sequences of H-84▽14x, generated through conventional directed mutagenesis, and H-84▽41x and H-84▽55x, generated through staggered-priming mutagenesis (shown in boldface for each construct). The sequence of unmodified H-Edm is shown in gray, and the positions of residue 84 in additional copies of the HR from positions 84 to 90 (84*, 84**, 84***, and 84****) or residue 118 in additional copies of the HR from positions 118 to 124 (118*), residues 111 and 117, and residues at the termini of the stalk duplications (90* and 117*) are indicated. Markings above the sequences represent the predicted “a” and “d” positions in the stalk helical wheel, and d* indicates HR stutters. (C) Graphic representation of elongated stalk H variant H-84▽41x in comparison with H-Edm. The 41-residue insertion is shown in the predicted helical configuration in light gray. Alignment with F, marking of individual residues and microdomains, and alignment bars are as described in the legend to Fig. 5A. (D) Microphotographs of Vero-SLAM cells cotransfected with 3 μg (each) of expression plasmids encoding F-Edm, H-Edm, or H variant H-84▽14x, H-84▽41x, or H-84▽55x as specified. Mock-transfected cells received F-Edm expression plasmids only. Photographs were taken 15 h posttransfection at a magnification of ×200. Representative fields of view are

shown. (E) Co-IP of surface-exposed, matured MeV F with MeV H after DTSSP cross-linking as in Fig. 2E. Values represent averages from four independent experiments ± SEMs. H-ER retained, an H variant carrying a cytosolic endoplasmic reticulum retention motif; IP, immunoprecipitation; αH, antibody to H.

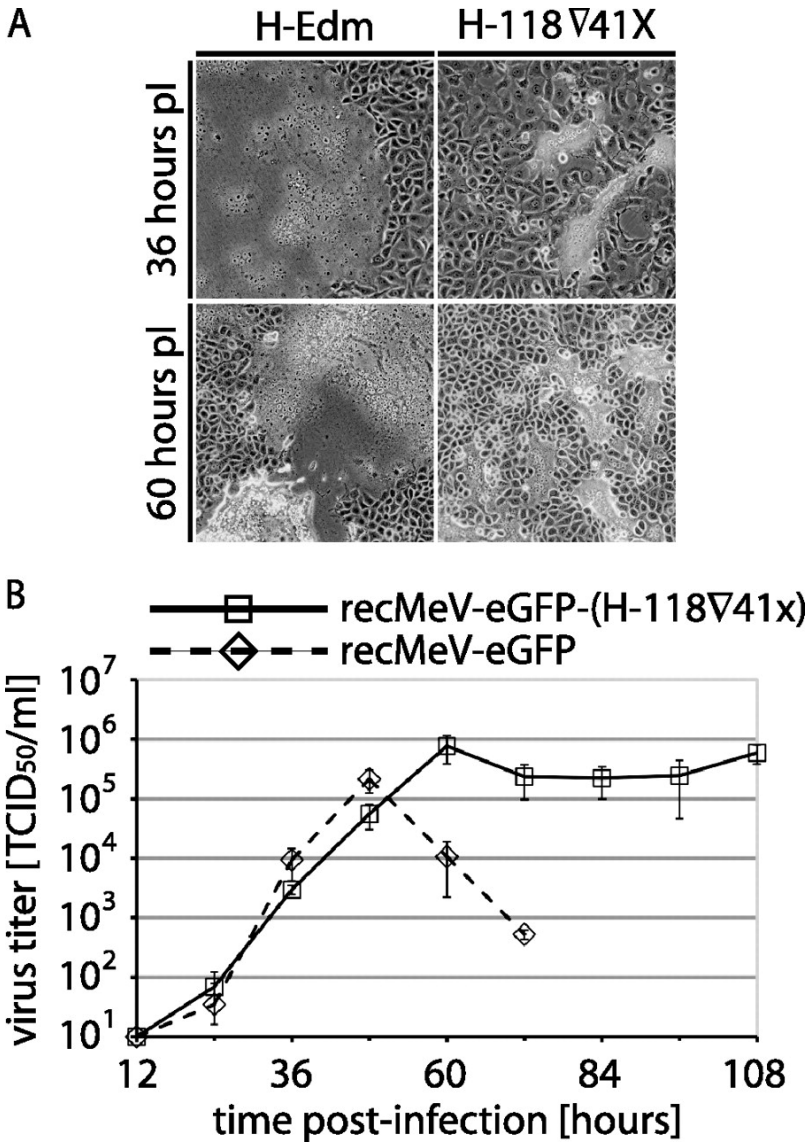

Figure 7. The H-84∇41x variant harboring the 41-residue membrane-distal stalk insertion supports virus infection and growth. (A) Microphotographs (overlays of phase contrast and fluorescence) of Vero-SLAM cells infected with recombinant recMeV-eGFP-(H-118□41x) that contains the H-118∇41x variant instead of normal H or unmodified recMeV-eGFP for comparison. Cells were infected at an MOI of 0.01 and photographed 36 and 60 h postinfection (pI) at a magnification of ×200. Representative fields of view are shown. (B) recMeV-

eGFP-(H-118▽41x) growth curves show an extended plateau phase of peak titers of progeny virus. Vero-SLAM cells were infected with recMeV-eGFP-(H-118▽41x) or recMeV-eGFP at an MOI of 0.001, and titers of cell-associated viral particles were determined at the indicated time points through $TCID_{50}$ titration. Average values from three independent experiments are shown, and error bars represent SDs.

Appendix 1 Acknowledgements

We thank J. J. Yoon and A. Shapiro for help with support experiments of the study and A. L. Hammond for critical reading of the manuscript.

M.A.B. was funded by the Molecular Mechanisms of Microbial Pathogenesis training grant T32 AI007470 from the NIH. This work was supported by U.S. Public Health Service grant AI071002 (to R.K.P.) from the NIH/NIAID.

Appendix 1 References

1. **Aguilar HC, Ataman ZA, Aspericueta V, Fang AQ, Stroud M, Negrete OA, Kammerer RA, Lee B.** 2009. A novel receptor-induced activation site in the Nipah virus attachment glycoprotein (G) involved in triggering the fusion glycoprotein (F). The Journal of biological chemistry **284:**1628-1635.
2. **Aguilar HC, Matreyek KA, Filone CM, Hashimi ST, Levroney EL, Negrete OA, Bertolotti-Ciarlet A, Choi DY, McHardy I, Fulcher JA, Su SV, Wolf MC, Kohatsu L, Baum LG, Lee B.** 2006. N-glycans on Nipah virus fusion protein protect against neutralization but reduce membrane fusion and viral entry. Journal of virology **80:**4878-4889.
3. **Ben-Efraim I, Kliger Y, Hermesh C, Shai Y.** 1999. Membrane-induced step in the activation of Sendai virus fusion protein. Journal of molecular biology **285:**609-625.
4. **Bishop KA, Hickey AC, Khetawat D, Patch JR, Bossart KN, Zhu Z, Wang LF, Dimitrov DS, Broder CC.** 2008. Residues in the stalk

domain of the hendra virus g glycoprotein modulate conformational changes associated with receptor binding. Journal of virology **82:**11398-11409.

5. **Bishop KA, Stantchev TS, Hickey AC, Khetawat D, Bossart KN, Krasnoperov V, Gill P, Feng YR, Wang L, Eaton BT, Wang LF, Broder CC.** 2007. Identification of Hendra virus G glycoprotein residues that are critical for receptor binding. Journal of virology **81:**5893-5901.
6. **Bossart KN, Broder CC.** 2008. Paramyxovirus entry. *In* Pohlmann S, Simmons G (ed.), Viral entry into host cells. Landes Biosciences, Austin, TX.
7. **Bossart KN, Crameri G, Dimitrov AS, Mungall BA, Feng YR, Patch JR, Choudhary A, Wang LF, Eaton BT, Broder CC.** 2005. Receptor binding, fusion inhibition, and induction of cross-reactive neutralizing antibodies by a soluble G glycoprotein of Hendra virus. Journal of virology **79:**6690-6702.
8. **Bowden TA, Aricescu AR, Gilbert RJ, Grimes JM, Jones EY, Stuart DI.** 2008. Structural basis of Nipah and Hendra virus attachment to their cell-surface receptor ephrin-B2. Nature structural & molecular biology **15:**567-572.
9. **Bowden TA, Crispin M, Harvey DJ, Aricescu AR, Grimes JM, Jones EY, Stuart DI.** 2008. Crystal structure and carbohydrate analysis of Nipah virus attachment glycoprotein: a template for antiviral and vaccine design. Journal of virology **82:**11628-11636.

10. **Buchholz UJ, Finke S, Conzelmann KK.** 1999. Generation of bovine respiratory syncytial virus (BRSV) from cDNA: BRSV NS2 is not essential for virus replication in tissue culture, and the human RSV leader region acts as a functional BRSV genome promoter. Journal of virology **73:**251-259.

11. **Burkhard P, Kammerer RA, Steinmetz MO, Bourenkov GP, Aebi U.** 2000. The coiled-coil trigger site of the rod domain of cortexillin I unveils a distinct network of interhelical and intrahelical salt bridges. Structure **8:**223-230.

12. **Cathomen T, Naim HY, Cattaneo R.** 1998. Measles viruses with altered envelope protein cytoplasmic tails gain cell fusion competence. Journal of virology **72:**1224-1234.

13. **Chen L, Gorman JJ, McKimm-Breschkin J, Lawrence LJ, Tulloch PA, Smith BJ, Colman PM, Lawrence MC.** 2001. The structure of the fusion glycoprotein of Newcastle disease virus suggests a novel paradigm for the molecular mechanism of membrane fusion. Structure **9:**255-266.

14. **Colf LA, Juo ZS, Garcia KC.** 2007. Structure of the measles virus hemagglutinin. Nature structural & molecular biology **14:**1227-1228.

15. **Colman PM, Lawrence MC.** 2003. The structural biology of type I viral membrane fusion. Nature reviews. Molecular cell biology **4:**309-319.

16. **Corey EA, Iorio RM.** 2007. Mutations in the stalk of the measles virus hemagglutinin protein decrease fusion but do not interfere with virus-

specific interaction with the homologous fusion protein. Journal of virology **81:**9900-9910.

17. **Crennell S, Takimoto T, Portner A, Taylor G.** 2000. Crystal structure of the multifunctional paramyxovirus hemagglutinin-neuraminidase. Nature structural biology **7:**1068-1074.

18. **Deng R, Mirza AM, Mahon PJ, Iorio RM.** 1997. Functional chimeric HN glycoproteins derived from Newcastle disease virus and human parainfluenza virus-3. Archives of virology. Supplementum **13:**115-130.

19. **Deng R, Wang Z, Mahon PJ, Marinello M, Mirza A, Iorio RM.** 1999. Mutations in the Newcastle disease virus hemagglutinin-neuraminidase protein that interfere with its ability to interact with the homologous F protein in the promotion of fusion. Virology **253:**43-54.

20. **Deng R, Wang Z, Mirza AM, Iorio RM.** 1995. Localization of a domain on the paramyxovirus attachment protein required for the promotion of cellular fusion by its homologous fusion protein spike. Virology **209:**457-469.

21. **Dorig RE, Marcil A, Chopra A, Richardson CD.** 1993. The human CD46 molecule is a receptor for measles virus (Edmonston strain). Cell **75:**295-305.

22. **Duprex WP, McQuaid S, Hangartner L, Billeter MA, Rima BK.** 1999. Observation of measles virus cell-to-cell spread in astrocytoma cells by using a green fluorescent protein-expressing recombinant virus. Journal of virology **73:**9568-9575.

23. **Federspiel MJ, Hughes SH.** 1998. Retroviral gene delivery, p. 179-214. *In* Emerson CP, Sweeney HL (ed.), Methods in cell biology, vol. 52. San Diego, CA, Academic Press.

24. **Gallagher P, Henneberry J, Wilson I, Sambrook J, Gething MJ.** 1988. Addition of carbohydrate side chains at novel sites on influenza virus hemagglutinin can modulate the folding, transport, and activity of the molecule. The Journal of cell biology **107:**2059-2073.

25. **Gravel KA, Morrison TG.** 2003. Interacting domains of the HN and F proteins of newcastle disease virus. Journal of virology **77:**11040-11049.

26. **Griffin DE.** 2007. Measles virus. *In* Knipe DM, Howley PM (ed.), Fields virology, 5th ed., vol. 1. Lippincott Williams & Wilkins, Philadelphia, PA.

27. **Hammond AL, Plemper RK, Zhang J, Schneider U, Russell SJ, Cattaneo R.** 2001. Single-chain antibody displayed on a recombinant measles virus confers entry through the tumor-associated carcinoembryonic antigen. Journal of virology **75:**2087-2096.

28. **Hashiguchi T, Kajikawa M, Maita N, Takeda M, Kuroki K, Sasaki K, Kohda D, Yanagi Y, Maenaka K.** 2007. Crystal structure of measles virus hemagglutinin provides insight into effective vaccines. Proceedings of the National Academy of Sciences of the United States of America **104:**19535-19540.

29. **Hu XL, Ray R, Compans RW.** 1992. Functional interactions between the fusion protein and hemagglutinin-neuraminidase of human parainfluenza viruses. Journal of virology **66:**1528-1534.

30. **Iorio RM, Mahon PJ.** 2008. Paramyxoviruses: different receptors - different mechanisms of fusion. Trends in microbiology **16:**135-137.

31. **Jain S, McGinnes LW, Morrison TG.** 2008. Overexpression of thiol/disulfide isomerases enhances membrane fusion directed by the Newcastle disease virus fusion protein. Journal of virology **82:**12039-12048.

32. **Lamb RA, Jardetzky TS.** 2007. Structural basis of viral invasion: lessons from paramyxovirus F. Current opinion in structural biology **17:**427-436.

33. **Lamb RA, Parks GD.** 2007. Paramyxoviridae: the viruses and their replication, p. 1446-1496. *In* Knipe DM, Howley PM (ed.), Fields virology, 5th ed., vol. 1. Lippincott Williams & Wilkins, Philadelphia, PA.

34. **Lamb RA, Paterson RG, Jardetzky TS.** 2006. Paramyxovirus membrane fusion: lessons from the F and HN atomic structures. Virology **344:**30-37.

35. **Lawrence MC, Borg NA, Streltsov VA, Pilling PA, Epa VC, Varghese JN, McKimm-Breschkin JL, Colman PM.** 2004. Structure of the haemagglutinin-neuraminidase from human parainfluenza virus type III. Journal of molecular biology **335:**1343-1357.

36. **Lee JK, Prussia A, Paal T, White LK, Snyder JP, Plemper RK.** 2008. Functional interaction between paramyxovirus fusion and attachment proteins. The Journal of biological chemistry **283:**16561-16572.

37. **Lee JK, Prussia A, Snyder JP, Plemper RK.** 2007. Reversible inhibition of the fusion activity of measles virus F protein by an engineered intersubunit disulfide bridge. Journal of virology **81:**8821-8826.

38. **Ludwig K, Schade B, Bottcher C, Korte T, Ohlwein N, Baljinnyam B, Veit M, Herrmann A.** 2008. Electron cryomicroscopy reveals different F1+F2 protein States in intact parainfluenza virions. Journal of virology **82:**3775-3781.

39. **Mahon PJ, Mirza AM, Musich TA, Iorio RM.** 2008. Engineered intermonomeric disulfide bonds in the globular domain of Newcastle disease virus hemagglutinin-neuraminidase protein: implications for the mechanism of fusion promotion. Journal of virology **82:**10386-10396.

40. **Manchester M, Eto DS, Valsamakis A, Liton PB, Fernandez-Munoz R, Rota PA, Bellini WJ, Forthal DN, Oldstone MB.** 2000. Clinical isolates of measles virus use CD46 as a cellular receptor. Journal of virology **74:**3967-3974.

41. **McGinnes L, Sergel T, Morrison T.** 1993. Mutations in the transmembrane domain of the HN protein of Newcastle disease virus affect the structure and activity of the protein. Virology **196:**101-110.

42. **McGinnes LW, Morrison TG.** 2006. Inhibition of receptor binding stabilizes Newcastle disease virus HN and F protein-containing complexes. Journal of virology **80:**2894-2903.

43. **Melanson VR, Iorio RM.** 2004. Amino acid substitutions in the F-specific domain in the stalk of the newcastle disease virus HN protein

modulate fusion and interfere with its interaction with the F protein. Journal of virology **78:**13053-13061.

44. **Melanson VR, Iorio RM.** 2006. Addition of N-glycans in the stalk of the Newcastle disease virus HN protein blocks its interaction with the F protein and prevents fusion. Journal of virology **80:**623-633.

45. **Melikyan GB, Markosyan RM, Hemmati H, Delmedico MK, Lambert DM, Cohen FS.** 2000. Evidence that the transition of HIV-1 gp41 into a six-helix bundle, not the bundle configuration, induces membrane fusion. The Journal of cell biology **151:**413-423.

46. **Naniche D, Varior-Krishnan G, Cervoni F, Wild TF, Rossi B, Rabourdin-Combe C, Gerlier D.** 1993. Human membrane cofactor protein (CD46) acts as a cellular receptor for measles virus. Journal of virology **67:**6025-6032.

47. **Navaratnarajah CK, Leonard VH, Cattaneo R.** 2009. Measles virus glycoprotein complex assembly, receptor attachment, and cell entry. Current topics in microbiology and immunology **329:**59-76.

48. **Navaratnarajah CK, Vongpunsawad S, Oezguen N, Stehle T, Braun W, Hashiguchi T, Maenaka K, Yanagi Y, Cattaneo R.** 2008. Dynamic interaction of the measles virus hemagglutinin with its receptor signaling lymphocytic activation molecule (SLAM, CD150). The Journal of biological chemistry **283:**11763-11771.

49. **Ng DT, Hiebert SW, Lamb RA.** 1990. Different roles of individual N-linked oligosaccharide chains in folding, assembly, and transport of the

simian virus 5 hemagglutinin-neuraminidase. Molecular and cellular biology **10:**1989-2001.

50. **Ng DT, Randall RE, Lamb RA.** 1989. Intracellular maturation and transport of the SV5 type II glycoprotein hemagglutinin-neuraminidase: specific and transient association with GRP78-BiP in the endoplasmic reticulum and extensive internalization from the cell surface. The Journal of cell biology **109:**3273-3289.

51. **Oldstone MB, Homann D, Lewicki H, Stevenson D.** 2002. One, two, or three step: measles virus receptor dance. Virology **299:**162-163.

52. **Ono N, Tatsuo H, Hidaka Y, Aoki T, Minagawa H, Yanagi Y.** 2001. Measles viruses on throat swabs from measles patients use signaling lymphocytic activation molecule (CDw150) but not CD46 as a cellular receptor. Journal of virology **75:**4399-4401.

53. **Peisajovich SG, Samuel O, Shai Y.** 2000. Paramyxovirus F1 protein has two fusion peptides: implications for the mechanism of membrane fusion. Journal of molecular biology **296:**1353-1365.

54. **Plemper RK, Hammond AL, Cattaneo R.** 2000. Characterization of a region of the measles virus hemagglutinin sufficient for its dimerization. Journal of virology **74:**6485-6493.

55. **Plemper RK, Hammond AL, Cattaneo R.** 2001. Measles virus envelope glycoproteins hetero-oligomerize in the endoplasmic reticulum. The Journal of biological chemistry **276:**44239-44246.

56. **Plemper RK, Hammond AL, Gerlier D, Fielding AK, Cattaneo R.** 2002. Strength of envelope protein interaction modulates cytopathicity of measles virus. Journal of virology **76:**5051-5061.

57. **Prussia AJ, Plemper RK, Snyder JP.** 2008. Measles virus entry inhibitors: a structural proposal for mechanism of action and the development of resistance. Biochemistry **47:**13573-13583.

58. **Radecke F, Spielhofer P, Schneider H, Kaelin K, Huber M, Dotsch C, Christiansen G, Billeter MA.** 1995. Rescue of measles viruses from cloned DNA. The EMBO journal **14:**5773-5784.

59. **Spearman C.** 1908. The method of 'right and wrong cases' ('constant stimulit') without Gauss's formulae. Br. J. Psychol. **2:**227-242.

60. **Sutter G, Ohlmann M, Erfle V.** 1995. Non-replicating vaccinia vector efficiently expresses bacteriophage T7 RNA polymerase. FEBS letters **371:**9-12.

61. **Takimoto T, Taylor GL, Connaris HC, Crennell SJ, Portner A.** 2002. Role of the hemagglutinin-neuraminidase protein in the mechanism of paramyxovirus-cell membrane fusion. Journal of virology **76:**13028-13033.

62. **Takimoto T, Taylor GL, Crennell SJ, Scroggs RA, Portner A.** 2000. Crystallization of Newcastle disease virus hemagglutinin-neuraminidase glycoprotein. Virology **270:**208-214.

63. **Tanabayashi K, Compans RW.** 1996. Functional interaction of paramyxovirus glycoproteins: identification of a domain in Sendai virus HN which promotes cell fusion. Journal of virology **70:**6112-6118.

64. **Tatsuo H, Ono N, Tanaka K, Yanagi Y.** 2000. SLAM (CDw150) is a cellular receptor for measles virus. Nature **406:**893-897.

65. **Tatsuo H, Ono N, Yanagi Y.** 2001. Morbilliviruses use signaling lymphocyte activation molecules (CD150) as cellular receptors. Journal of virology **75:**5842-5850.

66. **Thompson SD, Laver WG, Murti KG, Portner A.** 1988. Isolation of a biologically active soluble form of the hemagglutinin-neuraminidase protein of Sendai virus. Journal of virology **62:**4653-4660.

67. **Tomasi M, Pasti C, Manfrinato C, Dallocchio F, Bellini T.** 2003. Peptides derived from the heptad repeat region near the C-terminal of Sendai virus F protein bind the hemagglutinin-neuraminidase ectodomain. FEBS letters **536:**56-60.

68. **Tsuchiya E, Sugawara K, Hongo S, Matsuzaki Y, Muraki Y, Li ZN, Nakamura K.** 2002. Effect of addition of new oligosaccharide chains to the globular head of influenza A/H2N2 virus haemagglutinin on the intracellular transport and biological activities of the molecule. The Journal of general virology **83:**1137-1146.

69. **Tsurudome M, Ito M, Nishio M, Kawano M, Okamoto K, Kusagawa S, Komada H, Ito Y.** 1998. Identification of regions on the fusion protein of human parainfluenza virus type 2 which are required for haemagglutinin-neuraminidase proteins to promote cell fusion. The Journal of general virology **79 (Pt 2):**279-289.

70. **Tsurudome M, Kawano M, Yuasa T, Tabata N, Nishio M, Komada H, Ito Y.** 1995. Identification of regions on the hemagglutinin-

neuraminidase protein of human parainfluenza virus type 2 important for promoting cell fusion. Virology **213:**190-203.

71. **Vongpunsawad S, Oezgun N, Braun W, Cattaneo R.** 2004. Selectively receptor-blind measles viruses: Identification of residues necessary for SLAM- or CD46-induced fusion and their localization on a new hemagglutinin structural model. Journal of virology **78:**302-313.

72. **Wang Z, Mirza AM, Li J, Mahon PJ, Iorio RM.** 2004. An oligosaccharide at the C-terminus of the F-specific domain in the stalk of the human parainfluenza virus 3 hemagglutinin-neuraminidase modulates fusion. Virus research **99:**177-185.

73. **White JM, Delos SE, Brecher M, Schornberg K.** 2008. Structures and mechanisms of viral membrane fusion proteins: multiple variations on a common theme. Critical reviews in biochemistry and molecular biology **43:**189-219.

74. **Xu K, Rajashankar KR, Chan YP, Himanen JP, Broder CC, Nikolov DB.** 2008. Host cell recognition by the henipaviruses: crystal structures of the Nipah G attachment glycoprotein and its complex with ephrin-B3. Proceedings of the National Academy of Sciences of the United States of America **105:**9953-9958.

75. **Yao Q, Hu X, Compans RW.** 1997. Association of the parainfluenza virus fusion and hemagglutinin-neuraminidase glycoproteins on cell surfaces. Journal of virology **71:**650-656.

76. **Yin HS, Paterson RG, Wen X, Lamb RA, Jardetzky TS.** 2005. Structure of the uncleaved ectodomain of the paramyxovirus (hPIV3)

fusion protein. Proceedings of the National Academy of Sciences of the United States of America **102:**9288-9293.

77. **Yin HS, Wen X, Paterson RG, Lamb RA, Jardetzky TS.** 2006. Structure of the parainfluenza virus 5 F protein in its metastable, prefusion conformation. Nature **439:**38-44.

78. **Yuan P, Leser GP, Demeler B, Lamb RA, Jardetzky TS.** 2008. Domain architecture and oligomerization properties of the paramyxovirus PIV 5 hemagglutinin-neuraminidase (HN) protein. Virology **378:**282-291.

79. **Yuan P, Thompson TB, Wurzburg BA, Paterson RG, Lamb RA, Jardetzky TS.** 2005. Structural studies of the parainfluenza virus 5 hemagglutinin-neuraminidase tetramer in complex with its receptor, sialyllactose. Structure **13:**803-815.

80. **Zhao X, Singh M, Malashkevich VN, Kim PS.** 2000. Structural characterization of the human respiratory syncytial virus fusion protein core. Proceedings of the National Academy of Sciences of the United States of America **97:**14172-14177.